UNIVERSITÀ DEGLI STUDI DI MILANO

DEPARTMENT OF PHYSICS, ASTROPHYSICS AND APPLIED PHYSICS

PHD SCHOOL IN

PHYSICS, ASTROPHYSICS AND APPLIED PHYSICS

CYCLE XXXIV

STUDY OF THE MUTUAL INTERACTION BETWEEN THE EXTRACELLULAR MATRIX AND CELLS IN PERITONEAL METASTASIS

Disciplinary Scientific Sector < FIS/03 >

PhD Thesis of:

Ewelina Julia Lorenc

Director of the School: Prof. Matteo Paris

Supervisor of the Thesis: Prof. Alessandro Podestà

co-Supervisor: Dr. Matteo Chighizola

A.Y. 2022-2023

External referees:

Dr. Marco Pierotti
Head of CGT Lab & R&D Diagnostic and Scientific Director of BiLiGeCT project
Cogentech Società Benefit srl, Milan, Italy
Prof. Massimiliano Galuzzi
Associate Professor at Materials Interfaces Center
Shenzhen Institutes of Advanced Technology, Chinese Academy of Sciences, Guangdong, China

Commission of the final examination:

Prof. Małgorzata Lekka,
Full Professor at the Department of Biophysical Microstructure at the Institute of Nuclear Physics, Polish Academy of Science, Kraków, Poland

Prof. Felix Rico,
Associate Professor at Université Aix-Marseille and Institut national de la Santé et de la Recherche Médicale (INSERM), Force Microscopy lab, Marseille, France

Internal member:

Prof. Alessandro Podestà
Associate Professor of Department of Physics, Astrophysics and Applied Physics “Aldo Pontremoli”, Università degli Studi di Milano, Milan, Italy

Final examination:

13th March 2023
Department of Physics, Astrophysics and Applied Physics, Università degli Studi di Milano, Milan, Italy

Acknowledgements

First of all, thanks are due to my supervisor Prof. Alessandro Podestà for all the guidance, especially in the field of physics and mechanics. I am glad that I had an opportunity to work with such great and inspirational researcher. Special thanks to Matteo Chighizola, my co-supervisor, for all the help, advice and support, not only the scientific one. Thank you for guiding me in PhD life;) I'm very grateful to Hatice Holuigue, for all the years of working together and turning PhD studies into something more than just research. Thanks to you my PhD was an amazing adventure.

I want also to thank to everyone in Phys2BioMed network, for all interesting and simulating discussions about mechanobiology but also for great time we spent together. Special thanks to my friends from the project: Dominika, Maria Luisa, Maria Leonor and Sandra; I hope to work with you again. I would like to thank to Antonia Samorè for all the help within the project, but also during my first months in Italy.

Main part of my research was done in collaboration with Istituto Nazionale dei Tumori, thus I would like to thank Dr. Varinelli and Dr. Gariboldi for opportunity to work together. My research would not be possible without help of colleagues from urological research institute of Ospedale San Raffaele from research group led by Dr. Alfano and Federico Pezzotta from Officina Mecchanica of Department of Physics (UNIMI). Thanks to Prof. A. Moroni for cell storage and Prof. M. Mazzanti for providing vibratome. Special thanks to everyone at Department of Biophysical Microstructures at Institute of Nuclear Physics, especially Prof. Małgorzata Lekka. Kajangi Gnanachandran and Prof. Laidler and Dr. Gil from Medical Biochemistry department at the Jagiellonian University, where I had a chance to perform part of my studies. I am also grateful for opportunity to work with Prof. Ben Fabry and Prof. Wolfgang Goldmann, Dr. Ingo Thievessen, Msc. Thabang Matseke, Msc. Johannes Bartl at Biophysics group at Friedrich-Alexander-Universität

Thank you, Chiara, for your friendship, for believing that I am an engineer and for all the support (the fact that you’re reading this means that I’m a penguin, right?). Gianluca, thank you for all the words of support and motivation. I also had great time working at UNIMI with Federica, Filippo, Davide, Giacomo and Michele. All my years doing PhD will be an unforgettable time thanks to your friendship.

Thanks are also due to CIMaNiaCi group: Anita (for her contribution to emergency snack box), Sara (Buondi! It always brightened my day), Marco (all nice coffee breaks), Lorenzo (focaccia Friday and entertainment management), Matteo M. (despite our friendship, I will remain a Switzerland, sorry) and Matteo G. I was glad to see you and work with you every day.

I am very grateful for the help and support from my friends in Poland, especially Agnieszka and Monika (the real engineer).

The last but not least I would like to thank to my parents and family: for simply believing in me and motivating me with words of support. Despite the distance between us, you have always been there for me.

This project has received funding from the European Union’s
Horizon 2020 research and Innovation program under the
H2020-MSCA-ITN-2018 Grant Agreement n. 812772.

Funded by the European Union

“There is nothing like looking if you want to find something.

You certainly usually find something, if you look,

but it is not always quite the something you were after”

-J.R.R. Tolkien

I would like to dedicate this work

to my Grandparents Halina and Mieczysław and

to my Parents, who inspired my pursuit of knowledge

and encouraged me in this process.

TABLE OF CONTENT

1. INTRODUCTION 11

1.1. MECHANOBIOLOGY IN HEALTH AND DISEASE– NEW APPROACH IN BIOMEDICINE 11

1.2. CANCER AND ROLE OF ECM IN TUMORIGENESIS ON PERITONEUM 12

1.3. 3D BIOLOGICAL MODELS IN MECHANOBIOLOGY RESEARCH 15

1.4. AFM: A POWERFUL AND VERSATILE TOOL IN CANCER RESEARCH 17

2. AIMS OF THE STUDY 20

3. MATERIALS AND METHODS. GENERAL ASPECTS 22

3.1. ATOMIC FORCE MICROSCOPY IN INDENTATION MODE 22

3.1.1. COLLOIDAL PROBES 26
3.1.2. PYRAMIDAL AND CONICAL TIPS 26
3.1.3. CYLINDRICAL TIP WITH A "FLAT PUNCH" AND A TIPLESS CANTILEVER 27
3.2. CUSTOM COLLOIDAL PROBES 27

3.3. DATA ANALYSIS 32

4. STUDY OF THE IMPACT OF SAMPLE PREPARATION PROCEDURES ON THE MECHANICAL PROPERTIES OF TISSUES 33

4.1. INFLUENCE OF FREEZING ON NANOMECHANICAL PROPERTIES OF TISSUE SPECIMENS 33

4.1.2 INTRODUCTION 33
4.1.3. CURRENT METHODS FOR FREEZING BIOLOGICAL SAMPLES 34
4.1.3.1. Snap freezing in liquid nitrogen 34
4.1.3.2. Cool bath with dry ice and ethanol 35
4.1.3.3. Liquid nitrogen bath in isopentane 35
4.1.4. CRYOPROTECTANTS 35
4.1.5. STRUCTURE OF BLADDER 36
4.1.3. MATERIALS AND METHODS 37
4.1.3.1. Sample preparation and AFM measurements 37
4.1.3.1.1. Snap freezing in liquid nitrogen 39
4.1.3.1.2 Freezing with dry ice and ethanol 39
4.1.3.1.3 Freezing in liquid nitrogen bath 39
4.1.4. RESULTS 40
4.1.4.1. Snap freezing with liquid nitrogen 40
4.1.4.2. Freezing with dry ice and ethanol 42

4.1.4.3. Freezing in isopentane in liquid nitrogen bath 43
4.1.4.4. Comparison between techniques 44
4.1.5. DISCUSSION 45
4.2. PREPARATION OF FRESH TISSUE SAMPLES FOR AFM MEASUREMENTS 47
4.2.1. INTRODUCTION 47
4.2.2. MATERIALS AND METHODS 49
4.2.2.1. Developing protocol – use of the vibratome 49
4.2.2.2. AFM measurements 52
4.2.3. RESULTS AND DISCUSSION 52
4.3. CONCLUSIONS 54

5. STUDY OF THE MUTUAL INFLUENCE BETWEEN ECM AND CELLS DURING CANCER PROGRESSION IN PERITONEAL METASTASES 56

5.1. INTRODUCTION 56

5.2. DECELLULARIZED NORMAL AND TUMOUR SCAFFOLDS FOR CANCER ORGANOID CULTURES AS A MODEL OF COLORECTAL PERITONEAL METASTASES 59
5.2.1. INTRODUCTION 59
5.2.2. MATERIALS AND METHODS 60
5.2.2.1 Preparation of 3D-dECMs 60
5.2.2.2 dECM scaffolds characterization - AFM nanoindentation measurements 61
5.2.3 RESULTS 62
5.2.3.1 Mechanical properties of 3D-dECMs 62
5.2.3.2 Correlation of mechanical properties of 3D-dECMs with clinical data 63
5.2.4. DISCUSSION 64
5.2.5 CONCLUSIONS 66
5.3. CORRELATION BETWEEN EXTRACELLULAR MATRIX STIFFNESS DISTRIBUTION AND PERITONEAL METASTASIS PROGRESSION 67
5.3.1 FOREWORD 67
5.3.2. THE MANUSCRIPT 67
5.4. EXTRACELLULAR MATRIX SCAFFOLDS FOR CANCER ORGANOIDS CULTURES TO STUDY THE MECHANICAL ASPECTS OF CANCER PROGRESSION IN PERITONEAL METASTASES 88
5.4.1. INTRODUCTION 88
5.4.2. MATERIALS AND METHODS 90
5.4.2.1. Preparation of ex vivo PM lesions 90
5.4.2.2. AFM nanoindentation measurements 94
5.4.3. RESULTS AND DISCUSSION 94
5.4.3.1. Nanomechanical properties of ex vivo engineered PM lesions 94
5.4.3.2. Changes in elastic modulus distribution in ex vivo engineered PM lesions 97
5.5. CONCLUSIONS 99

6. STUDY OF NANO-MECHANICAL PROPERTIES OF SPHEROIDS 102

6.1. INTRODUCTION 102

6.1.1. SPHEROIDS AS A 3D MODEL IN BIOTECHNOLOGY RESEARCH 102
6.1.2. STRUCTURE OF SPHEROIDS 103
6.1.3 SPHEROIDS AS A TOOL TO STUDY MECHANOBIOLOGY OF CANCER 105
6.1.4 AFM IN MECHANOBIOLOGICAL RESEARCH ON SPHEROIDS 107
6.1.5. MICROFLUIDIC CYTOMETRY IN EXTENSIONAL FLOW 110
6.2. AIMS OF THE STUDY 112
6.3. DEVELOPMENT OF THE PROTOCOL FOR AFM NANOINDENTATION MEASUREMENTS OF MULTICELLULAR SPHEROIDS 113

6.3.1. MATERIALS AND METHODS 113
6.3.1.1. Cell culture 113
6.3.1.2. Spheroids culture 113
6.3.1.3. AFM nanoindentation measurements 117
6.3.2. RESULTS AND DISCUSSION 119
6.3.2.1. AFM nanoindentation measurements 119
6.3.2.1.1. Colloidal probes 120
6.3.2.1.2. Tipless cantilevers 123
6.3.2.1.3. Pyramidal tips 125
6.3.2.1.4. Comparison between used AFM probes 129
6.3.3. CONCLUSIONS 130
6.4. STUDY OF NANOMECHANICAL PROPERTIES OF MULTICELLULAR SPHEROIDS WITH MICROFLUIDIC CYTOMETRY IN EXTENSIONAL FLOW 132

6.4.1. DEVELOPMENT OF THE PROTOCOL 132
6.4.2. PRELIMINARY MEASUREMENTS AND DEVELOPMENT OF DATA ANALYSIS PROCEDURE. 138
6.5 CONCLUSIONS 139

7. CONCLUSIONS AND PERSPECTIVES 141

BIBLIOGRAPHY 143

1. Introduction

1.1. Mechanobiology in health and disease– new approach in biomedicine

Mechanobiology is an emerging field of science that focus on mechanical properties of biological specimens like cells and tissues, and it also investigates mechanical interactions and forces between cells, cells and their microenvironment and even between compounds of cells at single-molecule level[1]. Mechanical forces play a major role in the regulation of the function and organization of cells, tissues and organs. Because changes at the molecular and cellular levels have an impact on mechanical properties and may be associated with changes at the macroscopic level, studying biomechanical properties of cells and tissues in physiological and pathological processes, including cancer can help us better understand the pathophysiology and ethology of various malignancies and alternations in tissue homeostasis. This will offer a different and superior method for determining the stage of cancer development or progression as well as the targets for therapeutic treatments[1].

As an essential marker, tissue mechanics can provide information about the physiological or pathological status of the cells and extracellular matrix (ECM) during processes like differentiation, aging, or the progression of a disease, including cancer. In fact, this trait can offer profound insights into the study of many biological or medical processes, such as the differentiation between healthy and unhealthy cell types. As a matter of fact, aberrant alterations in tissue biomechanics are a major factor in several illnesses, including cancer, osteoporosis, osteoarthritis, cystic fibrosis, muscular dystrophy, ventricular aneurysm, and others. These pathological alterations in the mechanical characteristics of tissues begin at the cellular level and progress to higher levels of organization, such as tissues and organs[1,2]. The mechanical properties of cancer and stromal cells significantly change during tumorigenesis and progression due to a progressive loss of biomechanical homeostasis. The process by which a benign tissue becomes a malignant and invasive tumour entity happens both within the cells and in the tumour ECM [3–5].

1.2. Cancer and role of ECM in tumorigenesis on peritoneum

Cancer develops when the genes that control cellular development and repair are altered. The presence of cancer cells must be identified at the earliest stage feasible in order to successfully treat cancer[6,7]. This will aid in preventing them from metastasizing, which is the process of their spreading to different areas of the body[1]. One pathophysiological result of cancer is that affected cells are more deformable than non-malignant cells[3,8,9], while mechanical resistance increases in neoplastic tissue[3,4,10–15]. As a result, the difference in cell and tissue deformability but also adhesion and mechanics can be utilized to distinguish between normal and pathological states in the diagnosis of cancer[3]. Malignant cancer cells and tumours' ability to infiltrate, invade, or create metastases to distant places is another effect of alterations in the elastic properties of tissue main elements. There is currently little knowledge of how modifications in the biomechanical characteristics of cancer cells and tumours might influence cancer spread[1]. Early detection of cancer, if localized and controlled, makes it simpler to cure; nevertheless, after metastases have established, therapies are far more difficult and ineffective[6,7].

In every country, cancer ranks as a primary cause of mortality and a significant barrier to extending life expectancy. The World Health Organization (WHO) reported that the primary or second major cause of death before the age of 70 in 2019 is the cancer. The fact that cancer is becoming more prevalent as a leading cause of death is partially due to the notable decreases in stroke and coronary heart disease mortality rates worldwide[6,7]. About 25% of patients with colorectal carcinoma (CRC) may develop peritoneal metastasis, which is a significant cause of cancer-related death globally[16]. Although it occurs often, little is understood about the biology of colorectal-derived peritoneal metastasis (PM). For these individuals in their latter stages of illness, PM is linked to a poor prognosis and poor quality of life[16]. Even while receiving cytotoxic treatment, around 25% of patients who receive curative intent resection but do not have overt distant metastases at the moment of diagnosis, experience peritoneal recurrence, with a median survival of 6 months[17]. Modern chemotherapy, however, is less successful in individuals with colorectal PM. The peritoneal host defence is negatively impacted by current therapies including surgery, which causes a fast recurrence in many patients[16,18,19]. It is required to deconstruct the peritoneal metastasis process into several phases known as the "peritoneal metastatic cascade" in order to better comprehend the events involved. Although this divide is analytically helpful, it is vital to understand that each phase in the metastatic cascade indicates a continuous and interrelated process rather than necessarily occurring in isolation[17,19,20]. Alongside with biological and molecular studies, insight into mechanobiological aspects of cancer progression and PM cascade can be beneficial for further research.

One of the main elements of the tissue and important factor in carcinogenesis is the ECM[11,12,21–25]. The ECM is an intricate web of protein- and sugar-containing macromolecules that is distinguished by the presence of fibrillary and reticular structures, pores, and asperities at the nanoscale[26]. The ECM is essential for supporting cell development, controlling cell-cell and cell-matrix signalling, influencing cell mechanics mostly through cytoskeleton remodelling, and determining cell destiny[22,27–31]. The ECM and cells interact reciprocally, enabling active alteration of the ECM structure and content, which also impacts the mechanical characteristics of the ECM[11,32–34]. The growth and maintenance of multicellular tissues are controlled by a complex interplay between cells and ECM. Therein, it was discovered that the microenvironment's biophysical characteristics were essential regulators of several cellular responses, including proliferation, migration, and differentiation.

Tumour development and progression are influenced by changes in stiffness and deterioration of tissue microenvironment[11,22,30]. Connective tissues made of specific fibrotic proteins are part of the ECM and are overexpressed in the majority of malignancies. It is well recognized that the intricate web of macromolecules has unique physical, biochemical, and biomechanical properties, and that when a tumour develops, it goes through a significant remodelling process. Remodelling is being done to enable cancer cells to communicate with nearby tumour microenvironment cells[11,31–33]. Together, stiffening and degradation represent two significant ECM alterations. Stiffening may result from an increase in cross-linking between ECM proteins. On the other hand, this cross-disruption linking's causes the ECM to deteriorate. The sole mechanical characteristic of cancer in clinics that is employed for early screening in cancer diagnosis is ECM stiffness, which is a prevalent occurrence. A stiff or rigid ECM can encourage epithelial cells transition from normal cells to malignant cancer cells[11,21–24,28,35]. All stages of metastasis, including cellular separation of the primary tumour, invasion via the local ECM, and homing of cancer cells into the new metastatic location, are mediated by the ECM. Cancer cells exert physical pressure on the local ECM to develop invasive characteristics. ECM stiffness may result in intracellular contractions that stiffen the actin cytoskeleton and encourage the migration of cancer cells. In fact, substantial cancer cell motility depends on coming into touch with collagen bundles inside the ECM.

ECM stiffness activates many factors and signalling pathways[11], like transforming growth factor-ß (TGF-ß), leading to epithelial-to-mesenchymal transition in cancer cells[36,37]; phosphoinositide 3-kinase activity is enhanced by collagen cross-linking[38,39] extracellular signal-regulated kinase (ERK) pathway is indirectly activated by ECM stiffness what contributes to neoplastic cell proliferation and survival[40]. Overall, tissue microenvironment is an important element in cancer development and progression, playing a part in cancer cell proliferation and survival, and later invasion and metastasis, angiogenesis, hypoxia[11]. Before administering chemotherapy, it is necessary to disrupt the ECM because its rigidity might prevent chemotherapeutic medications from penetrating to the tumour site. This will facilitate drug penetration, reduce the dosage and subsequent side effects, and improve the prognosis for cancer patients[11].

1.3. 3D biological models in mechanobiology research

The nature of scientific research is to seek for novel techniques that will increase efficiency of measurements and provide more reliable, better quality results. There is a general shift from 2D to 3D models of cell culture and other more realistic biochemical and biomechanical microenvironments[41,42]. In 2D cultures, numerous crucial properties of cancer cells and tissue microenvironment cannot be accurately represented. Scaffold free system – spheroids and scaffold based system - organoids culture[41,4240], new 3D cell culture platforms that better resemble in vivo environment, are being developed to get around this constraint. These novel platforms have been shown to be better able to induce cell fates that are similar to those found in vivo for the particular processes being studied. Advances and applications of scaffold free systems: organoids and spheroids, will be discussed in detail in chapter 5.4.1 and chapter 6.1.1 respectively. Figure 1 shows comparison between spheroids and organoids, in the context of research of this work, to highlight the differences between these two systems.

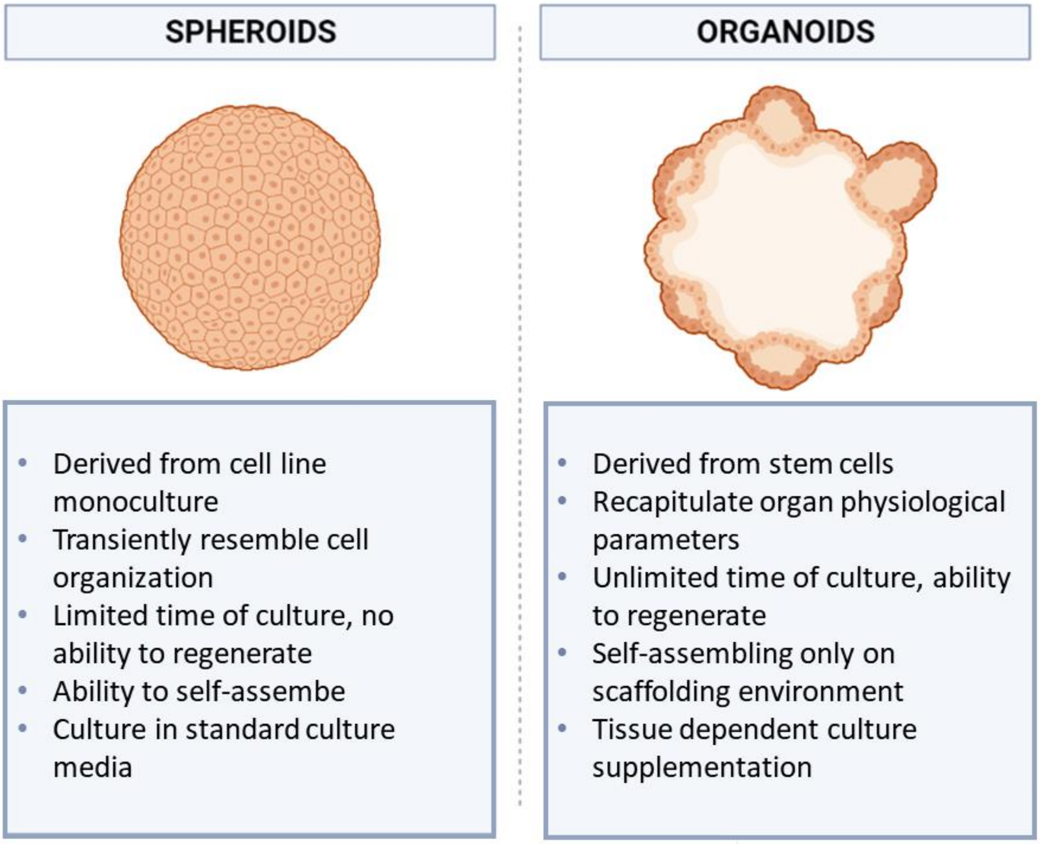

- Derived from cell line monoculture
- Transiently resemble cell organization
- Limited time of culture, no ability to regenerate
- Ability to self-assembe
- Culture in standard culture media

- Derived from stem cells
- Recapitulate organ physiological parameters
- Unlimited time of culture, ability to regenerate
- Self-assembling only on scaffolding environment
- Tissue dependent culture supplementation

Figure 1. *Main characteristics of spheroids and organoids*[42–46]*. [Made with BioRender].*

Findings from 3D research show that changing the ECM's dimension surrounding cells from 2D (fibronetin and collagen coating of culture surface) to 3D can have a big influence on their ability to proliferate, differentiate, and respond to mechanical forces[27,41,47,48]. 2D cell culture approaches can still accurately recapitulate in vivo behaviour for many bioactivities, and new developments in substrate design continue to add new capabilities to this platform. Overall, as technology advances to permit a larger range of operations, 3D platforms are expected to offer an increasingly alluring substitute for 2D cell culture[41]. The mechanical characteristics of three-dimensional systems may be adjusted to produce models that accurately represent a wide range of tissue stiffness[49]. Additionally, cell migration, adhesion, and dissemination are not limited to a single layer[42]. The utilization of 3D culture platforms (scaffold-free or scaffold-based techniques) is necessary to fully simulate natural tumour tissue biology as well as mechanical and biochemical features when mechanical limitations are included in the design of an in-vitro model. Tissue engineering frequently uses scaffold-based techniques to grow cells in a three-dimensional environment[42,50–54]. The use of bare ECM acquired by tissue decellularization as a scaffold for cell seeding or as an additional component of 3D gels to imitate the ECM architecture and chemical/biological characteristics in vitro is another encouraging development[25,50,53,55,56]. Additionally, adult, or pluripotent stem cell-derived organoids, which are self-organized 3D tissue cultures made from stem cells to recreate some or much of the complexity of an organ, can be used to imitate tissue physiology. By integrating decellularized ECM 3D in-vitro tumour models into high-throughput screening platforms and analysis via multiomics and single-cell profiling, it will be possible to provide new opportunities for developing more predictive and physiomimetic 3D tumour models[50,51]. All of these systems can replicate certain mechanical characteristics of natural tissue and range in complexity by providing complex three dimensional platform in which key cellular, biochemical and mechanobiological cues are present[42]. The subject of 3D disease models, including 3D scaffolds, spheroids, or organoids, is now flourishing and attracting significant interest from the pharmaceutical and biotechnological businesses, as well as from the medical and research communities.

1.4. AFM: a powerful and versatile tool in cancer research

Numerous experimental methods have been employed in the field of mechanobiology and cancer research[1,3,57–60], such as Atomic Force Microscopy (AFM) [61–63], micropipette aspiration[64], particle tracking microrheology[59,65,66], optical[67,68] or magnetic tweezers [57,69], magnetic twisting cytometry[68], rheology[14,59], hydraulic force spectroscopy (HFS)[70] or real-time deformability cytometry [71–73]. Focusing on cancer research and investigation of cell-microenvironment interaction, AFM may be very beneficial since it can be used as a force sensor with piconewton sensitivity as well as an imaging tool with high resolution[2,3,8,13,28,62,74–78]. Since magnetic resonance elastography, optical coherence elastography, and ultrasound elastography can only offer information on the mechanical characteristics of tissue at a relatively large scale, the nanoindentation approach has many benefits over other non-invasive methods. Additionally, these methods are unable to produce quantifiable data[79]. As the only microscope-based method that provides both high-resolution imaging and surface characterization, AFM is recognized as a versatile and effective method[3,80]. It can operate in a variety of environments (vacuum, air, and various liquids) and does not require special sample preparation such as dehydration, surface coating, or labelling. AFM can operate in a number of different modes, including contact (the tip is in contact with the sample surface), tapping (the tip-surface interactions are minimized), and non-contact (the cantilever oscillates at a certain distance from the surface)[3,80]. AFM has shown to be a valuable approach in treating cancer, assessing the impact of various medications on cell shape and mechanics[81].

In 1986 the atomic force microscope was developed as a tool for imaging non-conducting samples, both in air and under liquid[62,63,82]. Due to its capacity to detect small forces down to the piconewton scale, the AFM has since then been developed into a crucial instrument for researching surface interactions and giving quantitative data regarding material characteristics like elasticity, adhesion, surface potential, or surface charge density[83–85]. However, it quickly dragged attention of scientists from different fields, including biologists and biophysicists[2,58,61,86–89]. AFM has been widely used in clinical and biological applications during the last few decades, by mainly studying mechanics of variety of cells and tissues, demonstrating its potential in the diagnosis of numerous illnesses, including cancer and providing in-depth comprehension of cell and ECM physiological and pathological processes, as well as cell-cell and cell-microenvironment interaction in health and disease[2,3,8,13,28,33,75,77,81,90,91]. The range of the samples that can be studied with AFM is very wide: from tissues[4,15,76,92–94] to subcellular biomolecules[61,80,86]. The wide variety of applications of AFM comes from its simple principles of working. At the same time, there are opportunities for modifications and adjustments that make AFM suitable for variety of experiments[26,62,86,87]. By using cantilevers and tips with different properties it is possible to meet requirements of the experiment, depending on the measurement mode, type of studied sample (e.g., single cell, tissue, hydrogel) or the information that needs to be obtained (e.g., surface image, stiffness, adhesion force)[2,26,84,85,89].

Although technically difficult, the investigation of biological applications of the AFM is destined to be of crucial relevance. The new methods that combine AFM with traditional optical techniques help us understand the dynamics of biological processes better. They enable a variety of experiments, from identifying single molecule interactions to observing the responses of live cells[2] to ultimately determining the elastic properties of tissue biopsies[10]. In this way the full potential of AFM will be seen when combined with biological and molecular techniques[2,3,61,62].

2. Aims of the study

This thesis project has been carried out within a Marie-Skłodowska Curie ITN project called Phys2BioMed (Grant Agreement n.812772), which focuses on providing advanced and innovative tools for early diagnosis by mean of Atomic Force Microscopy AFM and correlative techniques.

The use of biomechanical approaches to study biological samples and cancer, in general, is still in its infancy and there are many outstanding questions that need to be addressed. Introducing AFM to research in mechanobiology requires adapting it to study variety of biological samples on micro and macroscale. Each type of sample, starting from tissue biopsies to DNA molecules calls for development of new protocols which adapt sample for AFM measurements[86]. A new, more specific aspects of sample preparation for AFM measurements were presented in the thesis. Each section of this work covers different aspects of mechanobiology research, focusing on adaptation of AFM measurements to study different biology samples and also to link study of mechanics with further biomedical research and to transfer these studies into clinics.

To fully exploit AFM advantages, work to adjust AFM for measurements on fresh, native tissue samples has been done, which is described in Chapter 4 of this thesis. Knowing that sample preparation is first, very important step in conducting research, new protocol for preparation of un has been developed. It allows to prepare tissue sections without use of any fixative that can affect nanomechanical properties of sample.

In this work AFM is used as main experimental tool to study cancer progression in peritoneum and interaction between tumour cells and its microenvironment. Aim of these studies was to have better insight into peritoneal metastasis from mechanical and biological point of view and to draw attention to AFM as potential tool in cancer diagnostic. The studies involved using experimental 3D models like organoids and ex vivo engineered PM lesions.

This research shows importance and advantages of 3D models in biological research and needs to adjust AFM measurements to new types of samples. Spheroids are common 3D models in research, including cancer research, thus there is high demand to develop protocol that will allow to study their nanomechanical properties. Hence, two attempts to characterize elasticity of spheroids were taken: with AFM in indentation mode and microfluidic cytometry in extensional flow.

3. Materials and methods. General aspects

3.1. Atomic force microscopy in indentation mode

The AFM operates by gently scanning or indenting the sample surface typically using a nanometre-sized tip positioned on a cantilever's free end[95,96]. The cantilever deflection is monitored using an optical beam deflection system[2,84,85,96]. In further detail, a laser source creates a beam that is reflected toward a photodiode by the back of the cantilever. The photodiode active region is often split into four quadrants, allowing for measurements of cantilever displacements in both normal and lateral directions (Fig. 2). By multiplying the cantilever deflection by the cantilever spring constant, the force is obtained, according to Hooke's law. Piezoelectric components are used to enable precise motions of the sample or cantilever. Then, qualitative, and quantitative data may be acquired by combining cantilever deflection with XYZ locations[2,3,59,61–63,95,96].

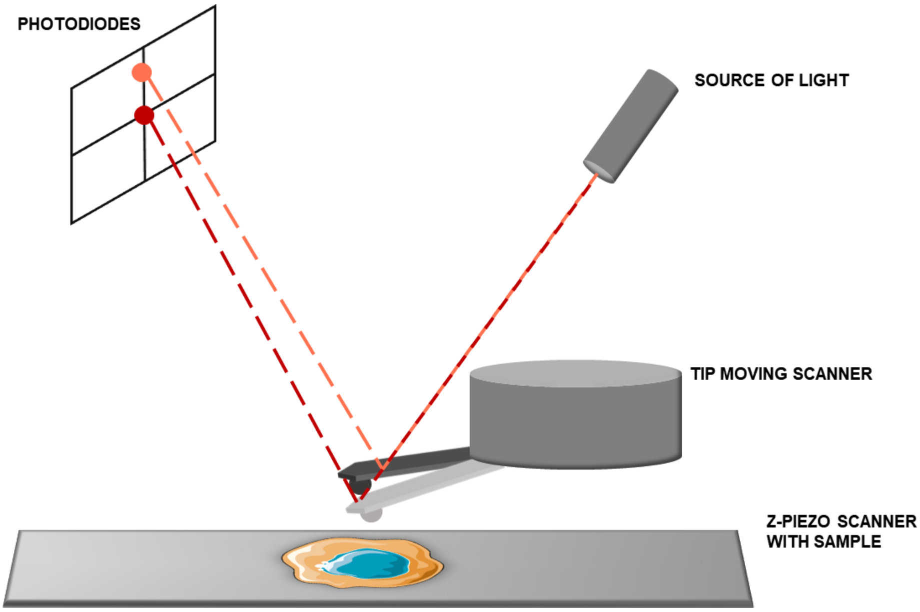

Figure 2. *Principles of AFM measurements*

The AFM nanoindentation method is the technique that is most frequently used to evaluate the mechanical characteristics of biological material at the nanoscale. This approach is based on applying a certain load to a nanoregion and then measuring the resulting indentation into the material, from which quantitative information about sample's elastic properties and intra- and inter-molecular forces can be obtained[2,79,83,97]. This mode involves the cantilever tip, which may be thought of as a spring, approaching the sample, indenting it until it reaches a certain deflection setpoint, and then retracting (Fig. 3). Force curves (FCs) may be captured by recording the raw cantilever deflection ΔV from the photodetector (in Volts units) vs. z-piezo displacement z [79,98,99]. The sample elastic characteristics are then determined by examining the force (F) versus indentation (δ) relationship (Fig. 2). These values cannot be measured directly, but it is possible to compute them using the relationships shown below:

$$\mathrm{F} = k_{CP,eff}^{LP}\mathrm{d}, \qquad \textit{Eq. 1}$$

$$\delta = \mathrm{z}+\mathrm{d} \qquad \textit{Eq. 2}$$

$$\mathrm{d} = \mathrm{S}\ \Delta\mathrm{V} \qquad \textit{Eq. 3}$$

where S is the deflection sensitivity of the OBD and $k_{CP,eff}^{LP}$ is the effective cantilever spring constant that accounts for cantilever tilt (see Eq. 10).

The Hertzian derivation from continuum mechanics serves as the foundation for the most basic and popular model to describe the elastic response of soft samples[2,61,79,97,100]. This model explains the local deformations caused by the interaction of two spheres with radii R1 and R2, each of which has a different Young's modulus (E1 and E2)[89]. The model, however, was expanded to account for the possibility that one sphere has an infinite radius and can therefore be thought of as an elastic half space:

$$F = \frac{3}{4}\frac{E}{(1-\nu^2)}R^{\frac{1}{2}}\delta^{\frac{3}{2}} \qquad \textit{Eq. 4}$$

where F is the loading force, δ is the indentation depth, and ν is the material-dependent Poisson's ratio (for cells and tissues is generally set to 0.5, since the volume is conserved during compression). R is the curvature radius of a parabolic tip. When the indentation is substantially lower than the bead's radius, this model can be applied to spherical tips[79,89,97,100]

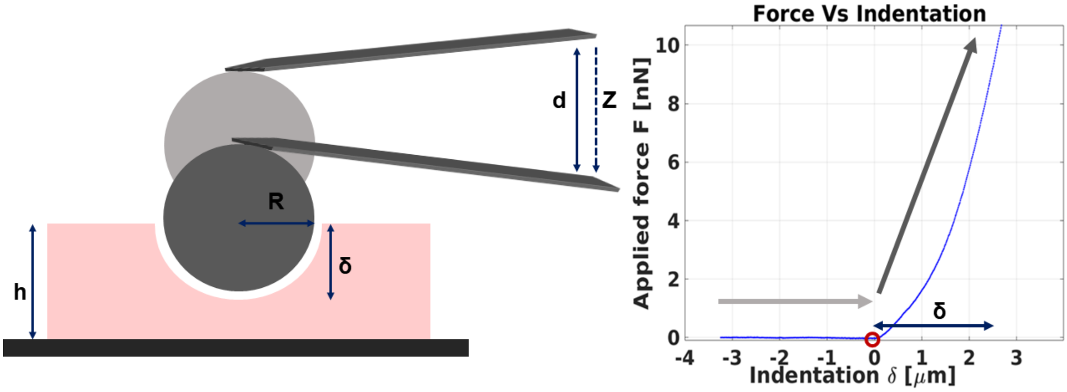

***Figure 3**. Principles of indentation mode in AFM measurements. As the AFM probe slowly approach the sample surface, no force is applied (bright grey arrow). Once the tip is engaged it starts to indent the sample and the indentation increases according to applied force.*

It is a truth that only in specific circumstances and with tight limitations can biological samples be approximated to elastic half spaces. The Hertz model is still the most often used mode, despite continued improvement and advancements in modelling of the mechanical properties of biological samples[79,100]. The aspects of relation between tip geometry and contact model are further investigated in Chapter 6.3.

When analysing biological samples and biomaterials for nanoindentation investigations, the Hertz model has been widely employed. The fundamental equations that result from the Hertz contact theory may be used to analyse the data from nanoindentation studies on bio-samples[79,97,98,100]. Numerous assumptions are necessary for the Hertz derivation, including homogeneity, isotropy, and an infinite sample thickness. To ensure a linear response of the sample, tiny stresses (also known as indentations) are required[98]. Despite the fact that all of these assumptions are crucial when using AFM data on biological specimens like cells and tissues, the majority of groups in the field have used this model with success[3,100–105]. The Hertz model describes with good accuracy the indentation of elastic bodies by spherical colloidal probes[79,97,98,100].

Under the assumption of a model for the tip-sample contact mechanics, the local elasticity (Young's modulus) of the sample may be determined by fitting the F(δ) model to the force curve. The data analysis of collected indentation FCs followed the protocol described in *Puricelli et al. 2015*[89]. Briefly, using Matlab environment, the baseline of each FC was removed to evaluate the contact point. Linearization to:

$$\delta - \delta_0 = \alpha F^* \qquad Eq.\ 5$$

, where $F^* = F^{2/3}$, δ_0 represents the point of first contact in the indentation axis and:

$$\alpha = \left(\frac{9}{16}\frac{1}{ER^{\frac{1}{2}}}\right)^{\frac{2}{3}} \qquad Eq.\ 6$$

allowed extracting the value of YM from FC by means of a simple linear fit[89]. The elastic behaviour of biological samples may be described using the following relations based on tip geometry[79]. It is common practice to simulate nanoindentation using the Hertz model, which needs knowledge of the tip's geometry and assumes that only elastic compressions of the specimen take place[79,98]. The earliest application of Hertzian contact mechanics was for the interaction of two fully elastic spheres. The model, however, was expanded to account for the possibility that one sphere has an infinite radius and can therefore be thought of as an elastic half space. It is a truth that only in specific circumstances and with tight limitations can biological samples be approximated to elastic half spaces. The Hertz model is still the most often used mode, despite continued improvement and advancements in modelling of the mechanical properties of biological samples[79,100]. What determines the properties of AFM tip, its advantages, and disadvantages, is its geometry. Among various geometries, the most common one is pyramidal and colloidal[84,85,95,98]. For the purpose of most of the research presented in this work, colloidal probes (CPs) were used. For AFM measurements described in Chapter 6.3additional tip geometries and contact models were exploited.

3.1.1. Colloidal probes

Colloidal probes, thanks to their large diameter (several microns) allow to reduce strain and stress and to indent a sample with a simple contact geometry (the contact area increases proportionally with indentation). Large contact area gives a higher signal to noise ratio[83,89]. Additionally, using colloidal probes in combination with stiffer cantilevers allows to obtain much higher indentation compared to pyramidal tips and also less strain and stress[95,106]. The mechanical properties of the sample can be obtained by applying Hertz spherical model on indentation data[106]. Although diameters up to 100 µm can be employed for certain purposes, the typical range for the diameter of the spherical bead is ~20 µm[95,106]. CPs can also be easily functionalized[26,107]. This advantage makes CPs perfect candidates for studying nanomechanical properties of biological samples, like cells, ECM and tissues[2,33,89–91,95,106,108–112]. The drawback of using colloidal tips is low lateral resolution[106,113] and a more pronounced bottom effect[89,98,114], which is typically an issue on thick samples, like spheroids.

3.1.2. Pyramidal and conical tips

The main advantage of pyramidal tips is that these tips can be sharp (with radii down to a few nm), thus providing high resolution in both topographic and mechanical maps[115]. These tips are commonly used for study mechanical properties of living cells at deep indentations (pyramidal) and for imaging deep and narrow features (conical). However, they can be a source of high strain and stress for the cells[113,115,116], which made many scientists questioning whether these tips are suitable for testing the mechanical properties of cells when high resolution is not a primary concern[108,112,114,117,118]. Additionally, pyramidal tips interact with nanometre-sized features and strongly modulate the contact area, making the mechanical readout more erratic[89,95].

The actual geometry of the pyramidal tip is a blunted pyramid, so it allows the Hertz model to be applied but only in case of small indentations (up to 500nm)[113]. Blunted pyramidal tip causes less damage and stress to the cells[113] . The geometry of this tip allows for small indentation which is sufficient for measurements on cells[90].

3.1.3. Cylindrical tip with a “flat punch” and a tipless cantilever

With a linear F-δ relationship and constant contact area, a cylindrical punch provides a constant and defined contact area during indentation[90]. This type of tip finds application in cell adhesion and study of nonlinear mechanical responses of cells[98]. Cylindrical tips are obtained by FIB method[90,116].

A tipless cantilever also presents a flat surface for contact with the sample (although titled with respect to it). The geometry of contact depends on the tilt angle (typically 10-15°) and cantilever width (typically 20-100 μm).

3.2. Custom Colloidal Probes

The force sensor, which consists of the cantilever, the tip and the photodetector, is the core of the AFM, and it is obvious that technical advancements have been made primarily to enhance the capabilities of this part[89]. Cantilevers come in a wide variety of shapes, materials, tip geometries, and sizes[62,83,85]. The force constant is the most crucial variable in biological studies. Utilizing very soft cantilevers allows to investigate living soft cells while stiffer cantilevers are more suitable for studying elastic properties of tissues. For the highest accuracy in mechanical measurements, the cantilever's force constant must also match the sample's stiffness. It is crucial to characterize cantilever spring constant k before each experiment in order to produce consistent and repeatable force readings[2,61].

The most important element of the AFM probe is tip, since its geometry determines the contact mechanics. For the studies on biological samples the most suitable are colloidal probes, when the half spatial resolution is not needed[79,83,89,100], however, large variety of biological studies and their differences recquire designing probes that will meet special needs of every sample and type of experiment[26,89,95,96]. Colloidal probes (CPs), which are produced by adding a spherical particle to a tipless (TL) cantilever, provide the following benefits for precise force measurements: in terms of geometry, the ideal interfacial system is a smooth spherical on a plane surface. Both the contact mechanics and the electrostatics of this system have analytical models that may be utilized for data fitting. Second, because of the wider contact area when utilizing colloidal probes, the signal-to-noise ratio is typically higher. It is highly helpful to examine weak interaction forces or the mechanics of materials over a wide range of contact area, averaging nanoscale inhomogeneities and local changes of the sample, in large CPs, where the radius R might be much bigger than 10µm. Large CPs enable for a more accurate comparison of AFM results to those from other indenters and, in theory, provide a link between macroscale and nanoscale mechanics[106,119,120]. Furthermore, functionalizing the spheres by grafting chemical groups onto them or by applying the right coatings makes it easier to control the chemical composition of the probe when using colloidal probes. Eventually, considerably lower pressures are often applied to the sample surface, assuming that working in fluid will keep tip-surface adhesion at a minimum. The lower lateral resolution of colloidal probes is their primary disadvantage[83,89,106]

Considering creation of colloidal probe, several issues have to be considered[89,106]:

- Contact radius (a) should be smaller compared to the radius of the sphere, which implies that the deformation of the sample is much smaller than the radius of the sphere.
- Contact radius and deformation are related by the equation (Hertz mechanics):

$$\delta = \frac{a^2}{R} \qquad \text{Eq. 7}$$

- Radius (R) of the sphere should be bigger than measured elements in the sample.
- R has to be smaller than thickness h of the sample (very important for measurements of thin sections), in particular, the following parameter should be (much) smaller than 1:

$$\chi = \frac{\sqrt{R \cdot \delta}}{h} \qquad \textit{Eq. 8}$$

A value closer to 0 indicates that the bottom effect is less significant; when this is not the case, corrections must be applied, which require the knowledge of the local thickness of the sample [89,98,121]. The finite-thickness effect does not depend only on the ratio of vertical lengths δ and h, but more on the ratio of the horizontal dimensions of the contact radius to the height[89].

For the purpose of research described in Chapter 4 and 5, large custom colloidal probes were prepared following protocol and guidance described in *Chighizola et al. 2021*[106] and *Indrieri et al 2011*[83].

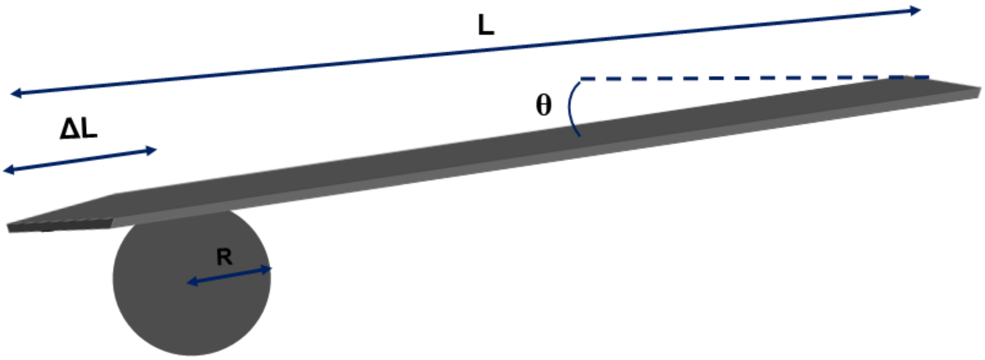

Figure 4*. Representative scheme of large colloidal probe. The sphere of a given mass and radius (R) is attach to cantilever with a length (L). The distance from the end of cantilever and point of attachment of the sphere is called loading point (ΔL).*

First step of characterization of colloidal probes was to obtain the intrinsic spring constant k_{TL} of the tipless (TL) cantilever, before the attachment of the sphere, by calibrating it by the thermal noise method[106,122]. k_{TL} is supposed to be equal to the intrinsic spring constant of the CP (k_{CP}) obtained upon attachment of a spherical bead to the tipless cantilever, the latter indeed is not influence by the added mass, as long as this is relatively small. If this is not the case, corrections are needed (see below). Three raw deflection vs. z-piezo displacement data were collected and averaged for the calibration of deflection sensitivity, in liquid, by ramping tip on a highly stiff surface (glass). The deflection sensitivity is derived as the inverse of the slope of the curves, if neither the tip nor the surface is deformed[99,106]. To create colloidal probes, soda-lime spheres with nominal radius of 30µm were used together with tipless cantilevers: ultrasoft (AppNano, USA) and force modulation (Nanosensors, Switzerland). The procedure described in *Indrieri et al. 2011* was followed. After the cantilever was mounted into the tip holder of AFM (Bioscope Catalyst, Bruker), the beads were captured using the AFM's XY motorized stage. An optical inverted microscope aided in finding and seizing the beads. Since there was large variety in sphere diameter regarding to nominal value, initial measurements of spheres radius were taken with optical microscope and ImageJ software.

Vaseline was used to secure the sphere to the TL cantilever, but in case of very large spheres, quick set epoxy adhesive (RC components, UK) was used (R>30µm), because very large CPs are too heavy to remain attached by adhesive capil~~a~~lary forces or even Vaseline (epoxy glue does not burn in the oven). After being moved into a high-temperature oven (PXZ series, Fuji Electrics) that was already at the desired temperature, the cantilevers with the connected beads were heated for two hours at a temperature of 700°C[83,106]. This temperature is just a little below the material's softening point, which is qualitatively described as the point at which a solid object starts to crumble under its own weight. The glass locally melted at the sphere-cantilever interface, generating a neck that is more or less stretched depending on curing time and temperature[106].

Once the CP was ready, the precise diameter 2R and ΔL were measured optically, using metallographic optical microscope equipped with calibrated 50x objective (AXIO, Zeiss).

The loading point -corrected spring constant of the colloidal probe (k_{CP}^{LP}) was calculated according to the equation: [99,106]

$$k_{CP}^{LP} \equiv k_{TL}^{LP} = \left(\frac{L}{L-\Delta L}\right)^{3} k_{TL} = \left(\frac{L}{L-\Delta L}\right)^{3} k_{CP} \qquad \textit{Eq. 9}$$

The intrinsic spring constant may need to be corrected by a factor accounting for the added mass, especially large, and dimension of the bead. The correction depends on nondimensional parameters like the reduced tip mass $\tilde{m}$ and tip radius $\tilde{r}$, normalized with respect to the cantilever mass and length, respectively[106,123].

The effective spring constant is used to convert the experimentally measured deflection into a force acting perpendicularly to the sample surface (and not to the cantilever, which is tilted); to this purpose a correction factor to the loading point corrected intrinsic spring constant of the CP is applied [106,122,124] :

$$k_{CP,eff}^{LP} = \left\{\left[1 - \frac{3R/L}{2(1-\Delta L/L)}\tan\theta\right]\cos^2(\theta)\right\}^{-1}\left(\frac{L}{L-\Delta L}\right)^3 k_{TL}$$

$$= \left\{\left[1 - \frac{3R/L}{2(1-\Delta L/L)}\tan\theta\right]\cos^2(\theta)\right\}^{-1} k_{CP}^{LP} \qquad Eq.\ 10$$

3.3. Data analysis

The data obtained during measurements were analysed in MATLAB environment using custom functions, which were written for analysis of nanoindentation data. All force curves from a single force volume were analysed together following the general procedure described in Chapter 3.1. The median values of Young's modulus of each force volume (FV) were extracted via linear regression of linearized curves on the selected indentation range. The contact part of linearized force curves was fitted by the Hertzian model. The fit is applied to the selected region of the contact part. In these experiments selected indentation range was from 10%-20% to 80%-90%.

4. Study of the impact of sample preparation procedures on the mechanical properties of tissues

4.1. Influence of freezing on nanomechanical properties of tissue specimens

4.1.2 Introduction

Preparation of tissue samples for experiments play a crucial role in the whole process of research, equally important as executing experiments and doing data analysis. Properly prepared samples will allow to perform many experiments without troubles and to obtain reliable data not burdened with errors and uncertainties. Moreover, standardized sample preparation procedures are mandatory to obtain comparable results in different laboratories, following standardized measurement and data analysis procedures.

Sample freezing is commonly used technique for shipment, storage and for some experimental protocols (including for AFM; freezing can preserve tissue functionality [10,125–129]. Performing studies on freshly collected biopsies has its advantages but it is also complicated since measurements must be performed within few hours after surgical resection[10]. Since freezing might affect tissue nanomechanical and chemicophysical properties, it requires proper optimization of the protocol. The challenge is to find a freezing technique that will allow to preserve structural and molecular properties of tissues and cells[126]. Freezing of the tissue requires presence of cryoprotectant, rapid freezing and low temperature (as low as possible)[130]. Slow rate freezing of biological samples allows the water molecules to line up during transition, which causes intracellular ice crystal formation, also during low rate freezing cells suffer from dehydratation[131,132]; this can cause distortion of tissue. Snap freezing slows the actions of proteases and nucleases to inhibit degradation of molecules (e.g., RNA, proteins) and allows water to remain in vitreous form (amorphous) and this form do not expand upon solidification [125,133]. However, vitreous ice requires very low temperature to avoid restructure, that is why proper storage of the sample is also very important. Amorphous ice restructure as cubic ice and expands above -121°C, in higher temperature, -80°C cubic ice becomes hexagonal ice and expands even more. Along with the temperature, rate of freezing plays crucial role. Rapid freezing is a function of the amount of specimen surface in contact with the cold source, the volume of water within the specimen, the starting temperature of the water (specimen), and how cold the source is[125].

The aim of this study was to verify if one cycle of freezing, which is very common in many biological experiments can affect mechanical properties of tissue and to understand how different freezing procedures affect the nanomechanical properties of fresh biological specimens. This series of experiments will highlight the main issues related to handling tissue biopsies in the context of AFM measurements and storage. To the purpose, samples of bladder tissue were studied with AFM in indentation mode to compare changes in mechanical properties of bladder before and after freezing. For this evaluation, three strategies of freezing of biological samples were selected, based on current knowledge of their advantages, disadvantages already presented in literature.

4.1.3. Current methods for freezing biological samples

4.1.3.1. Snap freezing in liquid nitrogen

Liquid nitrogen is one of the coldest liquids, providing temperature of -196°C that is able to freeze the sample in few seconds [134]. The drawback of using liquid nitrogen is the fact that it boils in contact with warmer objects because of low specific heat constant. As a result, it forms a vapor barrier (consisting of nitrogen gas layers), which works as an insulator and slows the rate of freezing in unpredictable fashion.

As a consequence, the outer layer of tissue is quick frozen and vitreous, meanwhile inner part freezes slower. It happens especially in case of large samples and might cause cracking of the tissue because of crystal formation inside the tissue[125,133].

4.1.3.2. Cool bath with dry ice and ethanol

This is another technique in which sample is rapidly frozen using a dry ice/alcohol slurry. This is a standard and commonly used procedure for preparing tissue samples for cryosections and it provides temperature around -72°C [134]. However, this procedure provides slower freezing rate comparing to other procedures (e.g., isopentane or liquid nitrogen). Another drawback of this technique is that contact with this cold source is non-uniform and it doesn’t provide even freezing [135].

4.1.3.3. Liquid nitrogen bath in isopentane

Isopentane has a high thermal conductivity and does not form vapor halo on specimen tissue. If the tissue sample has size around cubic centimetre in volume, the water inside will freeze all in the vitreous form. Isopentane chilled with dry ice will reach only a temperature of -78.5°C but with liquid nitrogen -160°C [133,134]. Such low temperature will freeze tissues more effectively and evenly compared to direct snap freezing in liquid nitrogen. It is important to fully immerse the sample in the liquid to maximize surface contact [125,133]. Snap freezing in isopentane is a promising technique since results from experiments on muscle biopsy indicate that values of Young’s modulus (YM) were nearly identical to values from freshly measured muscles [136].

4.1.4. Cryoprotectants

The main reason of cell and tissue injury during freezing is the purification of water during freezing process because water freezes as a pure substance. There are two mechanisms of damages. The first one is distortion of cell shape by ice crystals and the second mechanical damage is a result of chemical and osmotic effects of solutes in the residual unfrozen water between ice crystals. Cryoprotection is a process where water molecules are replaced with cryoprotectant molecules (molecules that cannot freeze). Cryoprotective agents (CPAs, cryoprotectants) can lower the melting point of water, prevent intra-cellular water loss, do not precipitate, or form eutectics or hydrates, and should not be toxic to biological samples [128,137]. Additionally, CPAs modify intracellular composition and prevent ice crystal formation because they interfere with hydrogen bonding between water molecules (it can be also a reason of non-specific toxicity)[128]. However, the highest cryoprotectant concentration that the tissue will tolerate prior to preservation is limited, and the concentration will increase during freezing as ice separates[138]. Comparing to cells, organized tissue is more vulnerable to freezing injury[139]

4.1.5. Structure of bladder

Urinary bladder is an organ whose main function is storage and excretion of urine; n elastic bladder is required for holding sufficient amounts of urine at low

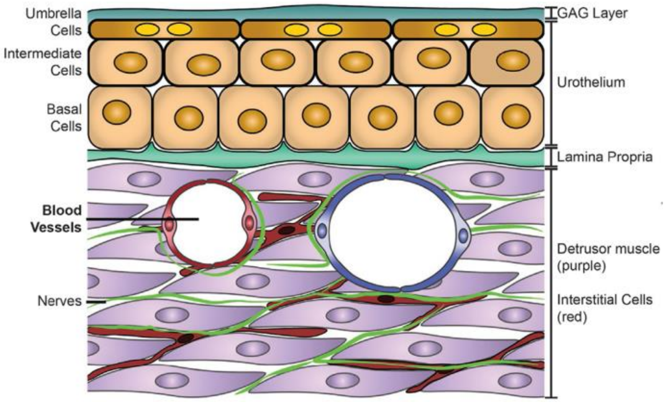

***Figure 5**. Section of bladder wall. Adapted from: Excitability and contractility in arterioles and venules from the urinary bladder, Tykocki N., Monson F., Academic press Inc., (2020), 301-326.*

pressures[140,141]. The wall of the mice bladder has thickness of 400µm (empty) to 200µm (filled)[140]. It is composed of several layers, starting from urothelium covered with glycosaminoglycan (GAG) layer. This part is facing lumen of the bladder. Later there is lamina propria (also called basement membrane) and detrusor smooth muscle layer (Fig. 5)[140,142]. Based membrane is mostly ECM composed of collagen IV or laminins[143]. The umbrella cells are interconnected to other cells through tight junctions and together with intermediate and basal cells form syncytium which is a barrier between urine and bladder[140,142]. As a matter of mechanical properties, bladder is a diverse heterogenous organ with a range from few to hundreds of kPa[141,143,144].

4.1.3. Materials and methods

4.1.3.1. Sample preparation and AFM measurements

For each experiment, healthy rats were sacrificed at Ospedale San Raffaele (OSR) with the use of carbonic anhydride[1]. The bladder was isolated from the body and cut into 4 pieces, from which only 2 were taken for the measurements. Each piece was fixed on the petri dish with two component epoxy glue (Fig. 6). The tissue was attached with inner part of bladder - urothelium facing up. After glue dried, PBS was added to every petri dish, they were closed and sealed with parafilm. Already prepared samples were transported to UNIMI in a cooling box and then stored in +4°C Before proceeding with AFM measurements, PBS in petri dish was changed to a fresh one.

---

[1] The studies on rats were approved by the Institutional Animal Care and Use Committee of San Raffaele Scientific Institute, and performed according to the prescribed guidelines (IACUC, approval number 942).

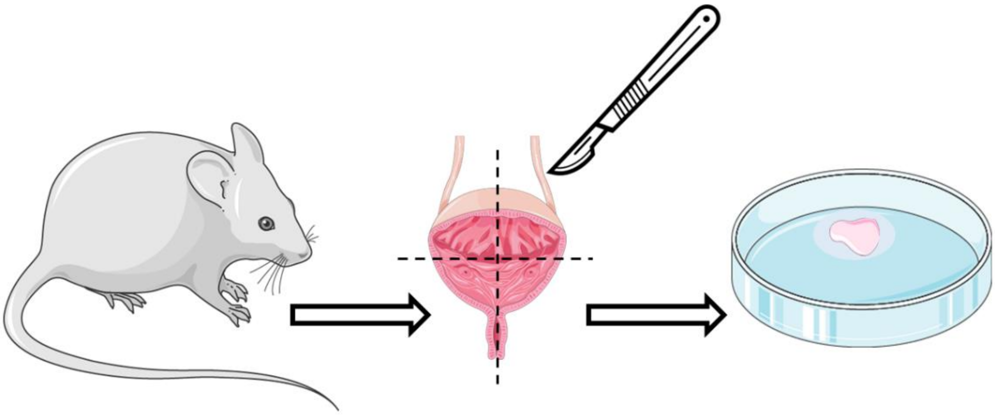

***Figure 6**. Steps of sample preparation for AFM measurements. The bladder obtained from rat was cut into 4 pieces. Fragments selected for measurements were fixed with the glue on the petri dish.* [*Parts of the Figure were drawn by using pictures from Servier Medical Art. Servier Medical Art by Servier is licensed under a Creative Commons Attribution 3.0 Unported License (https://creativecommons.org/licenses/by/3.0/)].*

AFM indentation experiments were performed according to the general procedures described in Chapter 3.1 with the use of soft custom colloidal probes (Chapter 3.2). The spring constant of AFM probes ranged from 0.23 N/m – 0.64N/m and the spheres had radius ~35µm. The contact radius for these probes was around 15µm. Applied force ranged between 30nN to 90nN effecting in indentation of ~ 2µm to 11µm.

Measurements on fresh tissue were done in several different, randomly chosen locations. The thickness of the sample did not allow for transparency, necessary to see the surface of the sample. Each region of interest (ROI) had size of 50 µm x 50µm with rows and columns space 5µm. Typically, a force volume (FV) of up to 100 FCs. After the measurements, PBS was removed from the petri dish and the tissue was gently dried with a small piece of paper towel. Next, optimal cutting temperature compound (O.C.T.) was added to petri dish in the amount that allowed to fully cover the tissue sample. The dish was closed and sealed with parafilm. The Petri dishes with samples were frozen according to one of the protocols studied in this research. One-week later, samples were thawed by putting them in room temperature (~ 22°C) for 30-60 min. After that time O.C.T. was removed with 1ml automatic pipette (the end of the tip was cut out to make it easier to remove viscous cryoprotectant). Remaining of O.C.T. was removed by washing tissue with PBS; petri dish with 1ml of solution was gently shake, later solution was replaced with fresh one. Washing was repeated 4 times. Measurements on thawed tissues were performed the same way as on fresh tissues.

4.1.3.1.1. Snap freezing in liquid nitrogen

Petri dishes closed with the use of parafilm were dipped into container with liquid nitrogen (sample was held with forceps). After around 30s. Petri dishes were removed from liquid nitrogen and stored for 1 week in freezer at -20°C.

4.1.3.1.2 Freezing with dry ice and ethanol

Petri dishes with samples were placed in the styrofoam box with dry ice inside. Ethanol was gently poured on dry ice, not too close to the samples, and the box was closed (~ 3 min). After that time frozen samples were stored in freezer at -80°C.

4.1.3.1.3 Freezing in liquid nitrogen bath

Petri dishes with samples covered with OCT were closed with the use of tape (parafilm crumbles in low temperatures). A styrofoam box was filled with liquid nitrogen and the Pyrex glass beaker filled with isopentane (5cm height, filled by $^1/_3$ or $^1/_2$ with isopentane) was put into the liquid nitrogen. The styrofoam box was closed for c.a. 10 minutes, after this time isopentane was slowly freezing on the sides of the flask. The samples were placed into the isopentane for 15 minutes. After samples freezed, they were stored in -80°C freezer for one week [145].

4.1.4. Results

4.1.4.1. Snap freezing with liquid nitrogen

Seven force volumes were collected from 2 pieces of fresh bladder tissue. The median values ranged from 204 Pa to 516 Pa (Fig. 7A). The typical maximum indentation was from 5,1 µm to 9,3 µm while the maximum applied force was constant for all measurements – 30nN.

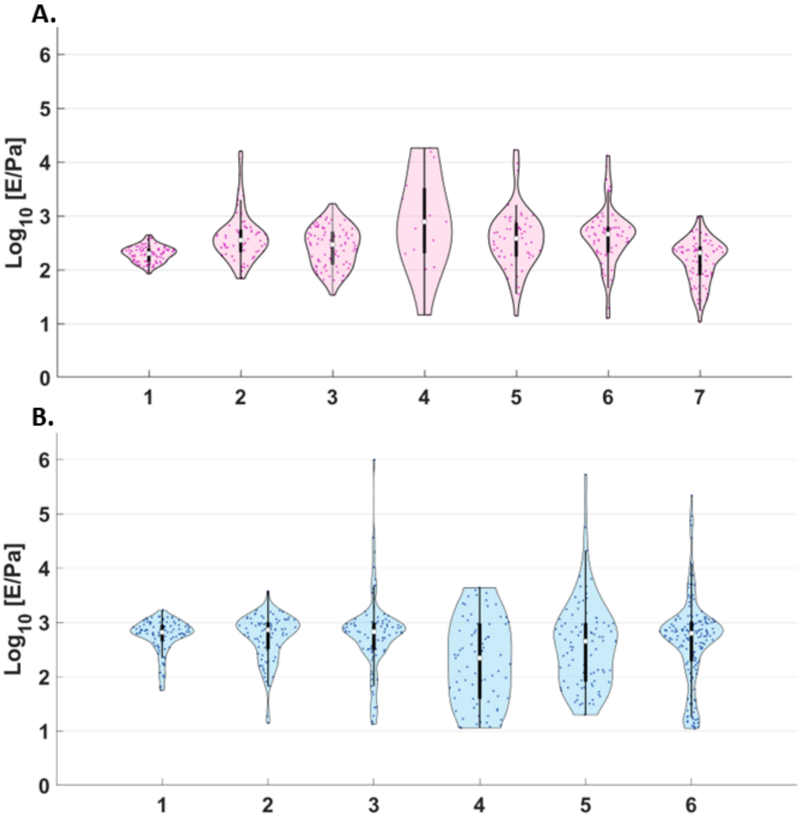

Figure 7. *Graphs presenting YM distribution and median logarithmic values of YM of fresh(A) and frozen/thawed (B) tissue measured on different areas of the bladder tissue. Each violin plot was plotted from single force volume, each point represents single force curve. The white point shows median value, thick black lines are upper and lower quartile*[146]

After 7 days, the samples were thawed, and 6 force volumes were collected. The range of measured values was wider comparing to fresh tissue: 263Pa to 854Pa (Fig.7B). Wider distribution of YM was not only between measured force volumes but also within single measurements – force volumes number 3, 5 and 6 of fresh/thawed sample (Fig.7B). After thawing the YM distribution of tissue become more heterogenous. The average indentation ranged from 2,4µm to 8,3µm with applied force of 30nN.

4.1.4.2. Freezing with dry ice and ethanol

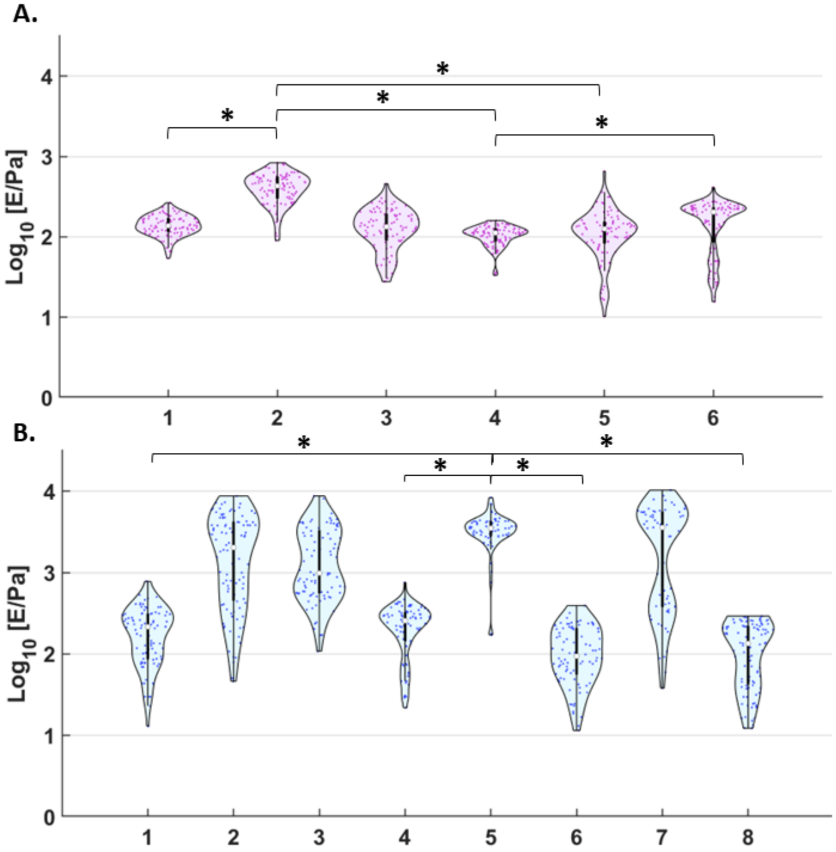

***Figure 8**. Graphs presenting YM distribution and median logarithmic values of YM of fresh(A) and frozen/thawed (B) tissue measured on different areas of the bladder tissue. Each violin plot was plotted from single force volume, each point represents single force curve. The white point shows median value, thick black lines are upper and lower quartile[146]. Asterisk means significance $p<0.05$*

Measurements from 1- 6 were done on 2 pieces of tissue. The median of Young's modulus of the fresh tissue ranged from 115Pa to 450Pa (Fig. 8A); the small differences in this value indicate that stiffness of bladder tissue is homogenous. On the contrary, stiffness distribution in thawed tissue was increased, both within single measured area and between single measurements. The values ranged from 96Pa to 1367Pa (Fig. 8B). As a matter of indentation, the average values were similar for fresh (9,8µm) and thawed (7,4 µm) bladder tissue.

4.1.4.3. Freezing in isopentane in liquid nitrogen bath

Based on previous experiments, some changes were applied during measurements. To make data analysis more efficient it was easier to collect more force volumes but on smaller areas.

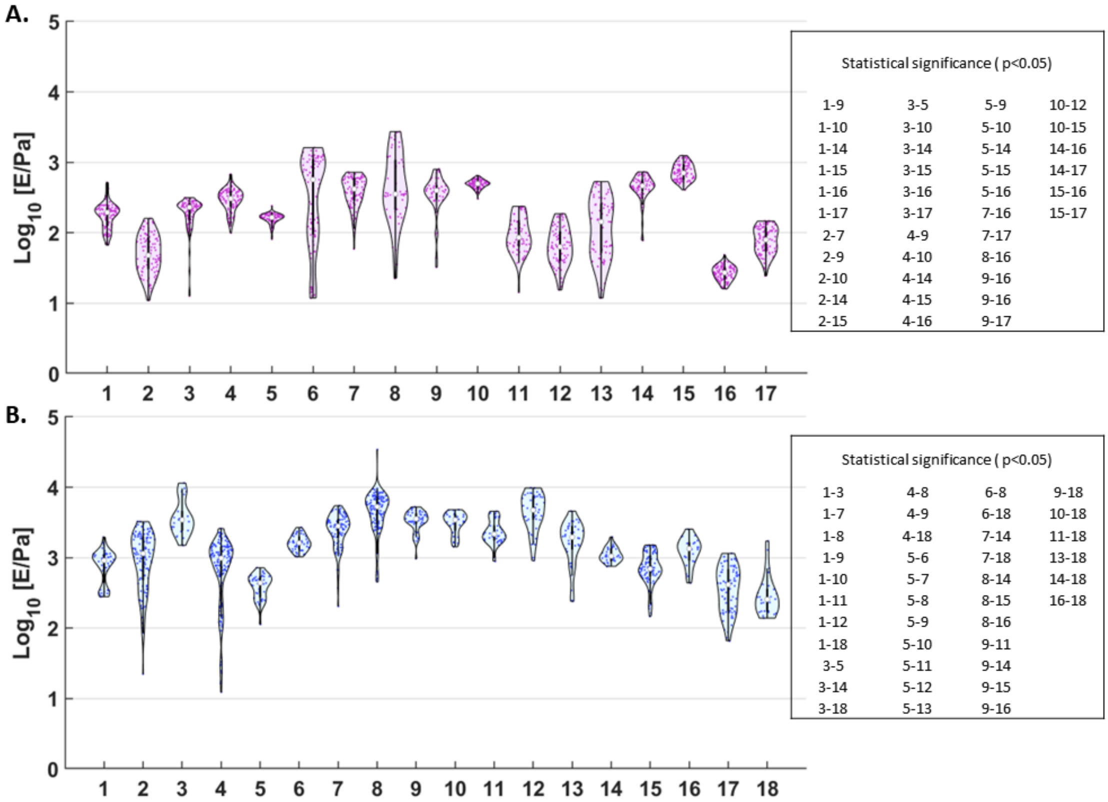

Statistical significance ($p<0.05$)

1-9
1-10
1-14
1-15
1-16
1-17
2-7
2-9
2-10
2-14
2-15
3-5
3-10
3-14
3-15
3-16
3-17
4-9
4-10
4-14
4-15
4-16
5-9
5-10
5-14
5-15
5-16
7-16
7-17
8-16
9-16
9-16
9-17
10-12
10-15
14-16
14-17
15-16
15-17

Statistical significance ($p<0.05$)

1-3
1-7
1-8
1-9
1-10
1-11
1-12
1-18
3-5
3-14
3-18
4-8
4-9
4-18
5-6
5-7
5-8
5-9
5-10
5-11
5-12
5-13
6-8
6-18
7-14
7-18
8-14
8-15
8-16
9-11
9-14
9-15
9-16
9-18
10-18
11-18
13-18
14-18
16-18

Figure 9*. Graphs presenting YM distribution and median logarithmic values of YM of fresh(A) and frozen/thawed (B) tissue measured on different areas of the bladder tissue. Each violin plot was plotted from single force volume, each point represents single force curve. The white point shows median value, thick black lines are upper and lower quartile*[146].

Results from 1-8 are from one piece and 9-17are from second piece. The stiffness of bladder ranged from 53,5Pa to 513,9Pa. In case of some measurements, distribution of YM values have wide range (6,8,13) and for others YM values range is very narrow (5, 10, 16) (Fig.9). The results from measurements on thawed tissue are more uniform comparing to the one made on fresh tissue. The median values vary from

139,5 Pa to 5649,4 Pa. Also, there was a huge difference between median indentations: 8,2µm for fresh tissue and 3,6µm after thawing.

4.1.4.4. Comparison between techniques

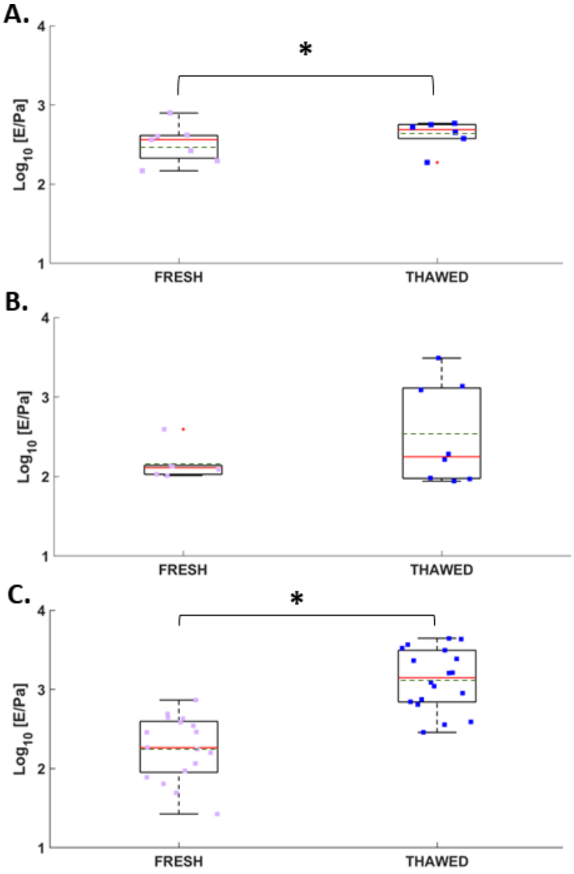

__Figure. 10__ Graphs presenting comparison of YM values between fresh and thawed bladder tissue frozen using different methods: snap freezing in liquid nitrogen (A); freezing with dry ice and ethanol (B); freezing in isopentane in liquid nitrogen bath (C). Red line shows median value and green dotted line – mean. Each square (pink and blue) stands for median value of single force volume. Error bars stands for standard deviation of the mean and asterisk means significance ($p<0.05$)

The aim of the experiments was to see how different techniques of freezing affects nanomechanical properties of tissue, using rat's bladder as an example, and which method is the best to preserve them. Figure 10 shows statistically significant differences between fresh and thawed tissue was observed for the method of snap freezing with LN_2 (Fig. 10A) and isopentane in LN_2 bath (Fig. 10C).

In case of snap freezing, the difference was statistically significant, however graph shows strong overlapping in median values of single force volumes. The mean value of fresh tissue was 318,4Pa while thawed one was twice stiffer: 662Pa. After freezing in vapours of ethanol the differences were not significant but on the other hand after thawing the tissue was much more heterogenous with 3 much stiffer zones (Fig. 10B). The biggest difference in YM values was observed on sample which was frozen using isopentane bath in liquid nitrogen. After thawing the mean value increased from 279,6Pa to 2112,6Pa (Fig. 10C).

4.1.5. Discussion

With AFM it is possible to study nanomechanical properties of biological samples, including tissues, nevertheless biopsy samples might need proper preparation. Freezing tissue specimens (i.e. cryosections) not only enables studying them with AFM setup but also allows to store them and facilitate the whole process of measurements in long term perspective. To find out whether freezing affects nanomechanical properties of tissue, rat bladder specimens were studied by AFM in indentation mode before and after freezing using three commonly used techniques of freezing.

Snap freezing is a very easy and fast method to freeze samples, however it carries the risk of micromechanical and macro-mechanical damages[125,133]. After thawing, bladder specimens were well preserved, as they yielded YM distribution that were close to those obtained from freshly measured tissue (Fig. 10A and 7). Similar AFM studies on human muscle also revealed that this method didn’t change nanomechanical properties of tissue[136]. In the studies on bronchoscopy samples described in *Zemła et al. 2018*, this method was also applied to freeze biological specimens, however with the use of another cryoprotectant – DMSO (dimethyl sulfoxide)[10]. The samples were studied by low-indentation AFM and most of the results reveal no significand differences between YM of fresh and thawed tissue samples[10]. Another commonly used technique is freezing by using dry ice and ethanol. No significant difference in resistance to indentation was observed (Fig. 10B), yet after thawing the heterogeneity of YM values increased (Fig. 8B). It might be due to the fact that this method doesn't provide even and quick freezing[135].

Another source of difference might be coming from mechanical damages that occur during sample preparation for AFM measurements. The measurements were done on bladder tissue pieces attached to the Petri dish with the urothelium facing up; this means that the load was applied on the urothelial cell rich layer with thickness typically below 10µm). We argue that the presented results refer mostly to the rigidity of cells (especially in the fresh tissue). Due to freezing process some cells die and detach (mostly during thawing and washing the tissue), which means that second measurements were done on cell depleted tissue, mostly on the basal lamina, which separates urothelium from the muscle layer. The basal lamina is mostly composed of ECM[143]; very likely, the rigidity of the ECM is higher than that of the cells which suggests that increase YM observed in thawed tissue comes from measurements of basal lamina and not urothelial layer, as it was in case of fresh tissue (Fig. 8 and 10B). The same explanation can be applied to the results of freezing in isopentane bath, where there was significant difference between mean stiffness of fresh and thawed bladder specimen (Fig. 10C and 9). In the work of *Van Zwieten et al., 2014* it was reported that the method of freezing in isopentane cool bath sufficiently preserved nanomechanical properties of tissue specimens [136]. However, in case of that studies different cryoprotectant were used – DMSO. 10% solution of DMSO in culture medium is a freezing solution commonly used especially for freezing cells while OCT is denser and more viscous, which makes it more difficult to wash it away. An attempt to clean bladder tissue from OCT probably caused detachment of cells in urothelial layer, thus measurements on thawed specimen were possibly done mostly on basal lamina.

Further experiments on three freezing techniques with use of DMSO as cryoprotectant could verify how different cryoprotectants affect measurements and obtained results. Unfortunately, there are more aspects of the experiments that hinder the clear interpretation of data and make comparison fresh vs. thawed less reliable. Since the size of the sample is very big, it is not possible to precisely select the region of measurements. In case when measurements were done on the edges of the sample, the presence of epoxy glue could affect the measurements what results in higher values of the stiffness.

A big improvement would be to perform measurements on tissue sections. It will allow to do measurements on different layers of the tissue and to have a control on chosen area for measurements before and after freezing (it will be possible to compare the same/close areas of the samples). Additionally, sectioning allows to prepare samples of chosen thickness, thus thin enough to have sufficient transparency to control locations of each measurement (what was not possible with big pieces of tissue, used in these experiments). Another improvement could be achieved by increasing number of measurements and collected FCs on single specimen, especially in case of first two techniques.

4.2. Preparation of fresh tissue samples for AFM measurements

4.2.1. Introduction

Based on the results and conclusions from the previous chapter, we studied whether it is possible to improve sample preparation process and help obtaining better data. Since most of the issues came from the peculiar layered and empty structure of the rat bladder, using tissue from different organs. To develop new protocol for sample preparation for AFM measurements, biopsies of human peritoneum were used[2]. For

---

[2] The study was approved by the Institutional review board (134/13; I249/19) and was conducted in following the Declaration of Helsinki, 2009. Written informed consent was acquired.

the purpose of these preliminary experiments and optimization of the protocol, I used the tissues samples that were already stored frozen. For further verification of freezing process, fresh tissue specimens (taken for analysis right after surgery) can be used. The samples were provided by research group of Manuela Gariboldi from Department of Experimental Oncology and Molecular Medicine of Istituto Nazionale dei Tumori (INT).

At this moment there are not many studies about how exactly freezing affects nanomechanical properties of tissues, although some works (including this) reveal that the impact of freezing is not very important [10,136]. Nevertheless, it would be beneficial to avoid this process; indeed, studies on fresh tissue samples would be more reliable since the measurement conditions are closer to the one *in vivo*. Vibratome sectioning is a common method used to obtain slices from different organs, like liver, kidney, lung, and brain. The thickness of the sample can be below 100 µm (in case of fixed tissues) or more than 100µm for fresh tissues[147]. Using this type of samples has its advantages for AFM studies, since the sample has proper size for nanoscale measurements and enables measurements in aqueous environment[10]. Challenging, yet crucial step is to fix specimen on sample holder surface (e.g. glass slide, Petri dish). For most of the studies, tissues are studied in form of cryosections. Often, tissue samples are evaluated as cryosectioned tissue strips, which can be immobilized by putting the positively charged glass slides[33]. Among substances used for immobilizing tissue can be listed histoacryl, ethyl cyanoacryle, or Cell-tak™ which are effective adhesives[10,148]. On the other hand, these substances can diffuse to the surrounding environment or even to tissue and, therefore, affect its nanomechanical properties, especially in the region of contact between tissue and the adhesive[148]. Poly-L-lysine (PLL) is a mild adhesive, thus limited only for application on cells and thin tissue sections[33,148] Additional improvement of attachment can be achieved by combining PLL coating with glutaraldehyde. Between glutaraldehyde and PLL is covalent binding and glutaraldehyde provides additional aldehyde group for binding[149].

The procedure of obtaining slices with vibratome can be difficult with soft tissues, especially if they are not fixed. It is common practice to fix the biological samples for example with glutaraldehyde or paraformaldehyde, yet it can affect nanomechanical properties of biological specimens, thus tissue sample deviates from *in vivo* conditions[148,150]. Another alternative is to make cryosections which provides slices with thickness of 5 µm -10µm, but since the effects of freezing on nanomechanical properties of tissues is not clear it is better to avoid this technique; additionally freezing decreases viability of cells, while vibratome preserves cell viability[148,151] As an effect, studies on such prepared samples are less reliable, especially regarding interaction between cells and ECM[151]. In the slices of some samples can be visible corrugations and vibratome lines, what affects sample roughness. This parameter is crucial for AFM measurements, and it can be simply solved by using good quality blades.

The main objective of this research is to create a protocol with the use of vibratome, that allows to obtain sample suitable for AFM measurements, what requires steps that will not affect mechanical properties of specimen. In this case the goal is to avoid freezing and usage of fixatives. Second aim is to obtain tissue sample of small size and firmly attached to glass slide.

4.2.2. Materials and methods

4.2.2.1. Developing protocol – use of the vibratome

To meet the needs of measuring fresh tissue sample, the following protocol has been developed. Due to difficulties coming from handling bladder tissue samples, described below protocol was developed using neoplastic tissue of peritoneum. The choice of peritoneal tissue for this research was based on its advantages: peritoneal biopsies are bigger what makes them easier to embed in agarose and immobilize. The main drawback of using bladder is the fact that this organ is empty inside which requires to fill it with agarose and avoid air bubbles (their presence impede immersion in agarose).

First step is to prepare 4% low-melting point agarose (LMPA) in PBS[151]. It melts at 65,5°C and remains liquid at 37°C. This property od LMPA excludes the risk of damaging tissue specimen with higher temperature that could cause collagen disorganisation, protein inactivation and denaturation[152,153]. The concentration of agarose (normal or low-melting point) used for vibratome slicing is between 2-4%, in some cases even 6%, however it is worth to keep in mind that that with the concentration, rigidity also increases. In case of 2% agarose, it is more adhering to the tissue. Control the temperature of LMPA; once it is between 25°C-37°C pour it into cryomold (volume ~15ml) (Fig. 11) and the tissue specimen can be placed inside, close to the bottom. It is important that the specimen is not wet by PBS or medium because wet samples tend to curl inside the agarose block.

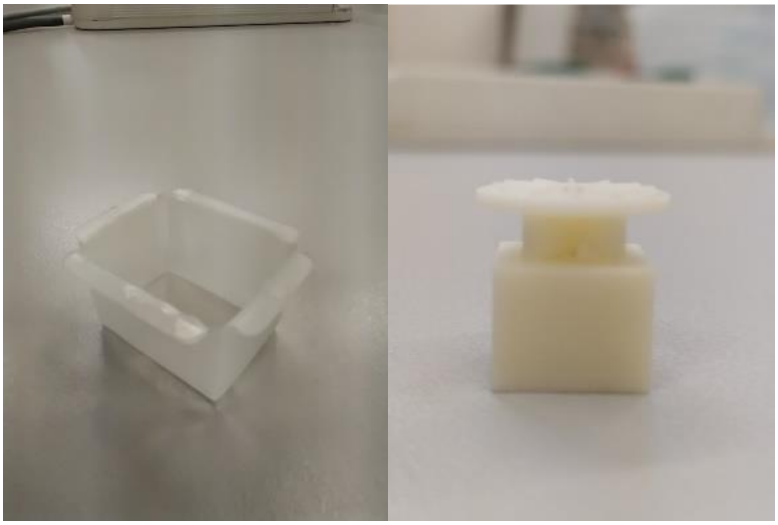

***Figure 11**. Cryomold (left) and sample holder (right)*

For the purpose of this research, special sample holder was designed, and 3D printed in collaboration with Federico Pezzota of Officina Meccanica (Department of Physics, Università degli Studi di Milano). When the LMPA is partially solid, vibratome sample holder can be placed a little bit inside the agarose (deep enough to dip the disc and the neck of the holder). The agarose block with sample holder can be removed from cryomold once the LMPA is solid. It is possible to cut off sides of the cube to make the block smaller thus more stable inside the vibratome. The sample holder can be placed inside vibratome [Vibratome Series 1500, St. Louis, USA] which is filled with cold PBS (4°C) (Figure 12)[151]. The vibratome was kindly borrowed from Prof. M. Mazzanti (Department of Bioscience, Università degli Studi di Milano). To keep the temperature low over time it is possible to put ice cubes into the water.

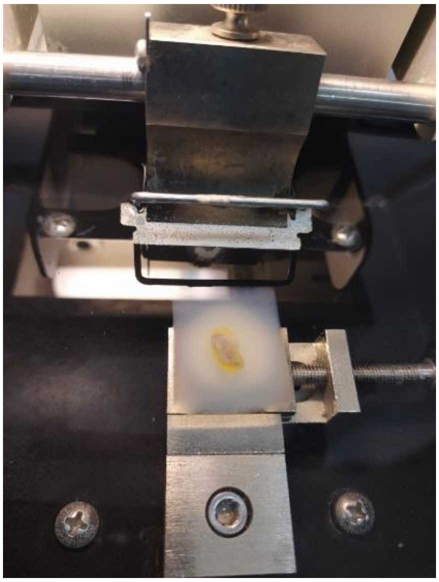

Figure 12. *Sample prepared for cutting.*

The samples were cut with parameters, optimized during preliminary trials: speed 1 (range 1-10) and amplitude 9 (range 1-10). These parameters allowed to obtain tissue slices with minimum thickness of 200µm. based on previous preliminary experiments the thickness of 200 µm was chosen as a most suitable for nanoindentation measurements. Such thickness allowed for sufficient transparency to controllably choose the position to collect force volume and avoid influence of bottom effect on collected FCs[98,114]. With the use of brush, the slice can be picked up gently from vibratome and placed on glass slide; LMPA surrounding sample can be gently removed using brush. An alternative is to wash tissue specimens in warm (37°C) PBS to remove residual LMPA[154]. The tissue slice can be placed on glass slide previously functionalized with poly-L-lysine [Sigma Aldrich] and 5%

glutaraldehyde [Sigma Aldrich][149] or glass slide covered with thin layer of two component epoxy glue. Crucial for measuring biological samples with AFM is to make sure that they are firmly attached to sample support, it this case: glass slide[75].

4.2.2.2. AFM measurements

The measurements on tissue slices were performed in aqueous (PBS) environment. The tissue slice with the droplet of PBS were concealed within hydrophobic ring (drawn with hydrophobic pen [Daido Sangyo Co., Ltd. Japan]). The main purpose was to see whether the slices stay attached and if the surface of the slice isn't too rough to perform set of nanoindentation measurements. A large colloidal probe (R=35,4nm) with invOLS=24.17nm/V was used. The maximum applied force was 2,9nN, aiming at indentation around 5µm. Two force volumes were obtained on each slice of both experimental classes.

4.2.3. Results and discussion

Attaching tissue slice to glass slide with glue was very fast and easy and allowed to keep tissue specimen attached during measurements. However, the glue gets stiffer once its dries and because it gets in contact and partially impregnate the tissue; it might also affect the samples rigidity upon drying in the area nearby. In that case the area of measurements will be limited to the middle part of the tissue.

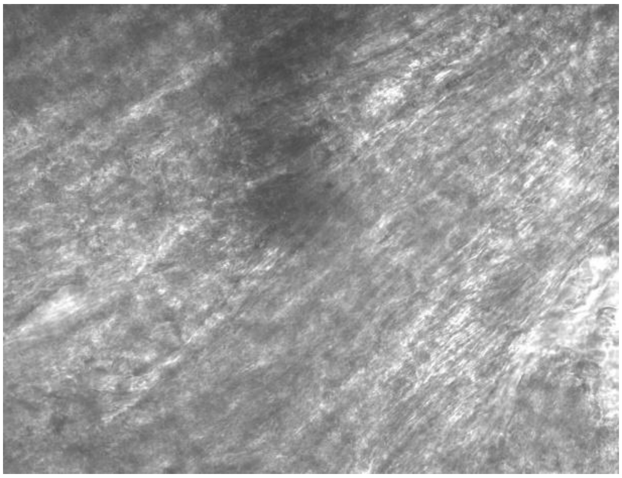

***Figure 13**. Image of 200 µm tissue slice under the AFM microscope (magnification 20x). The transparency of tissue was good enough to see its surface and the shade of the cantilever. However, it required increased brightness of the light. I case of longer measurements it will cause the problem of heating up the liquid (PBS with protease inhibitor).*

Coating glass slide with PLL and glutaraldehyde was also successful way to attach tissue slices. Slices of neoplastic peritoneum stayed attached for long time, even after adding droplet of PBS. The tissue was transparent enough to see the surface, however the tip was poorly visible (Fig. 13), nevertheless it was sufficient to have control over area selected for measurements It was possible to gently remove the tissue slice from the glass slide so it will be possible to store for future analysis. This is a great advantage over using two component epoxy glue since the sample cannot be removed from glass slide. Regarding AFM nanoindentation measurements, both techniques provided reliable results as a matter of obtained YM values and indentation range (Fig. 14). The mean indentation in glue attached tissue was 4,3µm and 4,7µm in case of tissue attached with PLL+glutaraldehyde. Lack of relatively higher YM in glued tissue indicates that this method of attachment does not change stiffness of the sample. Nevertheless, the measurements were performed on inner part of section, where the contact with the glue was limited compared to edges of tissue specimen.

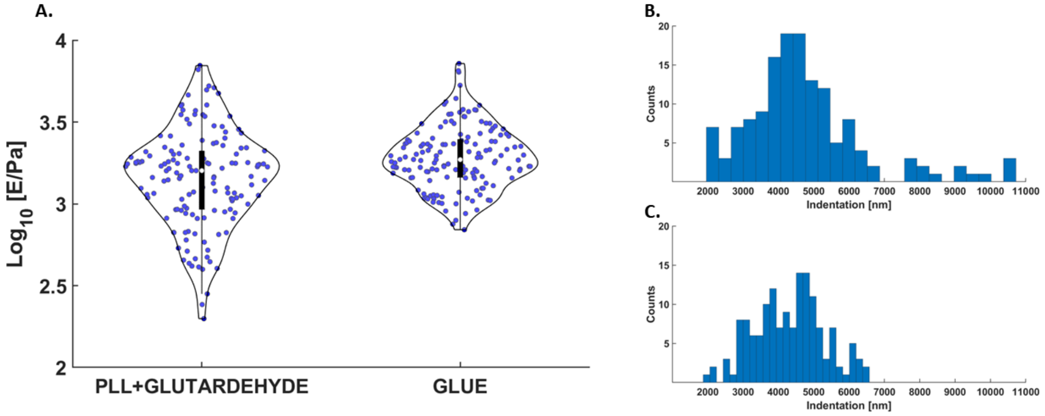

***Figure 14**. Verification on how different techniques of attachment to substrate affect AFM nanoindentation measurements of fresh tissue specimen. Comparison of the distributions of YM values between the samples of peritoneum attached to the glass slide with PLL and 5% glutaraldehyde coating and with two component epoxy glue (A). On the left histograms showing indentation distribution of samples attached to the glass slide with PLL and 5% glutaraldehyde coating (B) and with two component epoxy glue (C). On violinplots, the white point shows median value (median of all FCs collected per sample), blue dot stands for YM value of single FC, black thick lines are upper and lower quartile*[146]

4.3. Conclusions

AFM provides a great opportunity to study various biological samples [2,3,61,148,150]. Increased interest in studies of mechanobiology requires proper sample handling and preparation to make AFM more efficient and reliable. There are several studies on how freezing affects biological and nanomechanical properties of tissues, yet the answer is still unclear[10,136,148].

Presented studies revealed how freezing affects tissue specimen not only at microscale but also in macroscale. The obtained results do not unambiguously reveal which technique of freezing enables to better preserve nanomechanical properties. However, the results show that the mechanical properties of fresh and thawed samples are not markedly different, which is good since clinically relevant samples are typically frozen and frozen samples can also be transferred and exchange easily among labs. Moreover, the fact that frozen-thawed samples maintain their mechanical properties suggests that they can be used for sure in comparative studies without real loss of information. In addition, this study provides an insight into complexity of studying fresh tissue samples under AFM and freezing process. Uncertainties in the measurements originate to a great extent from quality of sample preparation.

To facilitate the AFM indentation measurements on fresh tissue samples the technique of vibratome has been explored as a great advantage over cryosectioning[151]. This technique allowed to obtain samples of peritoneum tissue assessable for AFM nanoindentation measurements. The great advantage of developed method is the elimination of factors, like freezing (including use of toxic cryoprotectants) or fixation, that affected reliability of AFM measurements and could alter properties of tissue compared to *in vivo* conditions, especially nanomechanical properties. With better quality samples and more controlled AFM measurements it is possible to continue mechanobiology research on tissue specimens and provide clear answer how freezing affects nanomechanical properties of tissue.

5. Study of the mutual influence between ECM and cells during cancer progression in peritoneal metastases

5.1. Introduction

The peritoneum is a serous membrane that covers intraabdominal organs and mesenteries in the human body. It is consisted of a monolayer of mesothelial cells supported by a basement membrane that is located on a connective tissue layer[19,155,156]. This membrane has many functions, mainly structural and protective functions for the contents of the abdominal cavity. It also plays a significant role in the transport of fluids and cells. Unfortunately, it might lead to the metastatic spread from colon cancer[17,19,157]. One of the biggest issues with cancer therapy is cancer metastasis. It is anticipated that a better understanding of metastatic pathways will offer crucial information to prevent metastasis[25].

Peritoneal metastasis (PM) affects about one out of every four patients with colorectal cancer (CRC)[18]. PM is linked to a poor prognosis and low quality of life in people in terminal stage of cancer because pathogenesis of colorectal PM is poorly understood[18,157]. The formation of PM is the consequence of multiple well-defined phases of molecular interaction between tumour cells and host components, especially extracellular matrix (ECM***)***[19,20]**.** Peritoneal metastasis is an outcome of peritoneal metastatic cascade, where tumour cells disseminate from primary tumour and spread to another organ – peritoneum (Fig. 15)[17–19,155]. The spread of cells is organ-specific in most of the cases[20,158]. Once the cells penetrate mesothelial barrier they attach to ECM by integrin-ligand interactions[159] and later invade the ECM. The main factor in this process are matrix metalloproteinases (MMP)[20,155]. However, prior to invasion of neoplastic cells in new tissue, it is necessary to alter foreign microenvironment by releasing tumour secreted factors like growth factors, hormones, cytokines, chemokines[158,160]. This mechanism and sequence of events are explained by “seed and soil” theory and lead to formation of pre-metastatic niche (PMN)[158].

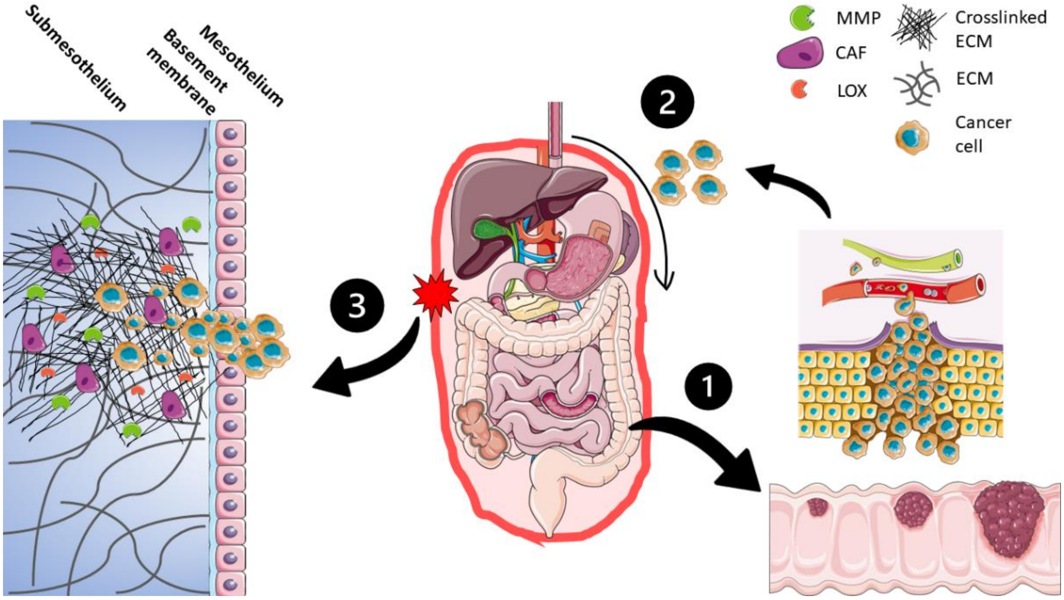

***Figure 15**. Pathophysiology of the peritoneal metastatic cascade from colorectal carcinoma. 1. Dissemination of CRC tumour cells and their transport to peritoneal cavity. 2. Tumour cells in regular peritoneal transport. 3.Attachment of neoplastic cells to peritoneum – invasion of submesothelium*[17–19]*. [Parts of the Figure were drawn by using pictures from Servier Medical Art. Servier Medical Art by Servier is licensed under a Creative Commons Attribution 3.0 Unported License (https://creativecommons.org/licenses/by/3.0/)].*

The pre metastatic niche is a tissue microenvironment in distant organs specialized to sustain and regulate neoplastic stem cell function and proliferation[158,160]. After extravasation, many tumour cells do not survive due to apoptosis, poor vascularization, or by immune defence action. The surviving cells can remain as isolated single cells or can form micrometastasis, which are difficult to detect since they are very small[158]. ECM active remodelling and deposition are the most important part in the process of PMN development[42,160] Abnormal ECM can promote many events, like the loss of differentiation state and polarity of cancer cells, the manipulation of stromal cells to foster their own proliferation at the main tumour and distant sites, and also disruption of tissue integrity[23]. Cell survival and proliferation are promoted by an increase in collagen deposition. Increased cross-linking of collagen and remodelling of ECM are caused by enzymes like metalloproteinases (MMP) and lysyl oxidase (LOX) (Fig 15) Therefore, defective ECM encourages the formation of a tumorigenic microenvironment and helps to maintain the local niche[23,161].

Growing evidence points to the importance of the peritoneal microenvironment in the formation and treatment resistance of colorectal PM. Any particular treatment, including surgery and chemotherapy, may cause the interactions between cancer cells and the peritoneal microenvironment to dynamically change. Bidirectional mechanobiological interactions between cells and their microenvironment are significant not only to sustain homeostasis but also play role in formation of pre-metastatic niche and tumour growth[33,109]. Cancer and stromal cells modify the local microenvironment as a result of the formation of tumours, and as a result, they both influence and are impacted by biochemical and biophysical signals. Changes in tumour mechanics can result from abnormalities in matrix deposition and degradation, elevated matrix crosslinking, impaired lymphatic drainage, blood vessel leakage (increased oncotic and fluid pressure), uncontrolled growth, and dense cell populations that produce solid pressure that inhibits cell movement. These mechanical signals are actively influencing tumour cell behaviour as they are converted into biochemical signals and sent from the cytoskeleton to the nucleus[42,161].

The combinatorial signals that support and encourage PM will be revealed by a deeper comprehension of this dynamic reciprocity. Novel insights into medication response and resistance may be produced by preclinical models with the required cellular and biomechanical features, including patient-derived cell populations in bioengineered tumours, which might make it possible to test out personalized treatments[18,32,160]. Current attempts focused on understanding of the mechanisms of peritoneal metastasis and other types of cancer are based on studies which use 3D models which do not fully recapitulate native tissue[17,52] This section focus on investigation of formation of pre-metastatic niche and the role of ECM by studying decellularized ECM (dECM) from patient derived biopsies and with the use of novel 3D ex vivo model of PM lesions.

5.2. Decellularized Normal and Tumour Scaffolds for Cancer Organoid Cultures as a Model of Colorectal Peritoneal Metastases

5.2.1. Introduction

As a part of collaboration with Dr. Manuela Gariboldi and Dr. Luca Varinelli from Istituto Nazionale dei Tumori I contributed to scientific paper "Decellularized extracellular matrix as scaffold for cancer organoid cultures of colorectal peritoneal metastases"[50] published in the Journal of Molecular Biology on 02 December 2022, written by:L. Varinelli, M. Guaglio, S. Brich, S. Zanutto, A. Belfiore, F. Zanardi, F. Iannelli, A. Oldani, E. Costa, M. Chighizola, E. Lorenc, S.P. Minardi, S. Fortuzzi, M. Filugelli, G. Garzone, F. Pisati, M. Vecchi, G. Pruneri, S. Kusamura, D. Baratti, L. Cattaneo, D. Parazzoli, A. Podestà, M. Milione, M. Deraco, M.A. Pierotti, M. Gariboldi. The aim of the study was to develop 3D engineered PM lesions and characterize properties of this biological model and its components. This chapter contains fragments taken directly from the publication, highlighting my contribution to the research. Experiments and methods described in this article were fundamental for further research described in Chapter 5.3 and 5.4.

The need to develop ex vivo engineered PM lesions rises from the fact that PM from CRC are associated with poor survival[18,157]. What is more, there are not many in vitro models available for the study of the peritoneal metastatic process and the mechanism underlying how metastatic cells interact with the ECM are still poorly known. The majority of the available knowledge on metastatic spread was compiled using patient-derived xenograft models or cancer cell lines, neither of which accurately represent the physiopathology of the original tumour[162]. One of the first steps of research was to obtain and characterize ECM scaffold that could be later used for culture of organoid cells. The samples of dECM provided by INT were studied at laboratories of C.I.Ma.I.Na, to characterize rigidity of the specimens. We studied its mechanical properties and structure with the use of AFM in indentation mode. Later, it was demonstrated that the decellularized peritoneal-derived ECM promotes the creation of three-dimensional (3D) nodules that retain the properties of in vivo PM by allowing the growth of tumour derived organoids (TDO) derived from PM[50]. This achievement was crucial for later research described in Chapter 5.4.

We expect that this approach and use of such ex vivo engineered model can be widely applicable in cancer research and can overcome present limitations of standard in vitro models of lower complexity and scale. Additionally, it might be a novel technique to create fresh therapeutic approaches in a physiologically pertinent setting to generate customized therapies.

5.2.2. Materials and methods

5.2.2.1 Preparation of 3D-dECMs

ECMs were extracted from the peritoneal tissue of five patients with CRC-PM (Table 1). The samples were taken after surgical resection at the Peritoneal Malignaces Unit of the Fondazione IRCCS Istituto Nazionale Tumori of Milan. The study was carried out in accordance with the 2009 Declaration of Helsinki and was given approval by the Institutional Review Board of Fondazione IRCCS Istituto Nazionale Tumori di Milano (134/13; I249/19). All experiments were conducted in compliance with the mentioned regulations and guidelines that were applicable. All participants gave their consent in writing after being fully informed. According to accepted clinical practices, non-tumour tissues were collected 10 cm away from the tumour[14].

Patient	*Age*[3]	*Sex*	*Diagnosis*	*Grade*	*Chemotherapy*
P1	43	Female	Mucinous Adenocarcinoma	G2	Yes
P2	60	Male	Adenocarcinoma	G3	Yes
P 3	63	Female	Mucinous Adenocarcinoma	G3	Yes
P 4	51	Female	Mucinous Adenocarcinoma	G2	Yes
P 5[4]	66	Female	Adenocarcinoma	G3	Yes

Table 1 *Characteristics of the patients from whom the tissue samples were obtained. All samples were at stage IV.*

Both the PM and the equivalent normal peritoneum were used to create 3D-dECMs. The decellularization was done in accordance with *Genovese et al. 2014*[109] instructions. Briefly, samples of normal and PM peritoneum (60-100 mg wet weight) were treated with solutions comprising detergents and enzymatic agents after being rinsed with ice-cold PBS supplemented with 50 ng/ml gentamicin and 50 ng/ml amphotericin B. Following an ice-cold PBS wash, the 3D-dECMs were placed in a chilled freezing solution (90% DMEM-F12, 10% DMSO) and frozen for later use.

5.2.2.2 dECM scaffolds characterization - AFM nanoindentation measurements

Five patients' 3D-dECMs derived from normal and neoplastic peritoneum were subjected to AFM mechanical investigation. OCT-embedded 3D-dECMs were then frozen in nitrogen-cooled 2-propanol. Slices with a thickness of around 100 µm were cut with a microtome (Leica) and mounted to positively charged poly-lysine coated

---

[3] *Age at surgery.*

glass coverslips (ThermoFisher Scientific). Samples were covered by a PBS droplet enclosed by a circular ridge of hydrophobic two-component silicone paste to nanomechanical tests were carried out in liquid (Leica). The Bioscope Catalyst AFM (Bruker) was used, and it was placed inside an acoustic enclosure while resting on an active anti-vibration base (DVIA-T45, Daeil Systems) (Schaefer). [150]

The measurements were performed with the use of colloidal probes with nominal spring constant k 3-6N/m and radii R 7.5 – 12.5 µm. The probes were prepared and calibrated following steps described in Chapter 3.2.

Every set of FVs had an array of generally 15x15=225 FCs, each of which had 8192 points and had a ramp length of 8–15 m, and a ramp frequency of 1 Hz. In order to produce a maximum indentation in the range of 4–9 m, the maximum load of 150–1500 nN was used. The probe typically approached at a speed of 16 to 30 m/s during indentation. Each condition's five samples were characterized. For a total of 10–25 independent P&S per patient and condition, 3–10 P&S were obtained in each sample at macroscopically distinct places (up to 2250-5500 FCs per patient and condition).

5.2.3 Results

5.2.3.1 Mechanical properties of 3D-dECMs

The results of an AFM nanomechanical investigation revealed that the neoplastic 3D-dECMs were significantly stiffer than non-tumoral 3D-dECMs and had a larger range of Young's modulus (YM) values (Fig. 16B). Additionally, there was a considerable overlap between the two conditions and the YM distributions were very dispersed (Fig. 16A).

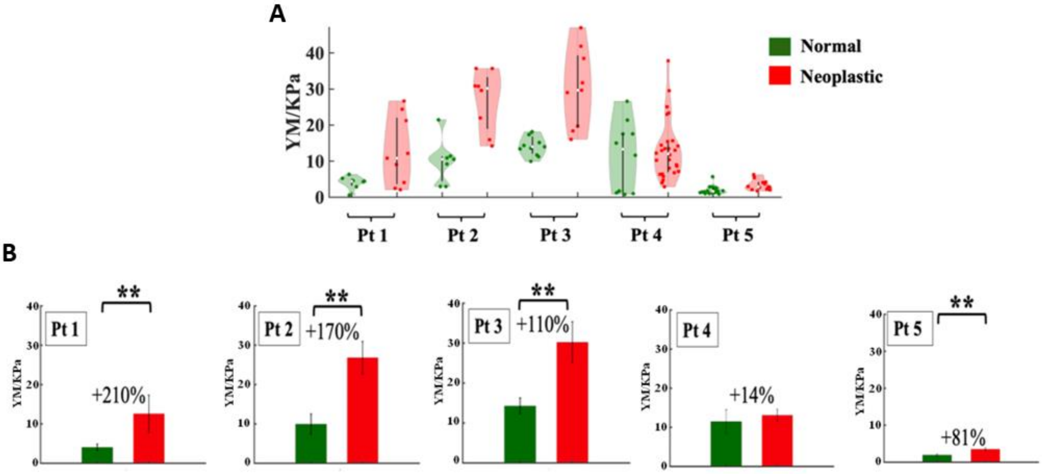

Figure 16. *Distribution of the YM values obtained for each patient and condition (normal and neoplastic). Violin-plots: each dot represents the median YMvalue extracted from a single measurement Point and Shot (P&S) made approximately by 225 FCs.Pt, patient. YM/KPa, Young's Modulus/Kilo Pascal (D). Result of the statistical analysis of the YM value for each patient and condition tested (E). The bars and error bars represent mean of the medianYM values and effective SD of the mean. The percentages represent the relative stiffening of the neoplastic ECM. Student's t-test (**P<0.01).*

These findings suggest that the ECM is a complex system that is still locally diverse at lengths between 10 and 100nm, which are representative of numerous typical cellular lengths. In terms of change in stiffness and structural organization, the shift from the normal to the malignant condition is not uniform across the entire macroscopic tissue region.

5.2.3.2 Correlation of mechanical properties of 3D-dECMs with clinical data

Obtained results of ECM rigidity were correlated with clinical data of patients. The idea was to better understand how ECM mechanics can be linked with

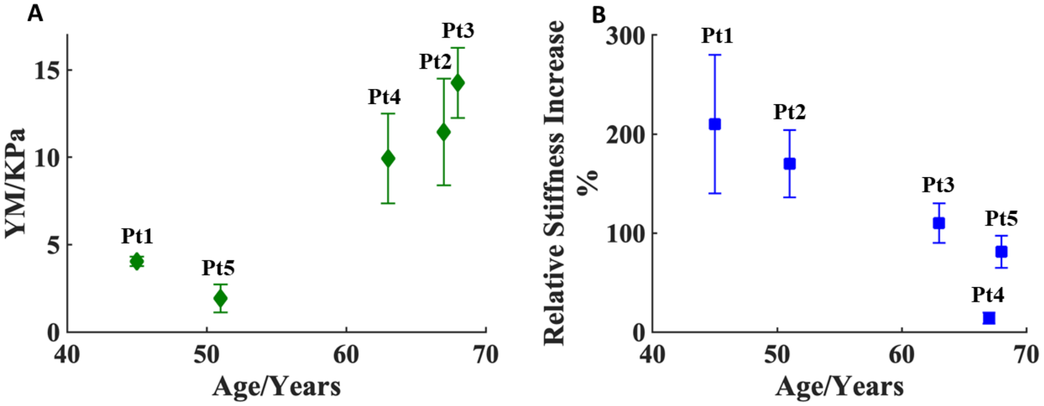

Figure 17. *YM values of analyzed cases correlated with clinical data. The rigidity of the normal dECM increases with the age of the patient (A). The relative stiffening associated with the age of the patient (B).*

Considering normal-derived dECM, it can be observed that samples from older patients are characterized by higher rigidity (Fig. 17A). It can be explained by the fact that an older tissue is mechanically weaker and less elastic but also more rigid than a young tissue due to the combination of increased and improper collagen crosslinking[11,22,163]. Interestingly, correlating age with relative stiffening revealed that increase of rigidity is more pronounced in younger patients, P1 and P2 (Fig. 17B).

5.2.4. Discussion

The main goal of work presented in *Varinelli et al. 2022*[50] was to develop and characterize ex vivio engineered PM lesions to study peritoneal matastasis. Understanding the distinctions between ECM obtained from normal and tumoral tissue and derived from various patients is made easier by researching the nanomechanical characteristics of the tissue microenvironment. It is possible to cultivate such scaffold for cell culture and build more physiological cancer models thanks to the ability to separate naturally decellularized ECM while preserving its

3D architecture and biochemical features. As my contribution to mentioned work, I characterized dECM, the main, next to organoids, component of studied model.

Observation of large patient to patient variability of rigidity showed that biological samples from different patients are very diverse. What is more, to proper characterize dECM and to understand PM mechanisms it is necessary to continue studies and supplement them with additional analysis of molecular biology techniques.

Additional AFM studies presented in this article showed that the observed stiffening of the neoplastic ECM can be partially attributed to the more compact fine structure of the matrix and to the linearization of the fibers in bundles. The topographical analysis of 3D-dECM revealed that matrices obtained from tumoral tissues exhibited a corrugated surface pattern, while normal tissues had an organization of very thin fibers that was characterized by homogenous and cross-linked reticular structures[50]. This highlighted the role of collagen in mechanics of peritoneal ECM.

What is more, linking changes of stiffness with clinical data and diagnosis of patients revealed that this information might be correlated. Due to low number of studied samples, proper conclusions could not be drawn, and the results were not published in the final version of the article. Nevertheless, these results gave a ground for further research, that were carried out to increase the number of studied specimens.

The strategy of culturing organoids on peritoneum-derived 3D-dECM scaffolds turns out to be successful, as this model supports colonization, infiltration, and proliferation of PM-derived organoids, maintaining the stem cell pool[50]. The aim was to create model of ex vivo engineered PM lesions, with intention for application in further research focused on mutual influence between cells and their microenvironment (what is later investigated and described in Chapter 5.4). It is well known that microenvironment and its mechanical properties affects cell behaviour[22,42,161]. Also, in work of *Varinelli et al. 2022* it was shown that neoplastic peritoneum-derived scaffolds, which are stiffer than conventional scaffolds, are preferred for the development of organoids. Gene expression studies performed on organoids developed on diverse substrates successfully characterized the clinical and biological characteristics of the organoids[50]. Such model could be used as pre-clinical platform to study the role of tumour ECM in the development of the PM niche. This could help in the future in the early diagnosis of cancer.

Organoids preferentially develop on neoplastic peritoneum-derived scaffolds, which are more rigid than regular scaffolds. Organoids grown on various substrates have gene expression analyses that accurately captured the clinical and biological properties of the organoids. It was also noted that the ECM influenced how well PM patients responded to conventional chemotherapy.

5.2.5 Conclusions

The novel work presented in *Varinelli et al. 2022*[50] showed importance of improvement of studied models in cancer research. Methodologies developed and optimized in these experiments, like decellularization and development of ex vivo engineered PM lesions of was fundamental for further research described in chapter 6 and 7. What is more, it highlighted the significance of ECM mechanical properties in cell proliferation and cancer progression. Studies have stimulated further research focused on correlation of ECM's mechanical characteristics with patients' clinical data and molecular aspects of PM (Chapter 5.3). Relation between cell proliferation and their microenvironment have stimulated studies of mechanical aspects of cancer progression in ex vivo engineered PM lesions, what is described in Chapter 5.4.

5.3. Correlation between extracellular matrix stiffness distribution and peritoneal metastasis progression

5.3.1 Foreword

Previous work described in Chapter 5.2 revealed that there might be significant correlation between mechanical properties of ECM, its changes, and clinical data of patients. The study presented in this chapter aimed to better characterize the ECM for its later use as a scaffold for cell culture and to complete and improve clinical data correlation by increasing the statistics of studied samples.~~.~~ To better understand mechanics of ECM and mutual influence between cells and their microenvironment I investigated nanomechanical fingerprint of ECM in health and disease. The results of this research are presented in the manuscript "The nanomechanical fingerprint of colorectal cancer – derived peritoneal metastasis" written by E. Lorenc, L. Varinelli, M. Chighizola, S. Brich, F. Pisati, M. Guaglio, D. Baratti, M. Deraco, M. Gariboldi, and A. Podestà. The paper is available on bioRχiv (doi: 10.1101/2022.08.17.504271) and currently is under revision in journal Scientific Reports (Springer Nature). The manuscript uploaded on bioRχiv is reported in the next section.

5.3.2. The manuscript

Abstract

Peritoneal metastases (PM) are one of the most common routes of dissemination for colorectal cancer (CRC) and remain a lethal disease with a poor prognosis. The compositional, mechanical and structural properties of the extracellular matrix (ECM) play an important role in cancer development; studying how these properties change during the progression of the disease is crucial to understand CRC-PM development.

The elastic properties of ECMs derived from human samples of normal and neoplastic PM in different pathological conditions were studied by atomic force microscopy (AFM); results were correlated to patients' clinical data and to the expression of ECM components related to metastatic spread.

Our results show that PM progression is accompanied by stiffening of ECM as a common feature; spatially resolved mechanical analysis highlighted significant spatial heterogeneity of the elastic properties of both normal and neoplastic ECMs, which show significant overlap in the two conditions. On the micrometre scale, ECMs that are considered normal according to the pathological classification possess stiffer spatial domains, which are typically associated with cancer associated fibroblasts (CAF) activity and tumour development in neoplastic matrices; on the other hand, softer regions are found in neoplastic ECMs on the same scales. Our results support the hypothesis that local changes (stiffening) in the normal ECM can create the ground for growth and spread from the tumour of invading metastatic cells. Mechanical changes correlate well with the presence of CAF and an increase in collagen deposition, which are well known markers of cancer progression. Furthermore, we have found correlations between the mechanical properties of the ECM and patients' clinical data like age, sex, presence of mutations in BRAF and KRAS genes and tumour grade.

Overall, our findings suggest that the mechanical phenotyping of the PM-ECM has the potential for predicting tumour development.

Keywords: colorectal carcinoma, peritoneal metastasis, extracellular matrix (ECM), nanomechanics, atomic force microscopy (AFM).

Introduction

Peritoneal Metastasis (PM) affects about one out of every four patients with colorectal cancer (CRC) [18]. PM development is characterized by several steps where cancer cells disseminate from the primary tumour to the peritoneal cavity [20], through a process also known as peritoneal metastatic cascade [19,20]. To colonize the peritoneum, the neoplastic cells must be able to infiltrate the extracellular matrix (ECM), starting from detachment from the primary tumour, attach to sub-mesothelial connective tissue and receive a favourable host response [20].

The ECM is an essential, acellular element of the tissue microenvironment, which plays a crucial role in several processes in tissue homeostasis [22]. The ECM determines the three-dimensional (3D) structure of the tissue and provides mechanical and biochemical support, playing a major role in cell-cell and cell-matrix communication and cell migration [22,23]. Moreover, in the last decades, the crucial role of the ECM in cancer progression has been clearly demonstrated [12,21,24,28,30,164].

The extra-cellular microenvironment is composed of water, various fibrous proteins (i.e. collagens, elastins, laminins, fibronectins), proteoglycans, glycoproteins, and polysaccharides; the ECM of the specific tissue has unique composition and topology, which results in developing the biochemical and mechanical properties of each organ and tissue [18,22,23].

The ECM can be considered a dynamic element of the tissue, as it undergoes several changes in its composition and rearrangements of own components, through covalent and non-covalent modifications, which are associated with cells activity in tissue development, and also severe diseases and cancer progression [23,163].

Both mechanical and biochemical changes in the ECM are regulated by growth factors, hormones, cytokines and metalloproteinase (MMP) [21]. The ECM elastic properties, together with the activity of specific biochemical factors, play a key role in tissue homeostasis, cell fate, cell adhesion, migration, cell cycle progression, differentiation and actin-related cytoskeletal reorganization and contractility [21,38,163,165].

During cancer progression, the ECM undergoes many structural and biochemical changes, such as an increase of collagen deposition, fibres cross-linking and also changes in gene expression[21–23,38,163,165]. Indeed, the stiffening of the ECM can be observed in pre-malignant and malignant tissues [21,163], is associated with high malignancy/aggressiveness and worse prognosis[24,38,165,166] and leads to enhanced treatment resistance in most of the tumours [21].

Cancer associated fibroblasts (CAFs) can originate from different cell types, including resident fibroblasts and mesothelial cells, which undergo a mesothelial-to-mesenchymal transition (MMT) [18,167] and are critical for the progression of the metastatic disease. CAFs oversee the production of ECM proteins such as collagen, fibronectin, and several others as well as proteases and other enzymes involved in post-transcriptional modification of ECM proteins [167–169]. CAF activation and collagen deposition, which lead to an overall increase of ECM elastic modulus (stiffening) are among the signs of cancer progression. Therefore, the detection of ECM stiffening at the cellular scale could allow us to spot the first signs of tumour development and monitor cancer progression from its beginning. Moreover, a better understanding of the ECM stiffening process and the associated cell-ECM interplay could help develop more efficient therapeutic strategies for the prevention or treatment of cancer.

Atomic force microscopy (AFM) is a powerful and versatile tool to study biological samples at the nano- and microscale, including the quantitative investigation of their morphological and mechanical properties [13,61,89,143,148,170]. The mechanical properties of cells, ECMs and tissues can be characterized by AFM [14,33,89,91,93,143,148,171–173] and could constitute a unique mechanical fingerprint of cancer progression [3].

Our work started from the hypothesis that the AFM study of nanomechanical properties of cells, ECMs and tissues, when complemented with the analysis of the expression of specific ECM components and with clinical metadata, can provide an important contribution to understanding the mechanisms that lead to the development of the PM. We have therefore studied the changes in the mechanical properties of the peritoneal ECM in patients affected by CRC-PM. In particular, we have characterized the Young's modulus of elasticity of ECM specimens through indentation measurements performed by AFM [89]. The results of the nanomechanical analysis have been correlated with CAF presence and collagen organisation in the ECM samples, to obtain information on the physicochemical differences between normal and neoplastic ECMs, and with patient metadata to try to identify mechanical markers related of specific physio pathological state.

Results

Changes in the nanomechanical properties of the ECM

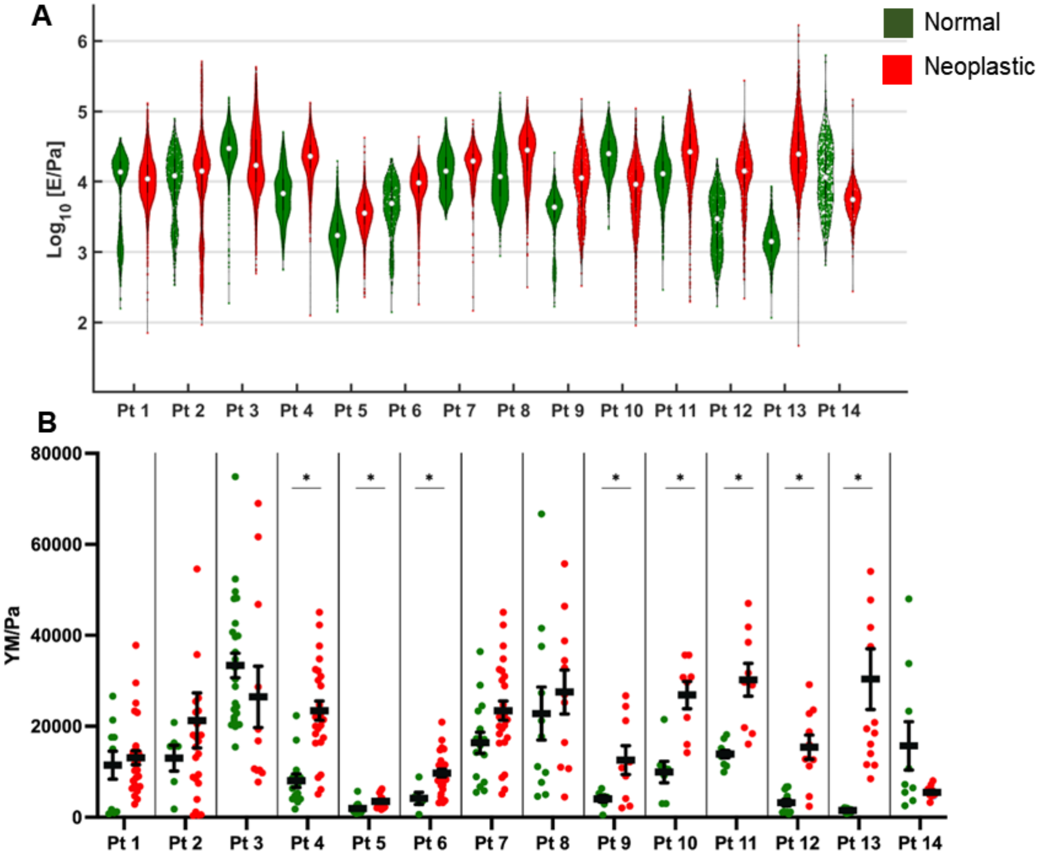

Figure 18. *YM distributions for the normal (green) and neoplastic (red) conditions from peritoneal ECMs for the 14 patients considered in the study. A) Violin plots obtained by pooling all YM values from all FCs acquired in all ROIs for a specific condition. The median value is represented by a white dot and black thick lines represent upper and lower quartiles. B) Plots showing the distribution of median YM values measured from all FVs collected in different ROIs for each specific condition. Black dots and bars represent the mean median values and the corresponding standard deviation of the mean, respectively. The asterisk indicates statistical significance of the difference ($p<0.05$).*

The heterogeneity of the ECM samples studied can be appreciated from the violin plots shown in Figure 18A. In several cases, the YM distribution appears as clearly multimodal. It turns out that often the YM value of the highest-order mode is similar (i.e., the distribution shows significant overlap) to the YM value of a leading mode in the distribution of the neoplastic sample (see for example patients 1,2,3,6,7,8).

Figure 18B shows the distribution of the median YM values measured at different locations of the ECM samples for the tested conditions and patients. In some cases, stiffening is statistically significant, in others it is not, although an increase in the median YM value is often observed. Statistically significant stiffening (i.e., increase of the YM value from the normal to the neoplastic condition) of the CRC-PM derived ECM was observed for eight patients (4-6 and 9-13), who were also among the oldest: 82, 66 and 71 years, respectively, for patients 4-6 and 63, 67, for patients 10-13. However, the stiffening process was also present in patients 7, 8 and 9, who are significantly younger (47, 43 and 45 years old) (Figure 18B).

For both normal and neoplastic tissues, the distribution of YM values is rather broad. Within the same tissue, we observed very wide patient-to-patient variability. For example, for the normal tissue, we observed a difference factor of ~17 between the YM value of patients 5 and 3; for the neoplastic condition, we observed a difference factor of ~8 between the YM value of patients 8 and 5. These results highlight, among other aspects, the importance of identifying internal references within the same patient; in our case, this is represented by the normal ECM collected several centimetres away from the cancer lesion.

Correlation of the mechanical fingerprint with αSMA overexpression and collagen fibers presence

To better understand the biological events that sustain the mechanical properties of the ECM, we selected six different cases (patients) and analysed CAF activity related to collagen deposition and orientation by αSMA, and Picrosirius Red staining (Fig. 19A,B). Patients whose ECMs exhibit different characteristic mechanical properties (no mechanical differences, moderate and significant stiffening) were selected.

Five of the six patients showed low expression of αSMA in normal-derived samples, although stromal regions showed high expression of localized αSMA (Fig. 19A). Interestingly, we also observed high expression of αSMA around blood vessels (see patients 6, 8 and 13), a sign of the process of neo-angiogenesis, a well-known hallmark of cancer and metastatic spread. Neoplastic-derived samples showed higher expression of αSMA in patients 2, 6, 8, 12; while no clear differences in CAF activity were observed in patients 13 and 14. Patient 13 showed low expression of αSMA in both normal and neoplastic tissues, while patient 14 showed high expression of αSMA in both tissues. For three out of six patients, clear differences in αSMA expression (Table 2) correlated with ECM stiffening, while patient 14 showed no differences in αSMA and no difference was observed in the measured YM of the two conditions. As can be seen in the case of normal-derived samples, αSMA expression is present, suggesting that neoplastic modifications of the environment are already occurring in a perilesional area (i.e., a region of the tissue that is healthy but close to the tumour mass). In patients 2, 8 and 12 (normal) stiffness distribution was bimodal (Fig. 18A) and a similar distribution was observed for αSMA expression.

We then evaluated the orientation of collagen fibers by Picrosirius Red staining (Fig. 19B). The results showed that normal samples had higher deposition of collagen fibers in stromal and blood vessel areas (Fig. 19B), while neoplastic-derived samples were characterized by an irregular and porous orientation of collagen fibers, with a corrugated-like morphology pattern (Fig. 19B, see patients 2, 6, 8, 12-14). Overall, collagen results correlated with αSMA expression (Table 2), demonstrating the active role of CAF in collagen production and deposition during metastatic spread (Fig. 19A,B). Again, we observed that some normal-derived samples exhibited a neoplastic-like collagen pattern, also in line with αSMA expression, particularly in patient 14.

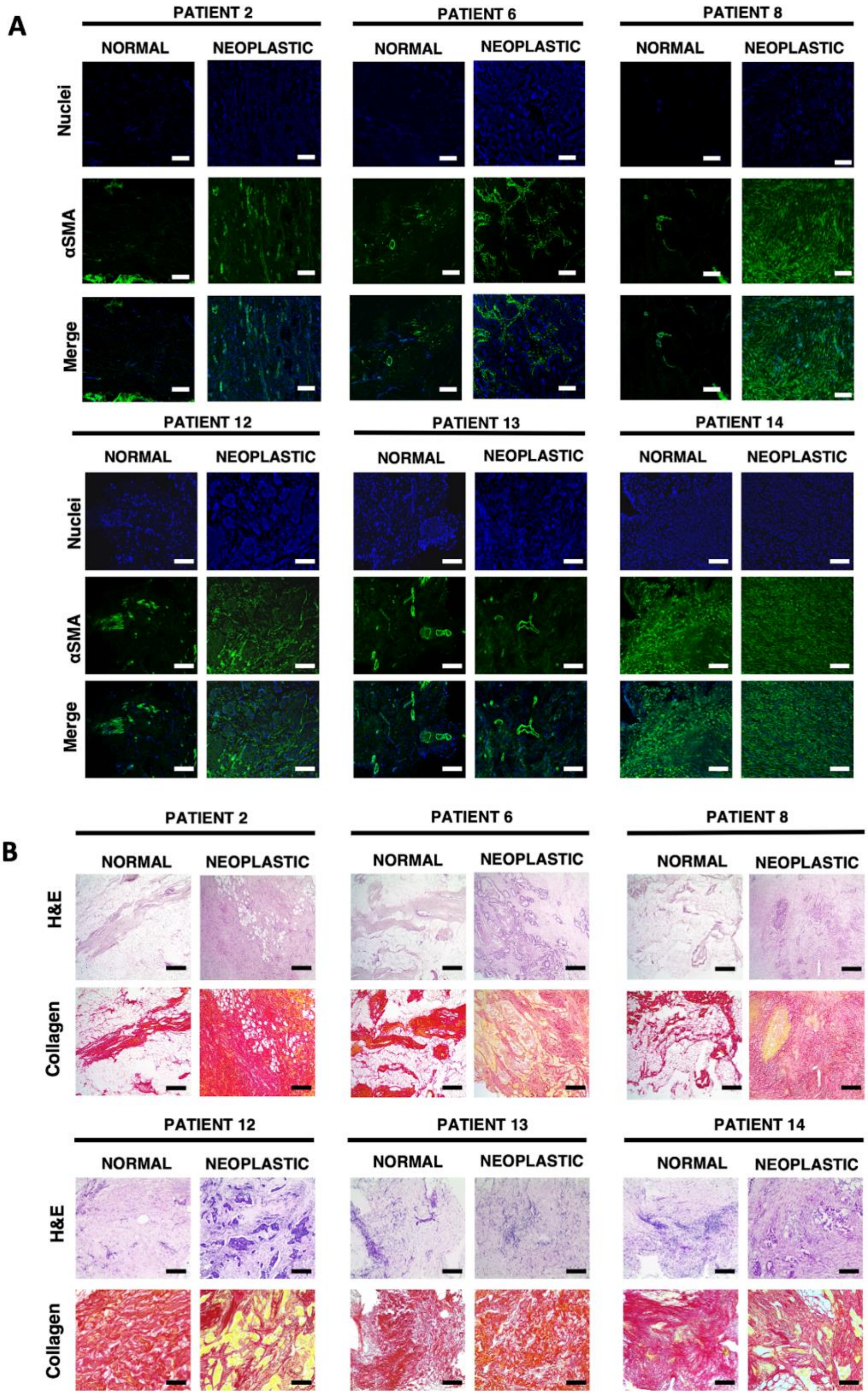

Figure 19. *Images of tissue samples from patients 2, 6, 8 and 12-14, for visualization of: A) cell nuclei (DAPI staining) and αSMA, magnification 10x; B) collagen and control staining (picrosirius Red and haematoxylin and eosin staining, respectively), magnification 4x. Length bar in 100µm*

Table 2. *Mechano-biological relevant cancer-related modifications. +: Observable differences, ++ marked differences (statistically significant in mechanics), -: no observable differences.*

PATIENTS	αSMA	*Collagen*	*Mechanics*	*Correlation*
2	+	++	+	✓
6	+	++	++	✓
8	++	++	-	
12	++	+	++	✓
13	-	-	++	
14	-	-	-	✓

Correlation of the mechanical fingerprint with patients' clinical data

To better understand how mechanical response and ECM modifications are related to PM, we looked for correlations between the observed biophysical properties and clinical data of the patients.

We first tested whether the Young's modulus of the normal ECM was correlated with the age of the patients involved, since age-related stiffening has been reported at both the cellular and ECM/tissue level [174–178]. The results are shown in Figure 20A. It is possible to observe a clear trend toward softening of the normal ECM as the age of patients increases (patient 13, with a colorectal neuroendocrine carcinoma, not included in Figure 20A, showed a decrease in line with the general trend).

To investigate whether the softening could be due to the treatments undergone by the patients, we checked for correlation with chemotherapy (Fig. 20B), but we found no significant evidence of its impact on the elastic properties of the ECM, despite a broader distribution of YM values for patients treated with chemotherapy. To avoid previous treatment-related biases, we calculated the relative stiffening of neoplastic versus normal ECMs within each single patient, as both tissues underwent the same treatments. The relative stiffening was calculated as the difference between the YM values of the neoplastic and normal ECM, normalized to the YM value of the normal ECM. Figure 20C confirms that chemotherapy is not correlated to stiffening of the ECM.

Figure 20D shows that there is a trend toward increasing relative stiffening with the age of the patients, although not significant. Note that patient 13, with a colorectal neuroendocrine carcinoma, showed the strongest increase in stiffness (up to 1200%, and four times larger than the second highest relative stiffening). The very high stiffening observed in patient 13, compared with the other patients, can be a sign of different mechanical modifications between tumour types. However, since neuroendocrine tumours are extremely rare, our observations are not statistically significant and a comparison with the PM group is not possible; patient 13 was therefore excluded from analysis reported in Figure 20.

We tested whether stiffening is related to the presence of mutations in the *KRAS* and *BRAF* genes, which are very frequent in metastatic CRC (Figure 20E). We observed a difference (although not significant) between the relative stiffening of ECMs carrying *KRAS* and *BRAF* mutations, which appeared to be greater in *KRAS* mutated cases. The non-mutated cases spanned a wider range of relative stiffening, encompassing that of the mutated cases.

In addition, we decided to look for correlations between relative stiffening and the sex of patients, since it is known that CRC is more frequent in males than females, although the differences in mortality appear to be insignificant [179]. Figure 3E shows that females have more pronounced stiffening, although not significant. There are no data on this issue, so it might be interesting to test for sex-related variations in the mechanical properties of other tissues, as in the case of cardiovascular disease, which is known to affect males more than females [180].

We also tested whether there are differences in mechanical properties in relation to the histopathological classification of the tumour (Table 2). Figure 20G shows that there are no evident differences in the relative increase of the YM of the ECM of the different histology.

Finally, we analysed the differences in the tumour grade of the samples analysed. Tumour grade describes a tumour in terms of abnormalities of tumour cells compared with normal cells. A low grade indicates a slower growing tumour than a high grade. All patients were diagnosed with grade 2 and grade 3; the results of the correlation between tumour grade and relative stiffening are shown in Figure 20H. It can be observed that the grade 3 group (G3) shows significantly greater stiffening than the grade 2 group (G2).

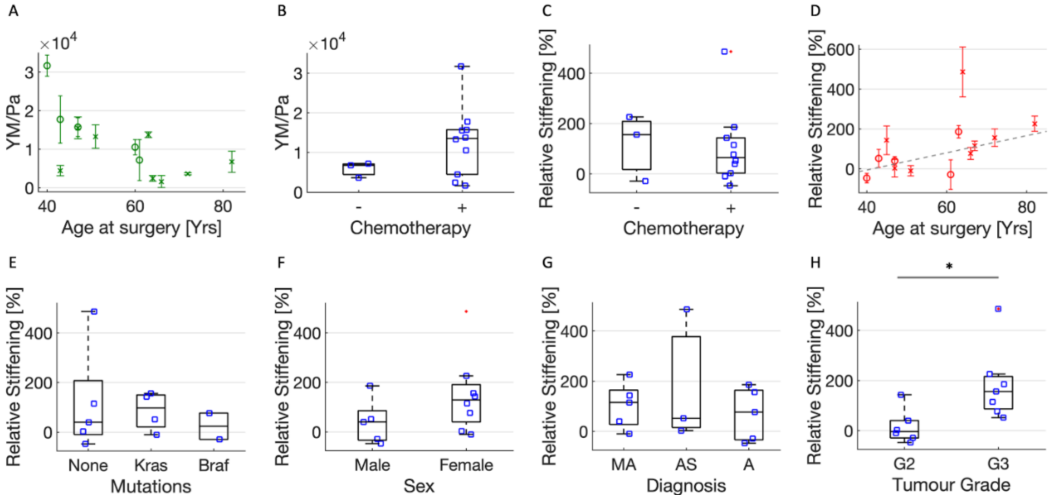

Figure 20. *A) YM values (mean median value +/- std of the mean) of healthy ECMs of the 13 patients affected by adenocarcinoma versus their age (circles and crosses represent men and females, respectively). B) YM values as in (A) for patients who did not (-) and did (+) undergo chemotherapy. C-H) Relative stiffening of the neoplastic ECMs from the same patients, versus: C) chemotherapy treatment; D) the patients' age; E) the presence of mutations in KRAS and BRAF genes; F) the patients' sex; G) histology – MA: Mucinous Adenocarcinoma, AS: Adenocarcinoma of the Sigma, A: Adenocarcinoma; H) Tumour grade.*

Discussion

Changes in the nanomechanical properties of tissues are one of the hallmarks of tumour progression. By understanding the processes behind them, we could exploit this knowledge to implement cancer diagnosis and other diseases based on nano- and microscale mechanical phenotyping. Here, we focused on the investigation of the mechanical modifications in decellularized ECM derived from CRC-PM.

Based on AFM studies on ECM samples from 14 patients, we observed a general trend of ECM stiffening during the development of the neoplastic lesion (Figure 18). Our results agree with previously published data on ECM of other cancer types [28,50,181].

The measured multimodal, not simply broad, distributions of YM values, suggest that the ECM possesses significant structural, compositional, and therefore also mechanical heterogeneity at the AFM measurement scale (10-100 µm). Moreover, the partial overlap of YM values distributions of different conditions (normal and neoplastic), revealed the complexity of disease progression during the metastatic process, which is characterized by high spatial heterogeneity at the cellular and supracellular scale. The seed and soil theory suggests that ECM undergoes changes, including mechanical ones, to prepare a microenvironment suitable for neoplastic cell proliferation [158]. The presence of stiffer regions in normal samples, comparable to those typical of the neoplastic cases, suggests that local changes that prepare the ground for metastatic invasion in the normal tissue occur far from the existing lesion, likely caused by the release of factors that can ultimately alter the mechanical properties of the ECM [158]. The common practice for cancer studies is to obtain non-tumoral sample 10-15cm away from the tumour [14]. Our results on the mechanical properties of the ECM show that the practice of considering the tissue located 10-15 cm far from the cancer lesion as non-tumoral can be incorrect.

Staining for αSMA, a CAF-specific protein expressed in fibroblasts, which is a sign of cancer progression and a typical marker of desmoplasia [167], detected changes in the surrounding microenvironment that typically lead to the development of specific metastatic niches. Since we also observed areas with high expression of αSMA in normal samples, it is likely that these may have undergone modification induced by specific pro-metastatic factors released by nearby PM metastatic cells. These results confirmed that the formation of pre-metastatic niches already occurs in normal derived tissue as we also observed areas of high αSMA expression in normal samples.

Higher expression of αSMA was also observed in areas rich in blood vessels (patients 6, 8 and 13). During the metastatic process, CAFs can distribute through blood vessels to develop the so-called perivascular metastatic niches, which can sustain the activation of stromal cells in normal tissue through TGF-ß and secretion of pro-inflammatory and pleiotropic interleukins and cytokines, which also contribute to initiate modifications in the ECM, including stiffening. The combination of these events generates a microenvironment more suitable to support metastatic spread, in particular angiogenesis [158,167,169]. Expression of αSMA in vascularized areas indicates early steps of metastatic invasion into normal tissues.

Expression of αSMA was higher than normal tissue in four of the six patients and CAF activity correlated with increased collagen deposition; nevertheless, two patients (8 and 13) exhibited uncorrelated results between staining and mechanical differences of normal and neoplastic ECM. Based on these results it appears that some of the tissue that was considered normal already had cancerous characteristics.

Another step to better understand the differences between normal and neoplastic ECM was to visualize collagen I and III fibers, as their overexpression and remodelling are strictly related to cancer progression[11,21–23,148]. Our results showed the typical expression and organization of collagen fibers already observed in previous studies on different types of ECM[28,31,173]. The organization of collagen fibers was strictly correlated with the expression of αSMA; expression of this protein confirmed collagen crosslinking in neoplastic ECM but also to a smaller extent in normal ECM. Tumours with high desmoplasia (fiber crosslinking) are considered more aggressive and with a worse prognosis [21]. In the neoplastic samples, increased crosslinking and restructuring of collagen fibrils in the ECM, and matrix stiffening produce an extracellular environment conducive to tumour invasion and growth. Changes in the vascularized and stiffer perilesional area could be a feed-forward loop to spread neoplastic ECM characteristics. Myofibroblasts are known for their ECM remodelling, which involves *de novo* deposition of specific receptors involved in mechanosignaling by the ECM, contributing to both normal and pathologic tissue remodelling [182].

Correlation of these results with patients' clinical data suggests a clear trend for tissue softening in older patients. This result is somewhat unexpected, considered that age-related stiffening at both cells and ECM/tissue levels has been reported [174–178]; damaging and inflammation of the tissue due to an extended inflammatory condition related to the presence of the tumour [171] could explain our observation. We exclude that the softening can be directly related to chemotherapy treatments, since we did not find any evident correlations in our patients (Figure 20B,C). These results show that human derived samples are complex and there are many factors (for example tissue repair or blood vessel formation) that contribute to the softening of ECM[183]. There are also reports that ECM degradation at invasive fronts renders a softer, less resistant ECM, facilitate invasion[183]. Nevertheless, it would be beneficial to increase the number of studied samples to see if the trend remains.

We then focused the analysis on the relative stiffening of neoplastic versus normal ECMs in each individual patient. The analysis of the mechanical properties according to the mutational status of *KRAS* and *BRAF* genes and across tumour grade showed that patients with mutations in *KRAS* gene had a slightly higher relative stiffnening, while a stronger relative increase is related to different tumour grade (G3 > G2). Since the presence of mutations in *KRAS* and *BRAF* genes is very common in PM and tumour grade is a parameter that characterizes tumour cell behaviour, they are probably associated to specific mechanical characteristics. These data are still preliminary and will be investigated with further experiments on a larger cohort of cases. We believe that such correlations would help to advance the development of biomechanical tests to complement standard clinical diagnostic techniques.

Understanding how modifications of the mechanical properties of the ECM influence the metastatic invasion may also have the potential in developing active tissue treatments that can impact on cell migration; ECM is already being used as a scaffold for cell culture to better understand the cell-microenvironment interaction mechanisms [50,51,148,184–187].

In conclusion, we provided evidence that in CRC-PM ECM stiffening correlates with collagen deposition and remodelling, CAF activity, age at surgery and tumour grade. Spatially resolved mechanical analysis of human-derived samples revealed significant spatial heterogeneity in the elastic properties of normal and neoplastic ECMs. The results, together with the high expression of αSMA, revealed that signs of pre-metastatic niche formation are already present in normal tissue, and correlation of mechanical data with patients' metadata showed interesting connections between the relative stiffening and characteristics of the tumour itself, in particular with patients' age and tumour grade. Our results suggest that nano- and microscale characterization of tissue mechanical properties can suggest the presence of metastasis and help in diagnostic procedures. A better comprehension of the mechanical properties of ECM will facilitate its use as a scaffold for culturing cells in future research, creating more reliable models of the disease.

Materials and methods

Sample preparation

ECMs were obtained from the peritoneal tissue of 14 patients diagnosed with CRC-PM (more detailed information is in ***Table*** 3).

The samples were collected during surgical resection at the Peritoneal Malignaces Unit of Fondazione IRCCS Istituto Nazionale Tumori di Milano as described in Varinelli et al. [50] The study was approved by the Institutional Review Board of Fondazione IRCCS Istituto Nazionale Tumori di Milano (134/13; I249/19) and was carried out following the Declaration of Helsinki, 2009. All experiments were performed in accordance with relevant named guidelines and regulations. Written informed consent was obtained from all participants.

Briefly, non-tumoral tissues were collected 10 cm away from tumour, according to standard clinical procedures[14]. Neoplastic-derived and normal-derived 3D decellularized extracellular matrix (3D-dECM) specimens were obtained as described in Genovese et al._[109]. 3D-dECM were embedded in OCT and then frozen in a liquid nitrogen bath of isopropanol. Frozen samples were cut into slices of 100-200μm thickness and immobilized on polarized glass slides (Thermofisher, Walthan, USA). Prepared samples were stored at -4°C and used for the AFM measurements.

Table 3 *Characteristics of the patients from whom the tissue samples were obtained. All samples were at stage IV.*

Patient	***Age***[5]	***Mutations at CRC-related genes***[6]	***Sex***	***Diagnosis***	***Grade***	***Location***	***Chemotherapy***
CRC-PM 1[3]	51	KRAS	Female	Mucinous Adenocarcinoma	G2	colon	Yes
CRC-PM 2	47	NONE	Female	Adenocarcinoma	G2	sigma	Yes
CRC-PM 3	40	NONE	Male	Adenocarcinoma	G2	colon	Yes
CRC-PM 4	82	ND	Female	Mucinous Adenocarcinoma	G3	right colon	No
CRC-PM 5[7]	66	BRAF	Female	Adenocarcinoma	G3	right colon	Yes
CRC-PM 6	71	KRAS	Female	Adenocarcinoma	G3	colon	No
CRC-PM 7	47	*NONE*	Male	Mucinous Adenocarcinoma	G2	rectum	Yes
CRC-PM 8	41	*KRAS*	Male	Mucinous adenocarcinoma	G3	sigma	Yes
CRC-PM 9[3]	43	*KRAS*	Female	Mucinous Adenocarcinoma	G2	right colon	Yes
CRC-PM 10[3]	60	ND	Male	Adenocarcinoma	G3	colon	Yes
CRC-PM 11[3]	63	NONE	Female	Mucinous Adenocarcinoma	G3	colon	Yes
CRC-PM 12	65	*NONE*	Female	Adenocarcinoma	G3	sigma	Yes
CRC-PM 13	82	#	Female	Colorectal neuroendocrine carcinoma	#	#	#
CRC-PM 14	61	*BRAF*	Male	Adenocarcinoma	G2	colon	No

---

[5] Age at surgery.

[6] KRAS and BRAF genes were analysed

[7] See Varinelli et al. 2022 [190].

AFM nanoindentation measurements

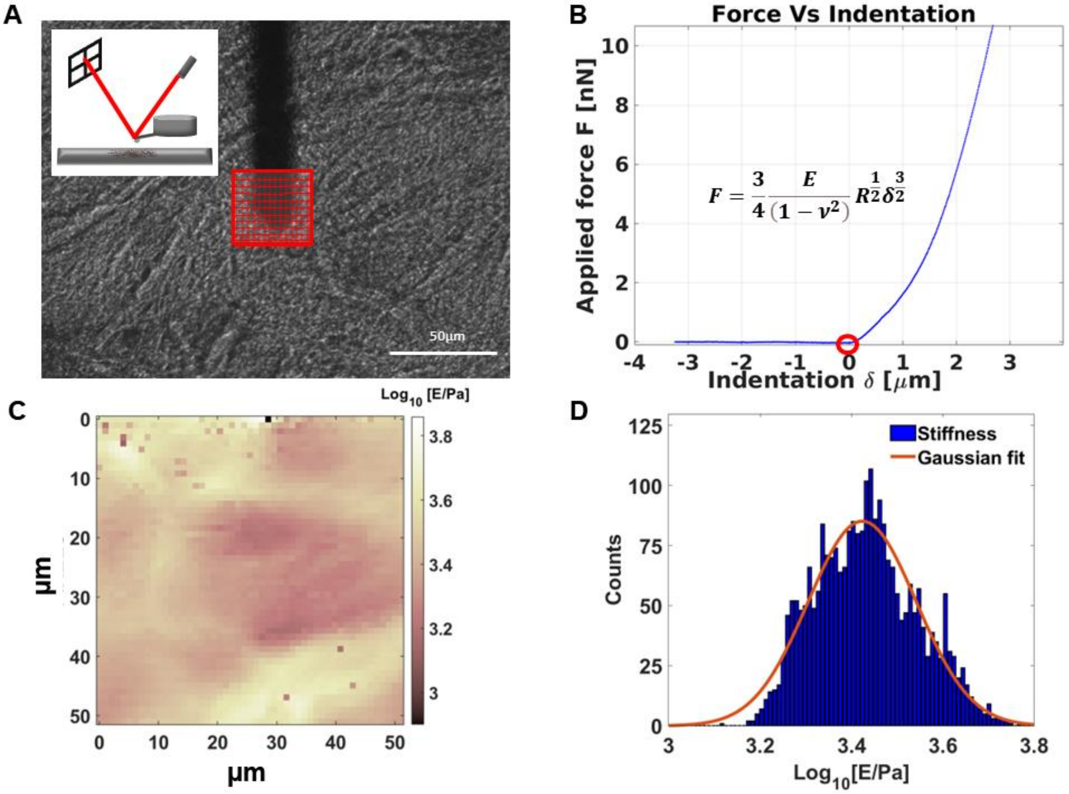

Figure 21. *Schematic representation of the nanomechanical measurement. A) Optical image of an ECM (normal peritoneum-derived from patient 8), with the AFM cantilever and the selected region of interest for the indentation experiment. Slices with thickness between 100 and 200 µm are semi-transparent, which allows to select regions for the analysis that look sufficiently uniform and smooth. The red grid represents the locations where force curves (FCs) are acquired (scale bar length – 50µm). In the inset, the experimental setup for indentation measurements and the optical beam deflection system are shown. B) Typical rescaled approaching force vs indentation curve. The red circle highlights the contact point. Only the portion of the curve characterized by positive indentation is considered for the Hertzian fit (Eq. 1 and also shown in the inset). C) The map of Young's modulus values extracted by the FCs acquired in the region of interested shown in A. D) Histogram representing the distribution of YM values represented in the mechanical map in C. Under the hypothesis of a log-normal distribution, a Gaussian fit in semi-log scale allows to identify the median YM value, as the centre of the Gaussian curve.*

The nanomechanical measurements were performed using a Bioscope Catalyst AFM (Bruker) mounted on top of an inverted microscope optical microscope (Olympus X71). To isolate the AFM from ground and acoustic noise, the microscope was placed on an active antivibration base (DVIA-T45, Daeil Systems) inside an acoustic enclosure (Schaefer, Italy). AFM measurements of cryosections were performed in a PBS droplet confined by a circle of hydrophobic ink.

AFM-based nanomechanical measurements were performed according to standard procedures, based on the acquisition of indentation curves, as described in Refs [89,99]. The measurement process is described schematically in Figure 21. We have used custom colloidal probes with spherical tips made of borosilicate glass beads with diameter (twice the radius R) in the range 18-25µm, produced and calibrated as described in Ref. [83]. The spring constant of the AFM probes (typically 5-6 N/m) was calibrated using the thermal noise method [106,122]. The deflection sensitivity of the optical beam deflection apparatus (in units of nm/V) was calculated as the inverse of the slope of the force vs. distance curves (simply force curves, FCs) collected on a stiff substrate (the glass slide holding the sample)[99] or using the contactless SNAP procedure[112].

The samples were studied by collecting set of FCs, also called force volumes (FVs), in different regions of interest (ROIs). Each FV typically covered an area between 50µm x 50µm to 125µm x125 µm and consisted of 100-225 FCs. The separation between adjacent FCs was chosen to be greater than the typical contact radius at maximum indentation, to reduce correlations between neighbouring FCs. For each patient's condition (normal or neoplastic), several FVs were collected on different, macroscopically separated locations on each sample, with 2-3 samples (cryosections) per condition (normal vs neoplastic) for each patient. In total, for each condition 2000-4000 FCs were collected. A FC typically contained 8192 points, with ramp length L = 15 µm, maximum load F_{max} = 800 – 1500 nN, ramp frequency f = 1 Hz. The maximum load was adjusted to obtain a maximum indentation of 4-6 µm in all samples.

Acquired data was analysed in MATLAB using protocol previously described in Puricelli et al.[89]. The elastic properties of the ECMs were characterized through their Young's modulus (YM) of elasticity, extracted by fitting the Hertz model [79,188] to the 20%-80% indentation range of the FCs (details in Ref. [13,89]):

$$F = \frac{4}{3}\frac{E}{1-\nu^2}R^{\frac{1}{2}}\delta^{\frac{3}{2}} \qquad (1)$$

, which is accurate as long as the indentation δ is small compared to the radius R. In Eq. (1), ν is the Poisson's coefficient, which is typically assumed to be equal to 0.5 for in-compressible materials, and E is the YM.

Finite thickness correction [89,114,121,189] was not applied since the thickness of the ECM slices (150-200µm) is significantly larger than the expected contact radius at maximum indentation. The first 20% of the FCs is typically ignored, due to the contribution of superficial non- crosslinked fibers, surface roughness issues, etc.[28].

Histochemistry (HC) and immunofluorescence (IF) analyses

Before HC and IF staining, formalin-fixed-paraffin-embedded (FFPE) blocks were prepared and cut as in Varinelli *et al* [50]. FFPE sections were stained with haematoxylin and eosin (H&E) for visualized nuclei and stromal regions. For HC analysis, sections were stained with picrosirius red (ScyTek lab), to visualize collagen fibers, following the manufacturers' instructions. Antigen retrieval IF analysis was carried out as in Varinelli *et al*[50] . For IF analyses, FFPE sections were stained with primary alpha Smooth Muscle Actin (αSMA,1:400), FITC conjugated antibody (Merck, KGaA) and DAPI (Merck, KGaA), following the manufacturers' instructions, to visualize respectively cancer associated fibroblasts (CAF) and nuclei. Images were acquired with a DM6000B microscope (Wetzlar, Germany Leica,) equipped with a 100 W mercury lamp, and analyzed using Cytovision software (Leica). All the experiments were performed in triplicate.

DNA sequencing

Presence of mutations in *KRAS* and *BRAF* genes was determined by DNA sequencing. DNA from FFPE sections of PM patient's tissues was used for mutational analysis and extracted as in Varinelli *et al*[50] . About 150–200 ng genomic DNA (measured with Qubit dsDNA HS assay kit, ThermoFisher Scientific), were sheared by the Sure Select Enzymatic Fragmentation kit (Agilent Technologies Inc., Santa Clara, CA, USA). NGS libraries, probe set design, DNA sequencing and data analysis were performed as in Varinelli *et al* [190].

Statistics

To evaluate the distribution of YM values that is peculiar of ECM in the different tested conditions, all values of the YM from all FCs were pooled together. This is justified in part by the fact that curve to curve distance is of the order of the maximum contact radius, and by the fact that separation between FVs from the same slice is comparable to the separation between FV from different slices obtained from the same patient. To highlight the diversity of local mechanical conditions met in the samples, we have used violin plots to represent the YM distributions (Figure 1A).

The evaluation of representative YM values for a specific condition of a specific patient has been done by pooling the median YM values obtained from all FVs collected in different ROIs and calculating their mean value and the corresponding standard deviation of the mean[171], assuming that the median values should be normally distributed according to the central limit theorem [191]. The distributions of median values are shown in Figure 1B. An experimental relative error of approximately 3%, evaluated using a Monte Carlo method [192], taking into account the uncertainties in the calibration factors (10% for the spring constant, 5% for the deflection sensitivity) was added in quadrature to the standard deviation of the mean to estimate the final error associated with the mean median YM values.

The statistical significance of differences between tested conditions was assessed using a two-tailed t-test. In case of a p-value <0.05, the difference was considered as statistically significant.

Data availability

The datasets generated and/or analysed during the current study are available from the corresponding authors on reasonable request.

Acknowledgements

This research was funded by the European Union Horizon 2020 research and innovation program under the Marie Skłodowska-Curie grant agreement No. 812772, project Phys2Biomed, and under FET Open grant agreement No. 801126, project EDIT. This work was supported by “5 per 1000” funds (2019 MUR and 2015 Ministry of Health, financial support for research) – institutional grant BRI 2021 “Harnessing the extracellular matrix to awaken the immune response in patients with peritoneal metastasis” assigned to Dr. Luca Varinelli, and by the Italian Ministry of Health, with a grant agreement No. RF2019-12370456. We thank the patients who participated in the study. We thank Hatice Holuigue for her valuable support and discussions.

5.4. Extracellular matrix scaffolds for cancer organoids cultures to study the mechanical aspects of cancer progression in peritoneal metastases

5.4.1. Introduction

Appropriate preclinical models are crucial for the effective dissemination of therapy options for patients affected by cancer. A great asset to cancer research and mechanobiology is to switch from simple 2D and in vivo models to more advanced 3D, ex vivo models [193]. The mechanical characteristics of 3D systems can be adjusted to create models that simulate a broad spectrum of tissue stiffness. What is more, in such models, cell adhesion, spreading, and migration are not limited to single layer. The sequestration/gradients of soluble biomolecules can be modulated to precisely control cell fate and differentiation, and the ECM can be tailored to produce the in vivo cell experience through various sets of chemical and mechanical signals. Many activities, whether through synthesis, degradation, directed migration, or mechanical signals, are fundamentally linked to cell-cell and cell-matrix interactions and cannot be adequately replicated in traditional 2D cell culture[42].

Developing 3D model requires the use of proper 3D culture platform. There are two types of platforms: scaffold-free and scaffold based (natural and synthetic), while the second one has application in tissue engineering and cell culture[25,42,194]. A highly innovative tool for building a tumour microenvironment (TME) with the necessary cellular and biomechanical properties is the combination of scaffolds and hydrogels. Patient-derived cell populations may be introduced into scaffold models, and further advancements may enable the use of bioengineered tumours as a platform technology to define clinical trial design[18,51]. There are several types of scaffolds which differ with their composition, mechanical properties, and degree of mimicking the real tissue[25,42,51] Among scaffold-based 3D models, the most represented ones are hydrogels, pre-made porous scaffolds[42,51,194,195], cell-derived ECM[25,51] and decellularized ECM from native tissue[25,74,109,185–187]. There is growing interest of using decellularized tissue since it provides more physiologically relevant and tissue specific microenvironment: closely recapitulate cell-ECM interactions and key biomolecular hallmarks and recapitulate the structure and composition of tissue-derived ECM[25,33,51,109].

Currently, there are many attempts to create 3D, scaffold free, artificial tumour microenvironment what helps to approach tissue complexicity[25,42,194]. Organoids are self-organizing 3D structures formed from stem cells, cancer cells, and other cells. This scaffold-free 3D model is considered to be one of the most physiologically relevant one. Organoids are easily able to include different cell types, and they can partially mimic organ function[42]. Patient-derived organoids have a lot of potential for molecular characterisation of tumour and individualized treatment. They have ability to self-organize, thus accurately recreate the original tumour's architecture and immunohistochemical markers[196]. Organoids derived from individuals with colorectal PM have been successfully created by many research groups, and they have been used to assess medication sensitivity[18,196,197]. There is an increasing interest in using organoids in cancer research, including screening of drugs against PM[196] or improving current therapies[198] because of its ability to accurate replicate the cancer landscape, including colorectal PM[18]. Organoids and engineered tissues derived from human tissue have the potential to be ground-breaking model systems. They can enhance drug discovery techniques and their efficiency as the starting point for advancements in regenerative medicine and cancer research[199].

Even though the tumour microenvironment plays a crucial role in the development and progression of cancer, surprisingly little is known about this environment's biophysical evolution. Unfortunately, there aren't many papers discussing the relationship between tissue mechanics and PM, but the findings of this study will provide light on the role of the ECM's mechanobiological properties in the development of pre-metastatic niches. The goal is to continue work initiated in *Varinelli et al. 2022* and to further evaluate the spatial 3D mechanical microenvironment of ex vivo engineered PM lesions and changes of nanomechanical properties in time. The "seed and soil" theory is being tested using normal and neoplastic dECM by looking at cancer cell colonization. This experimental study's goal is to create and verify a brand-new ex vivo model of the human peritoneum. The novelty of the model comes from using 3D native ECM as a scaffold to culture organoids. The aim of this study is to better understand the mechanisms that contribute to peritoneal metastasis development and, ultimately, to enhance treatment and prognosis.

5.4.2. Materials and methods

5.4.2.1. Preparation of ex vivo PM lesions

In this research samples from 2 patients diagnosed with PM from CRC were used. The detailed characteristics of patients are described in Table 4**.** The samples of peritoneal tissue were collected during surgical resection at the Peritoneal

Malignancies Unit of Fondazione IRCCS Istituto Nazionale Tumori. To obtain both normal and neoplastic 3D dECM, tissue biopsies were decellularized according to protocol described in *Genovese et al. 2014* [109]. In short, the protocol comprises of 6 washes with different solutions containing reagents that main aims are to dissociate cells stroma and to lyse them, remove lipid membranes and cell residues and finally degrade DNA and RNA[109].

Patient	**Age[8])**	**Sex**	**Protein mutation**	**Diagnosis[9]**	**Sample**
P2	47	Female	None	Adenocarcinoma, stage IV	Tissue and ECM from PM and normal peritoneum
P6	72	Female	Kras	Adenocarcinoma, stage IV	Tissue and ECM from PM and normal peritoneum
C1	70	Male	APC, G12S Kras, TP53	Moderately differentiated infiltrating adenocarcinoma	Organoids

***Table 4**. Characteristics of the patients from whom the tissue samples were obtained.*

The study was approved by the Institutional review board (134/13; I249/19) and was conducted in accordance with the Declaration of Helsinki, 2009. Written informed consent was acquired. The collection of the samples was previously described in the work of *Varinelli et al. 2022* [50]. The neoplastic organoids cell line was obtained from fresh tissue by following the protocol developed by *Fuji et al. 2015* [200].

To obtain engineered PM lesion we repopulated 6 specimens of 3D-dECMs derived from normal and neoplastic tissue with neoplastic organoids. The repopulation was done by following protocol described previously in *Varinelli et al. 2022* [50] . The night

---

[8] *Age of the patient on the day of the surgery.*

[9] *The stage of the cancer was determined according to the WHO classification* [157]

before repopulation, 3D-dECMs were incubated with fetal bovine serum (FBS) and antibiotics (penicillin and streptomycin). FBS was used to facilitate later proliferation and migration of cells after seeding. To seed neoplastic cells on 3D-dECM scaffolds, organoids were dissociated in single cells. To repopulate ECM scaffold, about one million of cells were resuspended in 1ml of Matrigel™ and poured onto 3D-dECM specimen Prepared samples were cultured for 5, 12 and 21 days. On each timepoint two specimens, normal and neoplastic, were taken to prepare samples for further analysis. Prior to snap-freezing procedure, ex-vivo PM lesions were washed with PBS and incubated in 10% formalin. This process aims to preserve integrity of sample before OCT embedding and freezing. However, using fixatives like formalin or glutaraldehyde can affect mechanical properties of biological samples by overstating elastic modulus[10].It is important to use protocol of mild fixation (low concentration of fixative, short time of incubation) or to find an alternative to strong fixatives After 1h samples were frozen in liquid nitrogen bath of isopropanol and cut into cryosections.

In this work, I studied and compared 10 different experimental classes, including 2 controls: native tissue and decellularized ECM (dECM) to verify to which extend 3D-dECM repopulated with cells recreates nanomechanical properties of native tissue and to see how presence of cells affects ECM stiffness (Fig. 22).

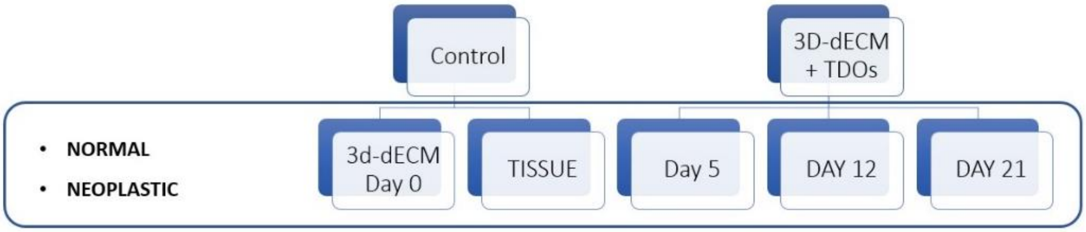

***Figure 22**. Diagram of experimental classes included in this research.*

5.4.2.2. AFM nanoindentation measurements

The steps of sample’s preparation were previously described in *Varinelli et al. 2022* [50]. Briefly, bulk samples of control and repopulated dECM were embedded in OCT and snap-frozen in liquid nitrogen bath of isopropanol and then cut into slices with the use of cryostat [Leica, CM1900-1-1].

The samples were measured as cryosection slices (thickness of 100 µm -200µm), prepared following steps described in Chapter 5.3[77].

The AFM nanoindentation measurements were performed following steps and using parameters optimized in previous works[13,50,77]. Cryosections were subjected to AFM measurements in a PBS droplet enclosed by a circle of hydrophobic ink. By gathering sets of generally 100–225 force curves per force volume (FV) in various macroscopically distinct locations of the sample, the mechanical characteristics of ECMs were investigated. Each FV normally covered a space from 50µm x 50µm to 125µm x125 µm. Each FC had 8192 points and had a maximum load of 800-1500nN and a ramp length of 15 µm. The aim was to collect around 20 FV per each experimental class, however, due to poor quality of cryosections, number of measured FV was below 10.

5.4.3. Results and discussion

5.4.3.1. Nanomechanical properties of ex vivo engineered PM lesions

The aim was to compare different samples (Fig.22), knowing that they contain or lack different elements, since repopulated sample aims to mimic native tissue; comparing dECM with repopulated one helps to understand the role of ECM in tumour progression and also as a scaffold for 3D models. AFM nanoindentation measurements revealed significant stiffening of both normal and neoplastic 3D-dECM repopulated with neoplastic organoids, from day 5/6 to 21 (Fig. 23AB). After repopulation with neoplastic cells, PM lesion model on day 6 of patient 2 was softer than ECM and tissue (Fig 23A) In case of repopulated normal sample, Young's modulus increases of 100% while for neoplastic one of 50% comparing day 6 and 21. Additionally, on 21st day both normal and neoplastic samples reached almost the same YM value, and it can be expected that longer cultured ex vivo lesions would reach the values of native tissue (Fig 23A). In patient 6 the stiffening was also significant especially in case of normal PM lesion – 140% increase of YM value from day 5 to 21 and 90% in neoplastic sample. (Fig. 23B)

Referring to control samples, in both patients' native tissue tends to be stiffer than bare ECM, which suggests that presence of cells in tissue significantly affects its mechanical properties and makes tissue more incompressible material. Single cells in standard 2D culture are softer than matrix microenvironment, nevertheless 3D environment and presence of cell-ECM interaction affects cells properties, including increase of cells elastic modulus[49,195,201]. Overall, normal ECM-based ex vivo PM lesions tend to become more stiffer comparing to neoplastic based samples. It indicates that processes of ECM remodelling (activity of MMP) and crosslinking (activity of LOX) are initiated in both normal and neoplastic PM lesion, however these processes are taking place more intensively in normal ECM based sample, what could be observed especially in case of patient 6. Live imaging experiments have demonstrated that cancer cells move quickly on collagen fibers in collagen-rich environments[23,202]**.** Since tumour cells migrate rapidly on collagen fibers already deposited in neoplastic ECM, there were no requirement of desmoplasia, nonetheless, cancer cells introduced to non-tumour microenvironment had to initiate ECM remodelling and collagen deposition causing strong stiffening (Fig. 23)[23]. Other research, performed on dECM derived gel from normal lung and liver tissue revealed that the normal derived dECM instructs cancer cells to develop greater metastatic potential[203].

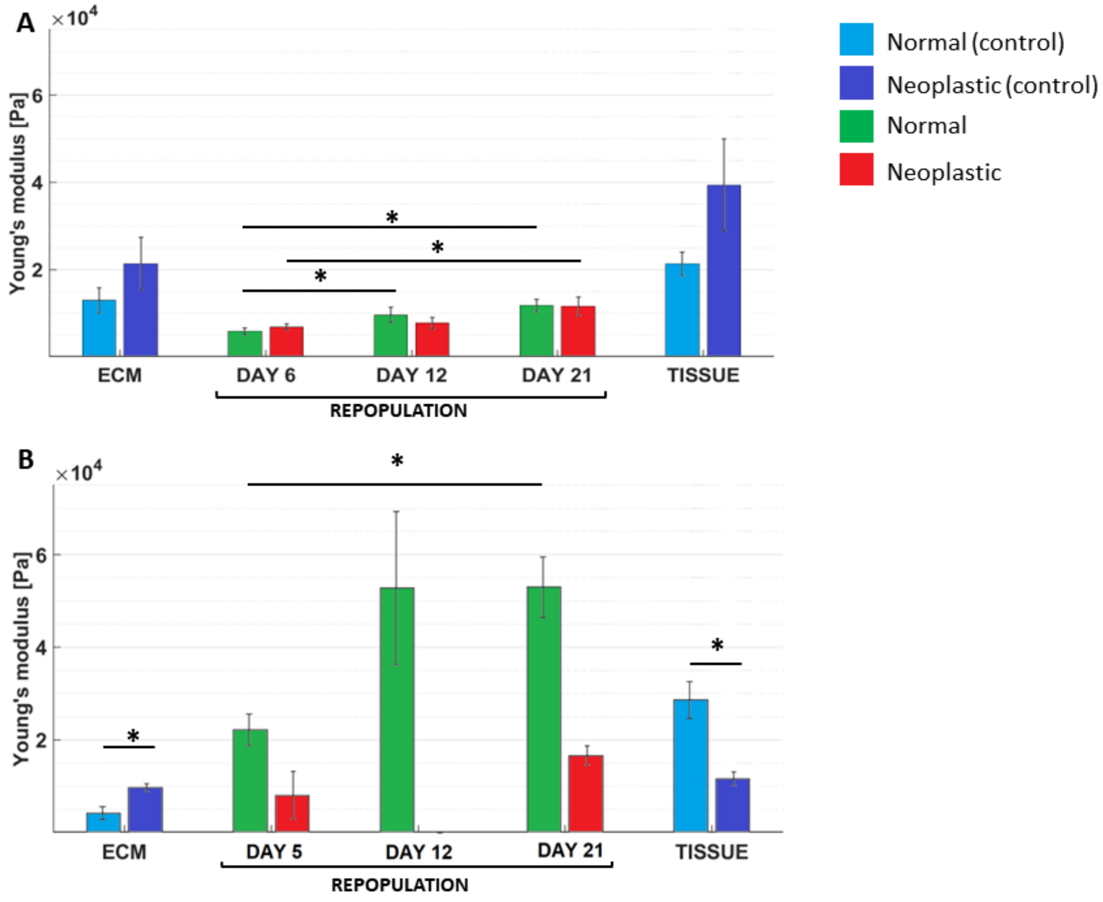

Figure 23*. The elastic modulus of control samples and ex vivo lesions in three timepoints of patient 2 (A) and patient 6 (B). The bars were plotted based on mean of the medians of force volumes collected in each experimental class. Error bars stands for standard deviation of the mean and asterisk means significance p<0.05.*

Similar research, performed by *Genovese et al 2014.* revealed that CRC-derived ECM supported the invasion of neoplastic cell lines (LoVo and SW480) which suggests that tumour cells and tumour-associated cells reorganize the original tissue to facilitate the invasion of the transformed cells[109]. These results support the hypothesis, that cancer cells introduced to neoplastic environment do not need to further modify ECM to migrate and proliferate.

It is well known that cells are able to detect and react to the topographical and mechanical characteristics of their substrates. Different cell activities, such as cell adhesion, migration, proliferation, and desmoplasia, are connected with differences in the stiffness and microscale properties of the ECM[49,195,201]. Based on this knowledge and presents results we can conclude that neoplastic cells introduced to microenvironment of different elastic modulus and biological characteristics (normal vs. neoplastic) will express different behaviour.

5.4.3.2. Changes in elastic modulus distribution in ex vivo engineered PM lesions

It was previously shown that insights into mechanical and structural heterogeneity of the samples can provide additional information about progression of changes in nanomechanical properties[77]. Nanomechanical properties of native tissue (both normal and neoplastic) were studied as a control to verify to which extend ex vivo PM lesions recapitulate native tissue. Presented model recapitulated variation in TME-ECM composition\macromolecular ration, and ECM mechanical properties during peritoneal metastasis. It is ideal to screen for more successful therapies using a patient-specific model that shows the changing environment of both the stage and the patient's TME. In order to serve as patient-specific platforms that can help doctors decide on the best therapeutic approaches, in vitro dECM tumour models should ideally aim to replicate tumour tissue specificity and cancer stromal cell heterogeneity[51].

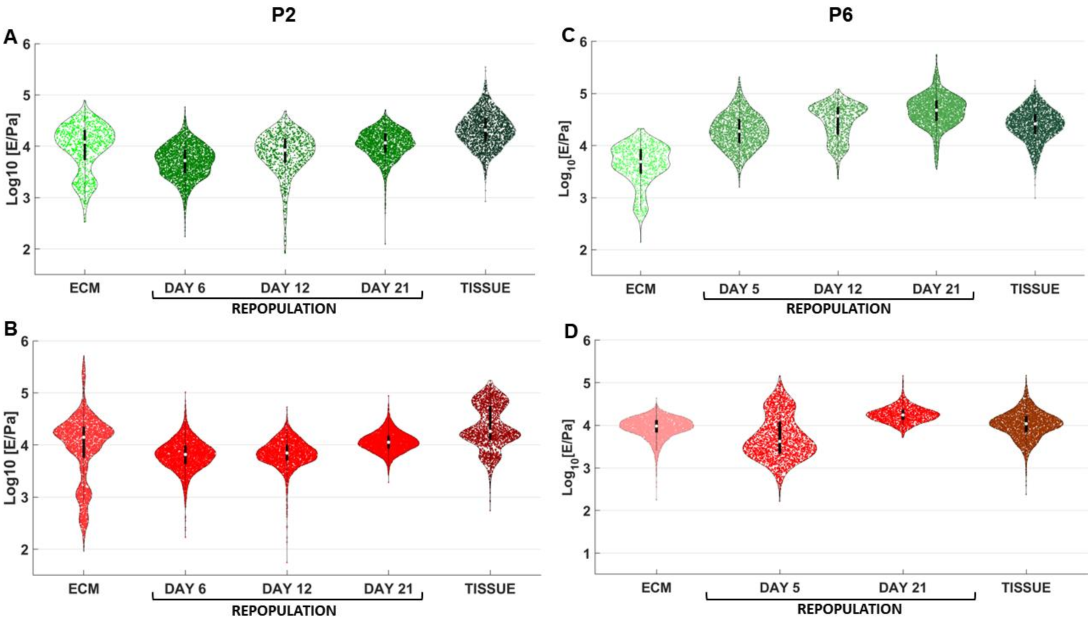

Figure 24 *Violin plot presenting distribution of YM values of normal (A) and neoplastic (B) samples from patient 2 and normal (C) and neoplastic (D) samples of patient 6. Each point represents single force curve. The white point shows median value, thick black lines are upper and lower quartile*[146]*.*

Violin plot is an alternative to standard boxplot because it better highlights the distribution of the data, allowing to see multimodal distribution[146]. In case of patient 2 we can observe bimodal distribution of YM values in normal ECM and to a small extent on day 6. With time, repopulated samples become more uniform, like the native tissue (Fig. 24A). Analogous situation occurs in neoplastic samples: before repopulation with organoids ECM is heterogenous; after repopulation, distribution of YM values narrows. However, in neoplastic tissue multimodal distribution can be observed (3 groups) (Fig 24B).

In patient 6, YM values arrangement in normal ECM is also bimodal (Fig. 24C), like it was observed in patient 2 (Fig.24A). Hence, on day 5th after repopulation, sample become stiffer and more uniform. Interestingly, after 12 days from repopulation, distribution becomes once again bimodal but with a strong shift towards stiffening what can be observed on 21st day (Fig. 24C). Neoplastic ECM of patient 6 is the only example where stiffness is uniform, yet after culturing cells on ECM scaffold for 5 days sample shows bimodal heterogeneity (Fig. 24D).

This event can be an outcome of sample preparation: organoids dissociated to single cells suspended in 1ml of Matrigel™ are seeded on top of ECM. Matrigel™ disintegrate in the first days after seeding and its residual components are removed during routine changes of medium. Despite that, some residues could be still present on 5th day and affect measurements as the Matrigel™ is a type of hydrogel with stiffness around 440Pa[204]. Matrigel™ is composed of mostly of laminin and collagen and aims at mimicking basement membrane which in peritoneum is composed of collagen IV and laminin[17,204,205]. As mentioned before in "Preparation of ex vivo PM lesions" (Chapter 5.4.2.1), cells are seeded on top of the scaffold and start to migrate into the dECM. 12-14 days is considered a period sufficient for the cells to colonize dECM matrix surface and also migrate into the deeper parts of the scaffold[50,206]. Knowing that cell distribution in not even through the engineered PM lesion, thus ECM remodelling and cell-ECM interactions occur at with different intensity. This could explain variety in YM values distribution PM lesion samples. In the work of *Jin et al. 2018,* MCF-7 (neoplastic cell line) were cultured both on normal- and neoplastic-derived breast tissue. Results showed that MCF7 cells could grow in cancer tissues, although normal tissues allowed the cells to migrate but prevented cell proliferation[207]. These results are in agreement with previous observations that cells behave differently when introduced to different microenvironment (normal or neoplastic).

5.5. Conclusions

Even though PM is associated with low survival rate, using more reliable and personalized approaches would help to better understand formation of pre-metastatic niche and mechanisms of PM development and ultimately to develop more effective therapeutic strategy.

Chapter 5.2 mentions the development of ex vivo engineered metastatic lesions: from successful decellularization to long term culture of neoplastic cells. The results prove effectiveness of this model in mimicking tumour microenvironment and its possible application in drug screening[50]. However, given the limited amount of tissue accessible and potential for introducing additional differences in composition or structure (based on clinical history), sampling from patient-derived ECM demands more caution regarding appropriate patient stratification and more detailed investigation of ECM mechanobiological properties[51].

Studies on dECM from patients diagnosed with stage IV adenocarcinoma has demonstrated broad variety of mechanobiological properties, which could be associated with patients's data: type of mutation, age and sex. By correlating AFM nanoindentation studies with additional biotechnology techniques, research revealed strict correlation between CAF activity, collagen deposition and nanomechanical properties of ECM. Studies in Chapter 5.3 revealed also that ECM of future metastatic organs are actively and selectively transformed by the main tumour before metastatic spread has taken place, as opposed to being passive recipients of circulating tumour cells[23,160,208]. Research on ECM from many patients, and further studying some of them as ex vivo PM lesions, revealed vast diversity between patients, and highlighted importance of patient-oriented approach in research. Moving forward it will benefit for more personalized treatment strategies[50,77]. ECM of future metastatic organs are actively and selectively transformed by the main tumour before metastatic spread has taken place, as opposed to being passive recipients of circulating tumour cells.

Using 3D ex vivo engineered PM lesions as an experimental model proved superiority over other models that allowed to perform studies for period of 72h[155] or 5 days[17]. Additionally, many models use commercially available cell lines, cultured as single cells or spheroids[17,155,194], while model presented in chapter 5.2 and 5.4 is based on using organoids, more advanced 3D model[50]. The disadvantage of native tissue-based models is dependency on surgeries while synthetic matrices can be easily prepared and modified to adjust components composition and stiffnes[194,195]. After seeing that rigidity of repopulated samples changes over time, what was an outcome of interaction between cells and their microenvironment. Thus, it would be interesting to decellularize again the PM models and to test the mechanical properties of dECM, exclusively. It would help to better understand the changes that have taken place in the dECM and to understand the influence of cells on ECM. Nevertheless, this approach will require pre-liminary research and optimization of decellularization procedure. Considering advances of this approach, research on ex vivo PM lesions will be extended of this additional step.

The remarkable adaptability of AFM has contributed significant quantitative insights to our current knowledge of the mechanical changes during PM and the function of the tumour cells in modifying ECM, to generate a more favourable and conducive milieu for tumour development.

The ECM is an active participant in the majority of important cell behaviour and developmental processes. The ECM's functional diversity and dynamic character make it a critical target whose dysregulation may be a rate-limiting step in the development of cancer; this makes an ECM an attractive target to study development of pre metastatic niche, not only in PM but also in other types of cancers. Tissue-derived ECM may be helpful to recreate human microenvironments for testing drug effectiveness in the tumour microenvironment and adverse effects on cells seeded in normal or tumour-derived ECM. What is more, this technology could potentially to limit the usage of animals[42,51,109].

6. Study of nano-mechanical properties of spheroids

6.1. Introduction

6.1.1. Spheroids as a 3D model in biotechnology research

The 3D architecture of human solid tumours, which offers ideal circumstances for cellular organization, proliferation, and differentiation, is one of their key characteristics[78]. Three-dimensional (3D) cell culture provides significant benefits in precisely mimicking the in vivo architecture and milieu of healthy tissue, organs and solid malignancies. In vitro 3D cell culture methodologies—both scaffold-based and scaffold-free—have developed in recent years as a workable alternative to both conventional 2D cancer cell cultures and in vivo animal testing[205]. Additionally, the mechanical characteristics of three-dimensional systems may be adjusted to create models that replicate a variety of tissue stiffness[209–211]. Spheroids are typically applied as study models in many types of research, especially in drug efficacy and toxicity trials but also in the investigation of organ development and congenital diseases, tissue engineering, and 3D bioprinting [42,43,205,212–216]. Spheroids are now the most desirable 3D model to create a uniform, repeatable cell structures and a potential starting point for building big tissues and intricate organs[41,42,212,213,217].

Spheroids generated by aggregating cells result from single cells in suspension self-assembling owing to embryogenesis, morphogenesis, and organogenesis. Complex homogeneous and heterogeneous binding of integrins, ECM proteins, and cell adhesion molecules is required to develop spheroids[43,218]. Intercellular adhesion molecules, among other systems and molecules with adhesion capabilities found in cells, are essential for intercellular communication. The cadherin superfamily (especially E-cadherins), regardless of whether it is dependent on calcium ions or not, is the principal mediator of cell-cell contacts, either by homophilic and heterophilic bonding or by affinity to specific receptors. Furthermore, proteins and cytoskeleton integrins stand out as possible causes of cell aggregation and compaction of 3D formations during advanced developmental stages[205,212]. A sequence of covalent cross-links is created to solidify the matrix-cell relationship when intercellular adhesion is established, resulting in the production of ECM, which binds to the cytoskeleton by the anchoring proteins and forms a complex network of connections. In truth, cadherins and ECM proteins types, as well as their concentrations, may change depending on the cell type, and cell-cell interactions with ECM proteins. This is what drives cell aggregation in addition to a spontaneous process of cell-cell contact[212,213,217,218]. Cell proliferation, differentiation, mechano-responses, and cell survival may all be greatly impacted by increasing the dimensionality of the ECM around cells from 2D to 3D[41,205]. When compared to monolayer cultures, the ECM composition of spheroids is significantly different[219].

6.1.2. Structure of spheroids

Spheroids feature three concentric zones with different cell populations: an outer zone with a high rate of proliferation and migration; a middle, quiescence zone; and an inside zone with necrotic cells (Fig. 25)[41,217,220]. The intricate circulatory networks that sustain tissues in vivo for oxygenation, nutrition, and waste elimination are still missing from the existing 3D systems. These tasks are the ones that 3D cultured cells can do through diffusion. This model still poses difficulties for bigger spheroids but is not problematic for smaller spheroids. The dispersed oxygen, carbon dioxide, and nutrition distributions of a 3D cell spheroid are schematically depicted in Figure 25, along with typical zones of cell growth. Because of this diffusion method, cells at various depths from the spheroid/aggregate surface are in various nutritional states and, as a result, are in various phases of the cell cycle[205,218]. As a result, the peripheral layer of the spheroids' cells is exposed to enough oxygen and the medium's growth factors, which encourage cell multiplication. The intermediate layer's restricted growth factor diffusion drives cells to enter the quiescent phase of the cell cycle[218].

In the proliferative zone and the quiescent zone ECM is equally distributed[220]. Therefore, the stiffness (linked with high density of ECM components) at the cell surface may regulate tumour metastasis, medication penetration, and tumour development and proliferation[201,220]. The necrotic death of cells at the innermost layer is brought on by the lack of nutrients and oxygen as well as the build-up of metabolic waste[217,218]. It is essential to evaluate anti-cancer medicines in the region of hypoxia, to better understand drug penetration; indeed, one of the factors that contribute to tumour treatment resistance is hypoxia. It is crucial to comprehend sample heterogeneity, especially when studying the mechanics of biological samples.

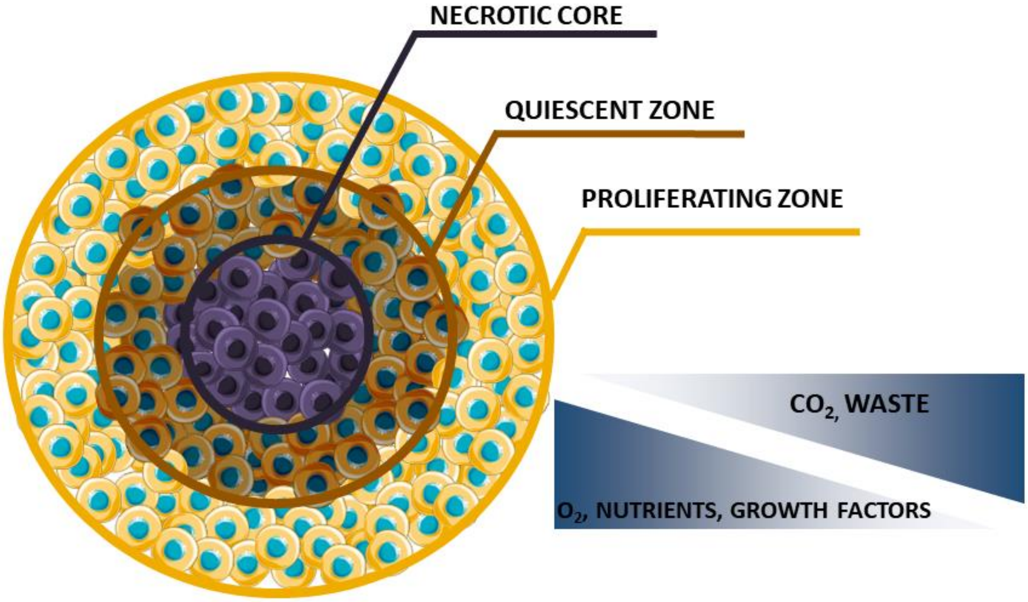

Figure 25. *Scheme of multicellular spheroid. The most proliferating cells are found on the aggregated spheroids' surfaces, whereas the most quiescent or necrotic cells are found inside the 3D cell bodies*[41,213,217,218]. *[Parts of the Figure were drawn by using pictures from Servier Medical Art. Servier Medical Art by Servier is licensed under a Creative Commons Attribution 3.0 Unported License (https://creativecommons.org/licenses/by/3.0/)].*

Using 3D cellular models in biotechnology has many advantages over traditional 2D cell culture method[41]. Spheroids' cells frequently start exhibiting traits that are distinct from those of monolayer cells, such as the deposition of ECM, the production of growth factors, and gene expression patterns. Researchers are interested in spheroid culture because it is straightforward, reproducible, and comparable to physiological tissues by mimicking *in vivo* processes like embryogenesis, morphogenesis and organogenesis[218]. The attractivity of using spheroids simply comes from many advantages provided by the 3D cell culture system[41,212,213,217,218,221]. Three-dimensional culture provides a much softer environment compared to the plastic, flat surface of the culture flask. This flat surface in 2D culture allows for stronger adhesion and cell migration; meanwhile the 3D environment and presence of ECM components restrain migration and invasion[41,218,221].

Another advantage of 3D models like spheroids is that they allow for gradients of soluble factors, and biomolecules based on diffusion through this gel or cell aggregates. The growth and proliferation of cells in 2D monolayers are homogeneous because they have access to an equal number of nutrients and growth factors available in the media[41,213]. Cells in 3D culture organize into spheroid-like structures, which environment privileges cell-cell and cell-ECM interactions over cell-substrate interactions[217,218]. The method of cell culture affects their polarization. 2D cell culture forces automatic apical-basal polarization while cells embedded in gel or surrounded by other cells generate apical-basal polarity on their own[41].

6.1.3 Spheroids as a tool to study mechanobiology of cancer

The spheroids can partially mimic the tumour microenvironment which allows for better recapitulation of patient tumour, which represents a promising challenge to improve the success rates in anticancer drug development and study of cell-ECM interaction, cancer biology, including cancer initiation, invasion and metastatic processes[78,213,217,220]. It is known that mechanobiology plays an important role in tissue homeostasis and affects cell behavior, thus it is important to study also mechanical aspects of carcinogenesis and metastasis. From increasing interest in studying mechanobiology and the role of mechanical properties of cells and ECM in cancer arise the need to study spheroids in the context of their rigidity. Characterization of spheroids' mechanical properties will enable the application of this model in further research, including the role of rigidity in PM and cell-ECM interactions.

Referring to the work presented in Chapter 5, to further focus on PM from CRC, two cell lines were selected to culture spheroids for this research.. HT-29 is a colon adenocarcinoma cell line, often resulting in metastasis to the peritoneum[19,157,222]. As a comparison, the CCD18-Co cell line (colon fibroblasts) was chosen.

The absence of straightforward and standardized procedures for spheroids imaging, analysis, quantification, and automation for future clinical uses is a major limitation to using of spheroids in preclinical investigations. In contrast to 2D cell cultures, there is less knowledge about the protocols, methodologies, and technologies that can be utilized to analyze spheroids' characteristics and mechanobiological aspects, making it difficult to standardize the output data analysis[205].

Understanding the mechanobiology of living cells requires precise measurement of their mechanical characteristics. Many techniques allow for studying the elasticity of cells. The most common ones are micropipette aspiration, AFM[76,103], particle tracking microrheology[223], magnetic twisting cytometry[224], and more[225]. The molecular foundations of cellular mechanics have been partly explained thanks to these techniques, but they are labour-intensive, expensive, and, most significantly, have limited experimental throughput[226]. Additionally, the recent shift towards 3D cellular models, like spheroids, requires adaptation or modification of current methods to new samples or even the developing new techniques.

Spheroids are complicated living materials, though; because of this, temperature fluctuations and cytoskeleton remodelling frequently allow them to display both viscosity and the elasticity of a solid. Typically, in such a case, the elastic constitutive relation in AFM data cannot be used to uniquely establish the mechanical properties of cells[225]. The great advantage of AFM is the possibility to use various measurements modes and AFM tips geometries that broaden the range of measurement approaches. On the other hand, AFM measurements are limited to interaction between the tip and sample surface. While it is not an issue in the case of samples like cryosections, it might be an obstacle for bigger samples with complex structures. Thus, it is expected that AFM nanoindentation measurements will be the most suitable tool to study spheroids up to the scale of multi-cellular organization.

Aiming at having a bigger picture of mechanics of spheroids it is beneficial to study sample with more than one technique. Microfluidic cytometry was adapted to determine the mechanical characteristics of spheroids in extensional flow and used as an alternative to AFM nanoindentation investigations. This method could supplement AFM experiments, provide a new approach to understanding the mechanics of spheroids as a single body. This method is based on standard assumptions of flow cytometry, yet here the focus is on the transition from deformation to relaxation state, while standard methods study only the deformation of particles during the flow through channel[71,227].

6.1.4 AFM in mechanobiological research on spheroids

In the recent years, AFM also found its application also in mechanobiology to study various biological samples like proteins, cells and their components, extracellular matrix, and tissues[61,74,78–80,85,86,89,91,154,228]. Each sample and experiment type requires choosing the most suitable AFM probe, considering its geometry and stiffness[85,106,115,229,230].

Nowadays, producers can provide different types of AFM probes made of different materials[61,84,115], with different lengths and shapes of cantilever[229–236], and tips with various geometries[115]. Among various geometries of tips, the most common are: pyramidal, conical, and colloidal ones. New approaches to AFM measurements required creating new, more customized shapes of the tip: blunted pyramidal[113], needle[121,237,238], or cylindrical[116] for more advanced and peculiar experiments[98].

The versatility of AFM and its components meets the requirements for studying complex samples like 3D biological systems, including spheroids. Knowing that spheroids are composed of different elements and their structure is organized in various layers (Fig. 25)[41,213,217,218], it is crucial to consider it while designing an experiment. Planning studies of the mechanical properties of spheroids, two main approaches can be considered: measurements of the spheroid as a single body or extracting YM values of single cells or ECM of the spheroid. Considering the complex structure of spheroids, their size, and the size of the tip, it is more likely that AFM will be more suitable for studying single cells and outer layers of the spheroids. AFM is a tool that allows for creating topographic maps of the samples, which have already been applied on spheroids[220]. The main advantage of AFM is that there is the possibility to adjust the experimental set-up of AFM, including measurement modes, parameters and especially AFM probes[85,95,96,98,115].

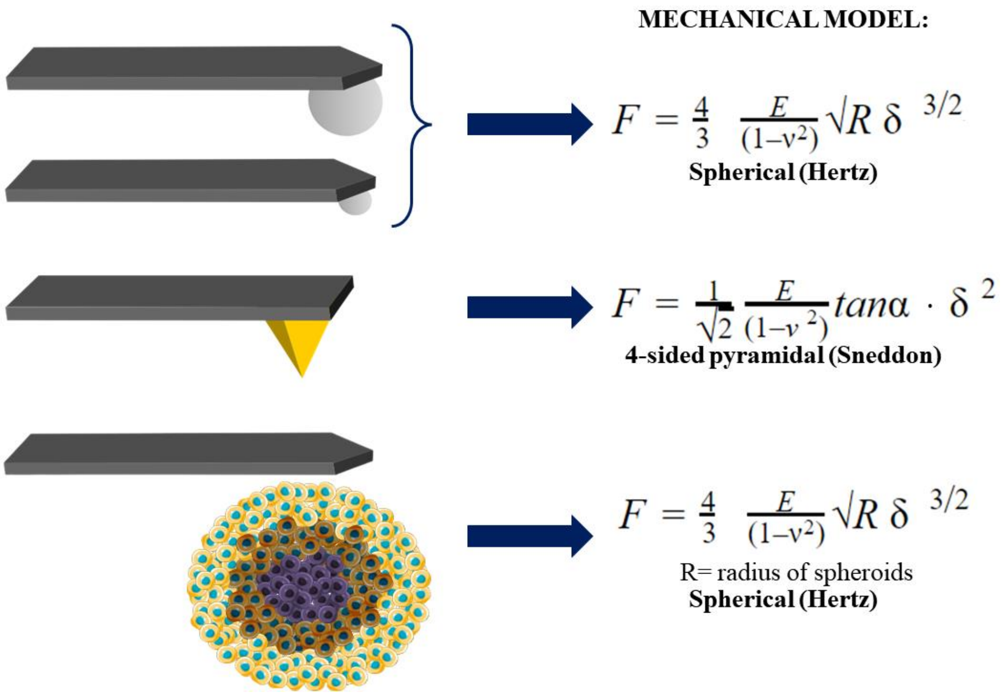

Figure 26. *Schemes of AFM probes with tips of different geometries and the models that can be applied to extract YM from measurements done with different probes*[95,98,113,188].

The choice of the contact mechanics model required to convert force-indentation curves into elastic moduli is the most fundamental and long-standing problem. Contact mechanics models based on Hertz, Boussinesq, or Sneddon theories are frequently used in cell nanomechanics. The relationships between Young's modulus, indentation, and force are expressed analytically in those models[98]. Hertz model, with some modifications, can be applied for different types of tips, depending on their geometry, mostly for spherical and pyramidal or conical tips indenting an elastic half-space (Fig. 26)[79,95,98,113,116]. It is important to note that the elastic response of the system to the force applied by the probe depends on the mechanical properties of the sample, probe, and on tip-sample contact geometry[79,90,113,239]. During tip-sample contact, the indentation depth (δ) and contact area (a) increase with applied force (F)[98]. Also, the stiffness of the cantilever, which depends on the cantilever length and shape (most commonly rectangular or triangular), plays an important role, since it should match the stiffness of the studied sample[115,229–231]. An important requirement for AFM studies is that the sample must be immobilized since AFM measurements need interaction with the studied specimen. Immobilization of adherent cells is easily accomplished by growing them in monolayers, typical two-dimensional tissue culture plastic or glass (referred to as 2D culture), or on top of ECM hydrogels (referred to as 3D culture on top)[33,240]. In the case of 3D models, e.g., spheroids, this issue is already under studies[70,220,240] but still requires optimization, and it will be further discussed in this section.

Eventually, the size (and geometry) of the indenting tip should be tailored to target the mechanical properties of specific components of the system (in the case of spheroids, the single cells or their compartments), or the effective combined response of several such components (cell clusters, the spheroid as a whole, or its layers – superficial, necrotic etc.). The characteristics of different probes was discussed in Chapters 3.1.1 – 3.1.3.

6.1.5. Microfluidic cytometry in extensional flow

Compared to traditional single-cell rheological tools, recent microfluidic technologies that infer cellular mechanical properties from analysis of cellular deformations during microchannel traversal have significantly increased throughput[71,72,227,241–243]. However, the extraction of material parameters from these measurements remains quite challenging due to issues like the dominance of complex inertial forces[226]. The viscoelastic response of complex systems made of several types of polymers, such as cells or tissues, is characterized by a continuum of relaxation times, therefore the relaxation dynamics develops across a large variety of time scales. The structure and mechanical characteristics of the polymeric network may be the cause of dissipative stresses inside the material, but the movement of liquid through the porous matrix may also have an impact[244].

Cell sorting and mutual tissue spreading are two examples of morphogenetic cell rearrangements that have been likened to immiscible liquid behaviour because of how similar they are. This resemblance has led to the hypothesis that tissues behave like liquids and have a distinctive surface tension, which is a collective, macroscopic feature of collections of moving, cohering cells[245].

The linear stress-strain relationship: $\sigma = E\epsilon$ (Hooke's law) between stress and strain is relevant for the majority of materials that are classified as solids, where E is the Young's modulus[244]. Shear stress in turn relates to strain rate $\dot{\epsilon} = \frac{d\in}{dt}$ in viscous fluids, which exhibits a completely different behaviour (with constant viscosity η):

$$\sigma = \eta\frac{d\epsilon}{dt} \qquad \text{Eq. 10}$$

Viscoelastic materials possess both characteristics of pure solids and fluids: their stress-strain relationship changes with time, which typically implies a time (or frequency) dependent Young’s modulus. Creep and relaxation are phenomena that viscoelastic materials display as a result of this time-dependency. The characteristic known as creep is when strain grows over time while the applied tension remains constant. Contrarily, stress relaxation refers to the reduction in stress when strain is maintained at a consistent level. In mechanobiology cells and tissues are considered as viscoelastic bodies[244,246], thus, the same assumption can be applied to spheroids as they are aggregates of cells.

Shear stress is the main cause for deformation of elastic particles, including cells and spheroids, e.g. inside a microfluidic channel[227]. The works of *Nyberg et. al 2017* and *Gerum et. al 2022* describe the use of microfluidic cytometry to characterize deformation of cells[71,227]. Methods of deformation cytometry have potential for application of mechano-phenotyping in variety of applications[247]. Cells are deformed by inertial flow's hydrodynamic forces on a microsecond time frame[227]. Although this method makes it easier to analyse large populations, it is difficult to predict and compute the external forces on single cells. A continuum elastic model[248] , which describes these shape changes accurately, allows to measure elastic modulus for individual cells. The shear stresses of fluid flow cause cell deformations. However, the initial deformation into microfluidic constrictions is dominated by particle deformability [227,249,250]; cells and particles with a higher elastic modulus exhibit longer deformation timescales. Other factors that can affect how quickly cells transit through microfluidic constrictions include cell size, channel size, and mechanical properties[248,250].

When cells are dispensed from the channel, they experience stresses due to extensional flow. It is significant for the design of new microfluidic approach in mechanobiology studies to assess the impact of the dispensing process.

Microfluidic cytometry in extensional flow has potential to be a novel technique that can be an alternative or supplement of existing techniques, for example standard microfluidic cytometry, AFM, optical stretching or micropipette aspiration. Extensional flow technique is a derivation of standard microfluidic cytometry that was already investigated in the context of studying cells viscoelastic properties[251]. It can be also applied study mechanical properties of spheroids, while standard microfluidic cytometry aims at studying small particles – cells. Considering that spheroids are complex biological model, consisted of several layers (Fig.25) and different components (cells and ECM) it is worth to consider their elastic properties with a focus on not only single elements but also on overall mechanical response of a spheroid as a single body, where these single elements and their interactions contribute to final elastic modulus.

6.2. Aims of the study

An attempt to develop and optimize suitable procedures was taken to meet the needs for studying the mechanics of spheroids. In this research, two methods were applied, AFM working in indentation mode and microfluidic technique.

The first objective was to optimize the culture of the spheroids to fit the technical needs of the instruments. In the case of AFM, another challenge was to develop an experimental setup that would allow data acquisition. Considering the different characteristics of AFM probes, and the complex structure of spheroids (see Chapter 6.1.2), a series of measurements were done. The measurements were performed using various tip geometries (see Fig. 26).

As an alternative to AFM nanoindentation studies, the technique of microfluidic cytometry was also adapted and applied to extract the mechanical properties of spheroids. The aim was to develop a method that could complement AFM studies.

6.3. Development of the protocol for AFM nanoindentation measurements of multicellular spheroids

6.3.1. Materials and methods

6.3.1.1. Cell culture

Two different cell lines were used in this research: HT-29 (colon adenocarcinoma) and CCD18-Co (colon fibroblasts). Both cell lines were kindly provided by prof. Małgorzata Lekka from the Institute of Nuclear Physics of the Polish Academy of Science. Cell lines were cultivated in an incubator at 37°C and 5% CO2 using RPMI 1640 culture media (for HT-29) and advanced MEM (CCD18-Co) supplemented with 5% and 10% FBS, respectively, 1% penicillin/streptomycin, and 1% amphotericin (Galaxy S, RS Biotech). If not stated otherwise, all bioreagents and materials came from Sigma Aldrich.

6.3.1.2. Spheroids culture

There are different strategies to obtain spheroids. Microfluidics, microchips, embryoid bodies (EBs), collagen gels (GELs), spinner flasks, matrix encapsulation and hanging-drop culture are a few of the techniques for spheroid cultures[41,43,212,217,218,252].

In this work low attachment method was used[212,217]. Spheroids were formed by seeding an adequate, previously calculated number of cells to U-bottom well plates (Thermo Fisher, Italy). The spheroids were cultured for 3 days in order to obtain intended size. Since both AFM and microfluidic measurements required suitable spheroid size for the measurements, it was necessary to optimize the procedure of seeding cells to grow spheroids.

The diameter of spheroids was calculated using bright field images, using ImageJ software[253]. After 3 days of culture, four different diameters were collected on every image of the spheroid, and the final diameter was calculated as average of all four measurements (Fig. 27). Measurements were done using ImageJ software[253].

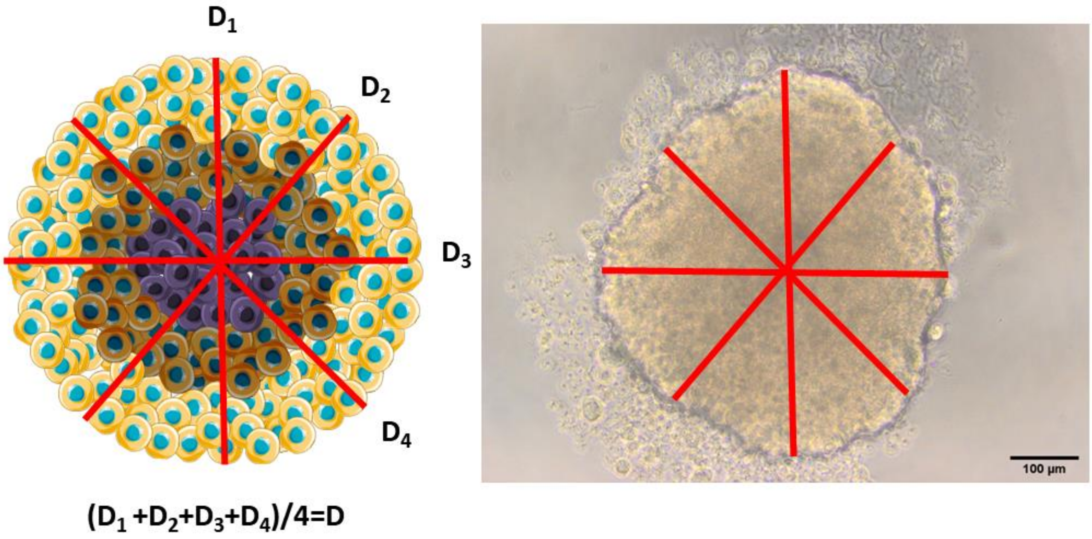

Figure 27. *Determination of spheroids size (diameter). [Parts of the Figure were drawn by using pictures from Servier Medical Art. Servier Medical Art by Servier is licensed under a Creative Commons Attribution 3.0 Unported License (https://creativecommons.org/licenses/by/3.0/)].*

The size of the resulting spheroids, in general, depends on the number of cells that were initially seeded for spheroid formation, although there can be some important deviations, which can come from random errors in cell counting. Additionally, the length of the cell type-specific division cycle affects how long it takes for the spheroid to develop, and this variation in time is substantial. As an effect, the final size of the spheroids might vary slightly between experiments. Based on literature research, a different number of cells were chosen to grow spheroids[52,217,254–257]. Several attempts were made to determine the number of cells most suitable to grow spheroids of the intended size. The most suitable size was chosen as 300-350µm. The latest experimental setups aiming at finding the most optimal diameter of spheroids considered the range of 4000 to 1000 cells/ well for HT-29 cell line, and 10000 to 3000 cells/well for CCD-18Co cells.

After three days of culture, five spheroids of each cell line and experimental class were measured. The mean diameter was calculated from the average of each spheroid (Fig. 28, Tab. 5).

Cell line	**Number of seeded cells** **Mean diameter ± SD [µm]**			
HT-29	4000	3000	2000	1000
	504.8±3.0	481.6±2.0	428.1±3.0	344.7±2.0
CCD-18Co	10000	5000	3000	
	319.1±19.5	223.9±16.0	173.9±6.0	

***Table 5**. Results of the obtained size of spheroids of two cell lines. The different diameters[µm] resulted from using the different number of cells to culture spheroids. Error is calculated as standard deviation.*

.

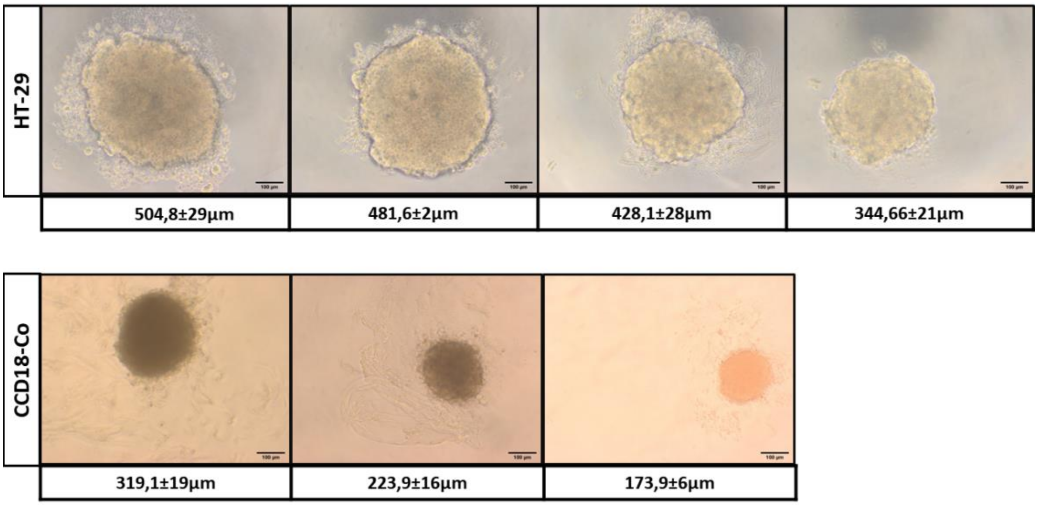

Figure 28 *Representative images of spheroids of HT-29 and CCD-18Co cell lines (magnification 10x). Images show results of determining the diameter of spheroids [µm] ±SD. Table mean diameter calculated from 5 spheroids of each size. Scale bar length is 100µm.*

For HT-29 cells, it was decided to use 1000 cells per well to grow spheroids, while for the CCD-18Co fibroblasts, it was 10000 cells per well. Macroscopic observation of spheroids of both cell lines confirmed that 3 days is the most suitable time for forming spheroids, since on 4th day and the following days, the increasing presence of necrotic core was observed. Three days was considered the most suitable time for generating spheroids, also other works used ≥3 days to obtain spheroids[52,255]. Considering that AFM and microfluidic measurements will apply different loads, the spheroid must be fully formed, otherwise, they will break. By simply vigorously pipetting the spheroid in the medium, it was possible to verify the resilience of the spheroid. After two days of culture, many spheroids fell apart into smaller pieces, while after three days, spheroids remained intact.

6.3.1.3. AFM nanoindentation measurements

Spheroids were measured in liquid environment, immobilized in a Micromesh array (Microsurfaces Pty Ltd, Australia) to confine them spatially. Micromesh is a polydimethylsiloxane (PDMS) grid of square wells with a depth of 100 µm and width of 500 µm (Fig. 20). The size of the Micromesh well was also an additional factor that determined choice of final size of the spheroids; the diameter of spheroid must be less than width of the well, so it fits inside. To provide additional attachment of cells of the spheroid to the substrate, the surface of a Petri dish was coated with poly-L-lysine (PLL) and 0.1% glutaraldehyde[149]. Glutaraldehyde can affect the mechanical properties of cells[258], however, a very low concentration was used for coating. Protocol also included 10 series of washing with PBS. Glutaraldehyde binds covalently to PLL, provides additional aldehyde group[149], and interacts only with cells from bottom part of spheroids, which does not affect tip-spheroid contact mechanics. The array was placed on a coated Petri dish and covered with small drop of ethanol to allow attachment of the grid to the surface. After the ethanol evaporated, the Petri dish was filled with advanced MEM culture medium (Gibco) for CCD-18Co fibroblasts and RPMI-1640 (Sigma-Aldrich) for HT-29 cells. Both media were not supplemented in phenol red (a weak acid that and can damage AFM equipment) and placed under the AFM. Several spheroids were collected from the culture multi-well plate to the Eppendorf tube and then gently placed on the top of the array, ensuring each spheroid fell into the well. The spheroids were taken for measurements on an ongoing basis to avoid measuring spheroids that were outside of culturing conditions for too long.

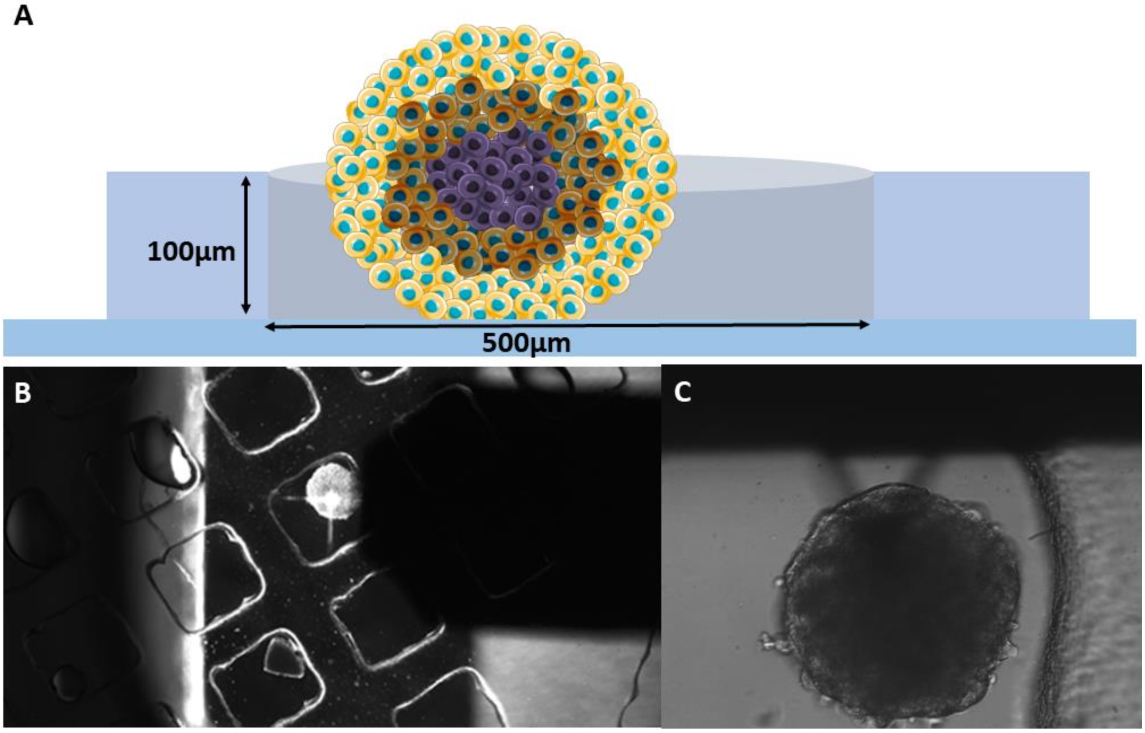

Figure 29*. Experimental setup of AFM measurements of the spheroid. Scheme presenting side view of spheroid inside the well (A); Planar view of spheroid and the PDMS array (B); Single spheroid inside the well with engaging cantilever (C). [Parts of the Figure were drawn by using pictures from Servier Medical Art. Servier Medical Art by Servier is licensed under a Creative Commons Attribution 3.0 Unported License (https://creativecommons.org/licenses/by/3.0/)].*

Four different AFM probe types were used to measure spheroids, and different measurements parameters were applied according to this (Table 6, Fig. 26). Overall, 3-6 FVs were collected on each spheroid and 10 spheroids of each cell line were measured with each AFM tip.

PROBE	Radius[µm]	Force map size [µm^2]	Force volume	Max. indentation [µm]	Applied force [nN]	Spring constant [N/m]	AFM tip
CP 5	4.3	35x35	100	~5	15-20	0.85	MLCT-SPH (Bruker)
CP 10	10	35x35	64	~5	15-20	0.23	CP-PNPS-BSG-C-5 (Nano and More
Pyramidal	0.02	20x20	100	2-4	5-10	0.79	MLCT-F (Bruker)
Tipless	HT-29 cell–177.7* CCD-18Co fibroblasts – 271.6*	40x40	49	~7	15-20	0.11	Arrow TL1 (Nano World)

Table 6. *Characteristics of used AFM and parameters of measurements. CP 5- colloidal probe with radius~5 µm. CP 10-colloidal probe with a radius of 10 µm. *Average radius calculated from five spheroids.*

6.3.2. Results and discussion

6.3.2.1. AFM nanoindentation measurements

Studying the nano-mechanical properties of spheroids with tips of different geometries and sizes provided various YM values. It is mainly an outcome of different contact mechanics between the probe and the spheroid and also applied Hertz model (Fig. 21)[79,83,85,100,106,113,116]. The main issues that can be discussed based on obtained results, are indentation depth which allows deciding which elements of spheroids were studied; heterogeneity of the YM distributions, which explains the contribution of spheroids components to the overall stiffness; practical application of various tip geometries in AFM nanoindentation measurements. Hence, the main aim was to understand which AFM tip geometry is most suitable for studying spheroids' elastic properties. The measurements also aimed to investigate whether there are differences between spheroids formed from colon fibroblasts and cancer colon cells.

6.3.2.1.1. Colloidal probes

In this research, two different colloidal probes were considered: large CP (CP10) with diameter of 20µm and small CP (CP5) with a diameter 8.7µm. Figure 30 compares YM for formed from both studied cells measured with different colloidal probes.

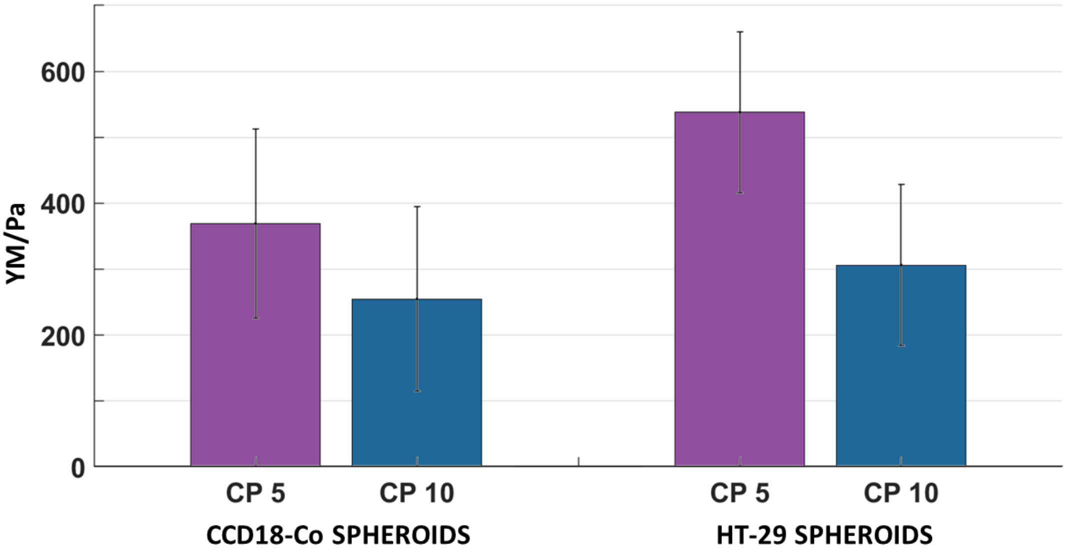

Figure 30*. Comparison of elastic properties between CCD-18Co (fibroblasts) and HT-29(colon cancer) spheroids, using small (R=4.3 µm) and large (R=10µm) colloidal probes. Each bar represents mean of the median values of spheroids included in measurements (n=10). The error bar represents the standard deviation of the mean.*

Nanoindentation measurements done with both CP5 and CP10 revealed that spheroids formed from colon cancer (HT-29 cells) and from fibroblasts (CCD-18Co) have very similar elastic modulus. It is well known that cancer cells are softer than normal one[3,8,75] while tissues become stiffer during cancer progression[11,12,75]. As explained in Chapter 6.1, spheroids can mimic tumour characteristics, including development of their own ECM, which suggests that spheroids made of neoplastic cells can be stiffer in the long term, even though they are composed of softer cells.

On the other hand, fibroblasts (in case of this research CCD-18Co cell line) have a much more well-developed cytoskeleton than colon cancer cells. It means that, they could be stiffer than colon cancer cells. It would be beneficial to compare the rigidity of spheroids with cells in 2D, using the same CPs, to better understand the mechanics of both cell lines in different systems. On the other hand, applying maximum force of 15-20nN resulted in quite wide range of indentations, from 2.7µm to 6.8µm, nevertheless, it allowed us to study only most outer layers of spheroids: the first few layers of cells and partially ECM (produced by the cells). In the research of *Rodriguez-Nieto et al. 2020* elastic modulus of CCD-18Co cell line was evaluated as 300Pa[259] what is close to the value obtained with large probe CP10 – 305.6Pa. It is worth considering the bottom effect, which occurs when the indentation is close to the sample thickness[89,98,114,121]. In the case of standard 2D measurements of cells, the influence of a very stiff surface (plastic or glass) must be considered and included in data analysis[89]. Regarding the 3D structure of spheroids, the bottom effect might come from underneath layers of cells and ECM and also from the lateral confinement exerted by the surrounding cells and lead to overestimation of YM in case the inner layers are much stiffer[98]. Bottom (and in general terms spatial confinement effects) are amplified by the use of large colloidal probes[89]

Using spherical probes with different diameters entails differences in the contact area and distribution of the force applied to the sample. Considering contact area, it can be expected that smaller CP (CP5) provides more heterogenous YM values distribution by detecting single elements in the studied surface, which larger standard deviation should quantify, while larger CP (CP10) measures across a larger contact area (and interaction volume) more averaged YM values.

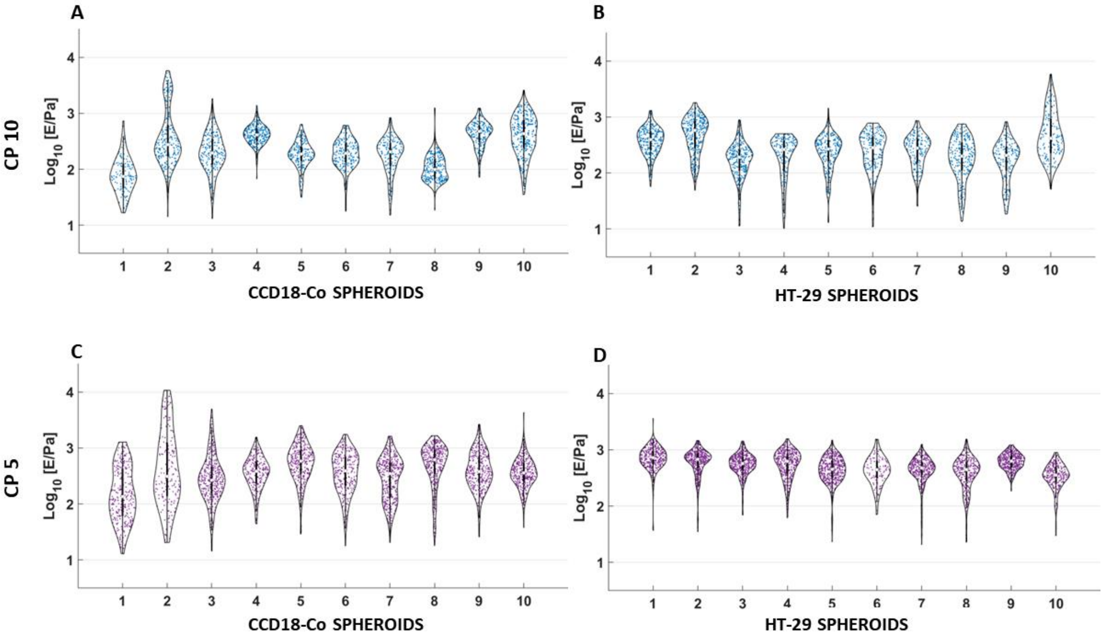

Figure 31. *Violinplots showing median YM values of each spheroid and distribution of YM obtained from single FCs within the different force volumes (4-6). (A) CCD-18Co spheroids measured with large CP; (B) HT-29 spheroids measured with large CP; (C) CCD-18Co spheroids measured with small CP; (D) HT-29 spheroids measured with small CP. The white point shows the median value, and thick black lines are the upper and lower quartile*[146]

To verify this statement in the context of spheroids mechanics, results of measurements were presented in violin plots (Fig. 31). This plot shows the distribution of YM values of every single FCs and the median value of all FCs measured within each spheroid. Results did not show any prominent characteristics in the distribution of YM regarding the used probe or cell line. By comparing spheroids within experimental classes, it was possible to observe low heterogeneity. Surprisingly, HT-29 spheroids measured with a small colloidal probe showed the highest homogeneity (Fig. 31), while multimodal distribution could be observed in spheroids of other experimental classes.

6.3.2.1.2. Tipless cantilevers

Another attempt to characterize the nano-mechanical properties of spheroids was made using tipless cantilevers. The great advantage of tipless cantilever is the large contact area between the tip and spheroid, due to the width of the cantilever (100µm). Tipless cantilevers would allow to indent a spheroid as a whole, rather than locally. In our case, we achieved a maximum indentation of 7µm. Using a tipless cantilever seems to be a promising tool for studying the elasticity of spheroids however it raises questions regarding the contact mechanics and mechanical model that should have been used. One can speculate that for smaller spheroids, an inverted flat-on-sphere geometry can be appropriate, where the radius of the indented body is the spheroid radius. In the case of large spheroids, with a diameter of several hundred µm, and wide tipless cantilevers, a flat-on-flat contact geometry, opposed to the sphere-on-flat geometry, can be appropriate. In this case, the approximation of a flat punch can be used, with the effective diameter of the circular cross-section equal to the cantilever width. In addition, one can assume that the flat cantilever indents the soft spheroid equivalently to a sphere with a diameter equal to the cantilever diameter.

To verify which model is most suitable, data from three spheroids were analysed to see which approach would be more suitable for further analysis. Three different Hertz models and assumptions were used:

- Hertz model for CPs with R equal to the radius of the spheroid (HertzSPH)
- Hertz model for CPs with R equal to half of the width of the cantilever (HertzCNT)
- Hertz model cylindrical probe with R equal to half of the width of the cantilever (HertzCYL)

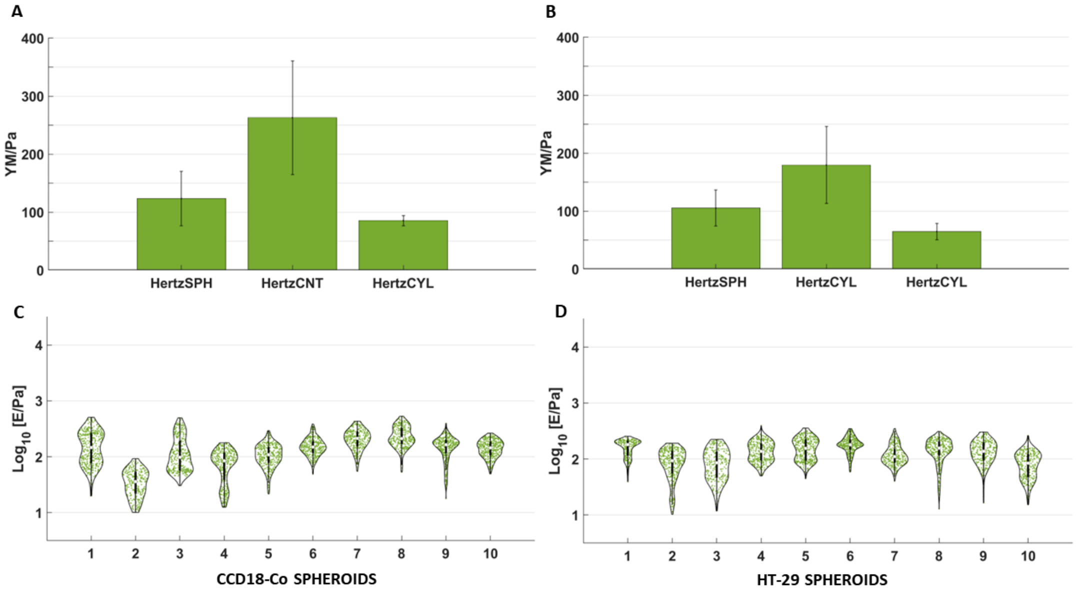

Figure 32. *Elastic properties of CCD18-Co (A, C) and HT-29 (B, D) spheroids measured with a tipless cantilever. Each bar represents the mean of the median values of spheroids included in measurements (n=3 analysed using three different contact models: HertzSPH– Hertz model where spheroid is treated as a deformable sphere and tipless cantilever as a rigid flat surface; Hertz CNT – Hertz model with R equal to half of the width of the cantilever;, HertzCYL – flat punch model, assuming the cantilever width as the diameter of the circular cross-section of the cylindrical indenter (A, B). Violin plots represent YM distributions, each value coming from all FCs collected in different locations of the same spheroid and analysed by applying the Hertz model for CPs with R equal to radius of the spheroid. YM values were extracted using mean radius of the spheroids (C, D). Error bars represent the standard deviation of the mean. The white point shows the median value, and thick black lines are upper and lower quartiles*[146]

First, we used the standard Hertz model (Fig. 26) but used an average radius of spheroids taken for measurements that day (Chapter 6.3.1.2). This is equivalent to considering a deformable sphere (the spheroid) pushed against a rigid flat surface (the tipless cantilever). The average size of HT-29 spheroids was 355.4µm. and for CCD18-Co - 543.2µm. Second, we have used the standard Hertz model (Fig. 26) but assuming that the cantilever can be treated as a sphere with an effective diameter equal to the width of the cantilever. In both cases (Fig. 32), the obtained values of the YM were very similar to those obtained using CPs (Fig. 30), especially in case of CCD18-Co.

The third option was to use the flat punch model, as discussed above, with half of the cantilever width taken as radius – 50µm (Fig. 26). However, the tipless cantilever does not provide constant contact area, like in the case of truly cylindrical tips[90,98]. The contact region can be considered as an ellipse with one axis determined by cantilever width and the other axis expected to increase with indentation. As a result, obtained data analysed using the flat punch approximation provided very different (lower) values of Young's modulus, compared to other models (Fig. 32 A,B). *Giannetti et al. 2020* performed similar research on spheroids made of T24 (transitional cell carcinoma). The obtained elastic modulus was in the range of 100-500Pa[216]. Elastic modulus measured in this research (using the Hertz model with the radius of the spheroid, HertzSPH) were quite similar: 158.1kPa for CCD-18Co and 213.2kPa for HT-29 spheroids, while results obtained using the cylindrical model were lower than reported in *Giannetti et al.* 2020 and for Hertz model used in these studies[216]. This also confirms that using the model for a cylindrical tip is not optimal while indenting with a tipless cantilever.

Considering the results of data analysis, the most suitable and reliable model for further studies is the Hertz model for CPs, with a radius equal to the radius of spheroids. Both quantitative values of YM and considerations of contact mechanics are in favour of this approach. Further data analysis for all 10 measured spheroids was performed using this model (Fig. 32 C,D).

6.3.2.1.3. Pyramidal tips

Data analysis of the FCs obtained with pyramidal tips revealed that in some measured regions of interest there are two ranges of indentation. Based on this observation, FVs were analysed considering small (10%-30%) and large (30% - 90%) indentation ranges (Fig. 33). In the work of *Vyas et al. 2019* pyramidal tip was used not only to study cells but also ECM in proliferation zone of the spheroid and results presented in that work revealed changes in stiffness as a function of indentation[220].

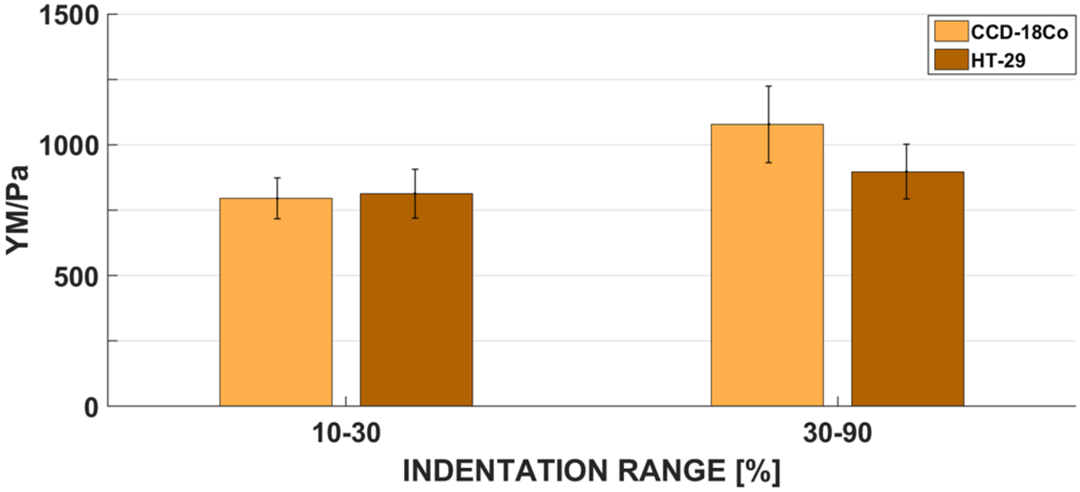

Figure 33. *The mean elastic modulus of spheroids formed from: CCD-18Co and HT-29 cells studied in within two ranges of indentation. The bars were plotted as the mean value of ten spheroids in a given indentation of each cell line. Error bars represent the standard deviation of the mean.*

Hence, the comparison of the two indentation ranges did not reveal any significant differences in elastic modulus for spheroids of both cell lines. Stiffening can be observed in large indentation range, nevertheless the difference is not significant. The lack of differences can be explained by the fact that overall indentation was not very high as it was limited by the height of pyramidal tip, what is one of the drawbacks of using this tip geometry. In case of CCD-18Co spheroids, median indentation for the first range was 1,5µm and the second range – up to 90% resulted in the median indentation of 4.4µm, while for HT-29 spheroids, median indentation was respectively 1.2µm and 3.7µm. Preparation of spheroids of smaller size could enable access to deeper layers, accessible within indentation limited by the height of the tip. Additionally, the pyramidal tip is good in the case of studies focused on extracting elastic modulus and visualizing smaller elements of samples rather than measuring the overall stiffness of big samples[95,115]. This approach was described in the work of *Vyas et al.* where with a pyramidal tip, it was possible to study many features of the spheroid, like collagen fibers, ECM-cell membrane interface, and even cells inside the ECM, in lower layers of the spheroid[220].

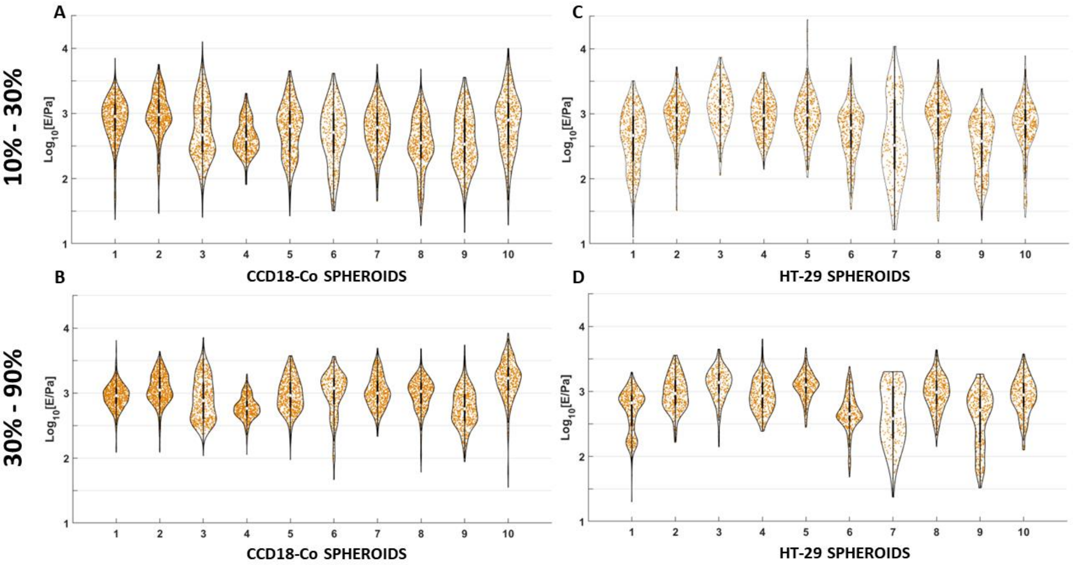

***Figure 34**. Violinplots showing median YM values of each spheroid and distribution of YM obtained from single FCs. CCD-18Co spheroids measured with indentation of 10% - 30% (A); CCD-18Co spheroids measured with indentation of 30% - 90% (B); HT-29 spheroids measured with indentation of 10% - 30% (C); CCD-18Co spheroids measured with indentation of 30% - 90% (D).*

Using pyramidal tips has its drawbacks. Mechanics-wise, sharp tips are more prone to explore non-linear elastic regimes in the sample already at relatively small forces. A systematic overestimation of Young's modulus has been reported by several authors[112]. *Vyaas et al. 2019* reported that when the pyramidal probe is repeatedly poking the spheroid surface, some of the matrix components may disintegrate in an aquatic environment. Due to the gelatinous nature of the ECM and the mixture of different molecular and structural components, there can be significant variations in modulus near the surface of spheroids[220]. To better understand the elastic properties of spheroids within outer layers, the distribution of single FCs was plotted for each spheroid in both indentation ranges (Fig. 34). In the first indentation range, the distribution of YM values is slightly wider for both cell lines compared to the second part of indentation. These results suggest that the surface of spheroids is more heterogenous than their inner parts.

Similar AFM studies were recently done on bladder cell-derived spheroids using pyramidal cantilever[78]. Based on the results presented in that research, we can conclude that pyramidal tip studies the mechanical properties of cells on the spheroid's surface. Obtained values in *Gnanachandran et. al 2022* are in a similar range as in this research (while studies with CP provided values of hundreds of Pa (Fig. 30 and 35)). Additionally, studies on bladder cancer cells and spheroids showed that YM values are similar for cell monolayers (2D) and spheroids (3D), indicating the role of actin filaments in cell-cell interaction and spheroids formation[78].

YM values of HT-29 and CCD-18Co spheroids can be compared with nano-mechanical properties of cell lines in 2D systems. Based on literature research, these values are 1.3 kPa (pyramidal, single cells)[260], 10 kPa (conical, single cell)[259] for HT-29, and 15kPa (conical)[261] for CCD-18Co. It is important to remember that differences in YM values can come from different measurements and tip parameters, spheroid culture, and experimental setups. Nevertheless, YM values obtained from measuring spheroids are lower than those measured on cells studied in 2D. This shows that cell express different mechanical properties when cultured on a flat surface, and when are a part of aa aggregate.

Pyramidal tip measures the elastic modulus of cells within the spheroid instead of the whole specimen, as pyramidal tips sense a smaller volume; thus, they provide more local analysis.

6.3.2.1.4. Comparison between used AFM probes

To summarize the series of measurements, a final comparison between used AFM probes was made (Fig. 35).

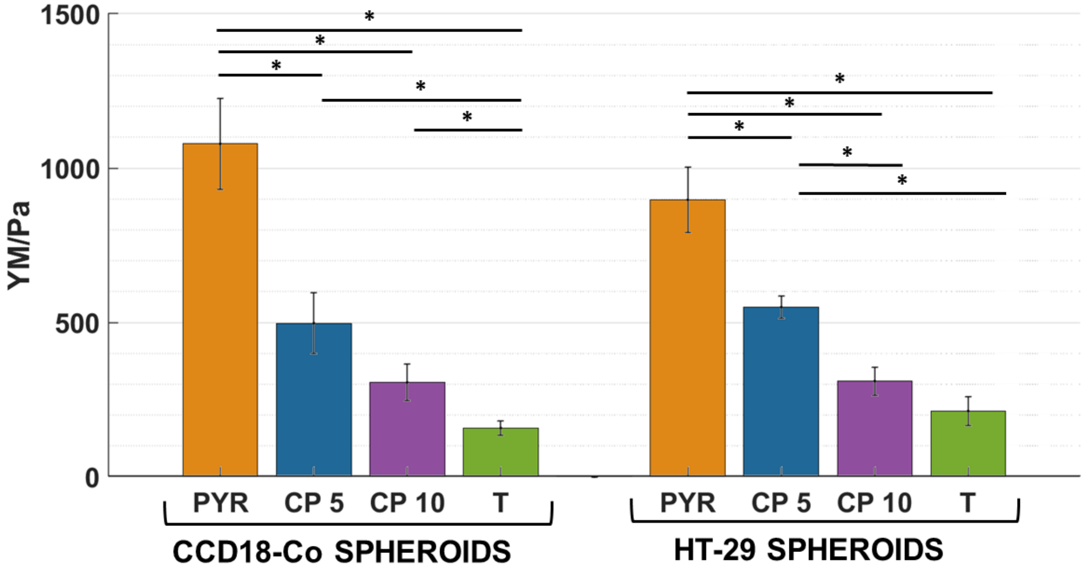

Figure 35 *Comparison of elastic modulus of two spheroids (CCD18-Co and HT-29) measured with different AFM tips: PYR – 4-sided pyramidal (indentation range 30%-90%), CP 5 – colloidal probe with R=4.3μm, CP 10 –colloidal probe with R=10μm, T – tipless cantilever (using Hertz model for CPs with radius of spheroids). Each bar represents mean value of 10 spheroids measured in each experiment and error bar is standard deviation of the mean.*

It is clearly seen that with the increase of radius used in the contact mechanics model, obtained YM is significantly lower. With larger tips (larger contact area, larger interaction volume, more averaging), it was possible to study elastic properties of spheroids on a multicellular level while using pyramidal tips allowed to extract values corresponding to individual elements of the system (i.e., single cells) in the spheroid outer layers.

Comparison between used AFM probes revealed that using different contact geometries in the fitting procedure results in significantly different YM values (Fig.

35), highlighting the importance of a precise experiment design and choice of the AFM probe. Based on results discussed in detail in previous chapters: 6.3.2.1.1 – 6.3.2.1.3 we can conclude that pyramidal tip is more suitable for studying cells on the surface and cell-cell interactions[220], while colloidal and tipless probes allowed to study elastic modulus of the whole spheroid. This conclusion can be based on the fact that tumour cells are softer than normal one[3,8,75] and it is the opposite for whole tissues[11,12,75]. Results of this study showed that measurements on HT-29 spheroids gave slightly lower values than on CCD18-Co spheroids done with pyramidal tips. The opposite trend could be observed to a small extent in measurements performed with other tips.

6.3.3. Conclusions

The versatility of AFM and its probes allowed us to study the elasticity of spheroids in different terms. AFM seems to be a promising tool for studying mechanical properties; however, some issues still have to be solved or improved. A great improvement of AFM studies would be to increase the sampling number because the AFM technique has low throughput for measurements. Collecting data from one spheroid took about 40-60 min. The number of spheroids analysed in these studies was limited to only 10 spheroids per experimental class, which might not be sufficient to draw proper conclusions.

Different values of YM values might come from different sizes of spheroids. Researchers use spheroids in various sizes, depending on the aim of the study. Research by *Mahajan et al 2021*. revealed that spheroids of different sizes (growing in the gel of different stiffness) had different stiffness (measured by Brillouin microscopy)[201]. Additionally, within the same research, spheroids' size can vary by a random error in calculating cells for seeding or even the small differences in the growth rate of cell lines between each experiment. As is generally seen with cell measurements, there is some data fluctuation due to cell differences. Since there are no significant variations between the smallest and largest spheroids, it appears that size has no impact on the results[216]. On the other hand, research by *Giannetti et al. 2020* on spheroids with tipless cantilever revealed no differences between YM values and spheroids of different size[216]. The presence or lack of differences might come from many factors like scale of size differences or type of cell line; concerning that, this issue might require further investigation.

Another crucial factor in spheroids nanoindentation measurements is their bigger size and complex layer structure. By using sharp pyramidal tips, it was possible to extract the elasticity of the first outer layers of in proliferating zone of the spheroid, with more focus on single elements, because indentation is limited to the height of the tip. While pyramidal and colloidal probes seem to be better for measuring single cells in spheroids, a tipless cantilever provides a much bigger contact area, and indentation force was applied to the spheroid as a whole. Considering larger indentation (around 7µm), inner zones of the spheroid might contribute to obtained YM value as a bottom effect[98,121].

Studying spheroids with AFM requires them to be in free form to allow for indirect spheroid-tip contact. In that case, the compressive stress is lost (present in spheroids cultured in hydrogels), which may have an impact on the mechanical phenotype of the spheroids[201]. Additionally, the immobilization of spheroids is a challenge. The technique of using coated Petri dish and a special grid allowed to fix spheroids for the time of measurements partially. Another method described by *Vyas et. al 2019* suggests using a thin layer of agarose gel to fix spheroids by their bottom part[220]. However, this method has the risk of embedding or covering the whole spheroid with the gel. In that way, the AFM tip could indent through agarose gel on the top of spheroids instead of cells of the outer layer. It is crucial to comprehend sample heterogeneity, especially when using these techniques on biological samples. It is also challenging to place the probe precisely above the point at which the sample and substrate come into contact. This would lead to measurements on the side part of the sphere, where the sample is also moving, and the mechanical model does not take this additional compliance into consideration[70].

To summarise, pyramidal tips are a good choice for studying single elements in multicellular spheroids and revealing sub-surface heterogeneities[220], while tipless cantilever allows studying large-scale mechanics of spheroids, or even spheroids as a whole in case of very wide tipless cantilevers; however, their use still requires some improvements, especially in the modelling part. A good alternative to tipless cantilevers is (very) large colloidal probes, as they provide a large contact area and reliable application of the Hertz model.

6.4. Study of nanomechanical properties of multicellular spheroids with microfluidic cytometry in extensional flow

6.4.1. Development of the protocol

In this study, we focused on the development of a novel technique for measurements of deformation creep and force relaxation of spheroids in a microfluidic flow. The method is based on approach to calibrate the method using air bubbles. They are spherical in an undisturbed state. Based on that, the strain can be calculated, also the surface tension is known between air and water (alginate solution is mostly water).

First step for the development of the technique was to arrange and adjust the experimental setup present at Department of Physics, Friedrich-Alexander University, Erlangen, Germany, in prof. Ben Fabry’s lab.

The scheme presented in Figure 36 explains the basics of the experimental system. Spheroids are resuspended in a 2 % alginate water solution. Alginate is a naturally occurring anionic polymer; the obtained solution is characterized by relatively high viscosity, which is crucial to apply shear stress on the surface of dispersed spheroids. Resuspended spheroids were stored in medical syringe connected to a pressure pump. The syringe had 800µm diameter needle, which was inserted into another container already filled with alginate. Upon application of a constant pressure by means of a pressure pump controlled by Phyton based program, the motion of spheroids in the alginate extensional flow exiting the needle and entering the reservoir was recorded with a camera (Blaster ace, acA640-750um) that provides 751 frames per second at VGA resolution. The thickness of the reservoir must be very small (only thick enough to fit the needle) in order to prevent dispersion of spheroids in z axis and getting out of focus of the camera. Without sharp images of spheroids, it would not be possible to measure precisely the geometrical parameters of the spheroids that are later crucial for data analysis. The duration of recorded video was equal to duration of pressure pump operation time. The excess gel in container was regularly drained by another pump. The software for operating the experimental setup was developed in Fabry's lab in Python environment.

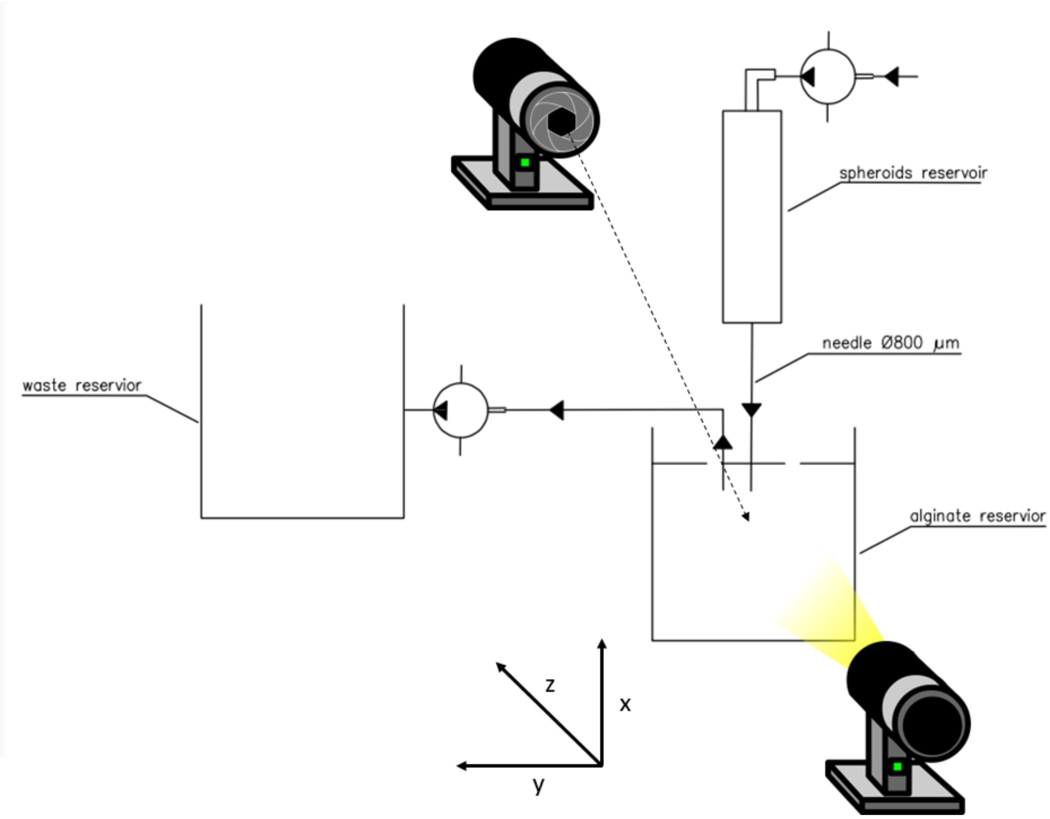

Figure 36. *Experimental setup used to acquire videos of spheroids in alginate extensional flow. Spheroids in the first container are pushed at constant pressure through a needle into another reservoir. Excess of alginate is taken away with second pump.*

The experimental strategy consisted in recording videos of spheroids exiting from the needle subjected to shear stress in the extensional flow and analysing the frames to determine relevant geometrical parameters of the spheroids (major and minor axes and perimeter of the spheroids' cross section, centre of mass to trace the spheroid motion, etc); the dynamics of the spheroids in the extensional flow can then be modelled to extract relevant mechanical properties and deformability indicators.

In this study, two cell lines were used to develop spheroids: HT-29 and CCD-18Co. First part of preliminary experiments was to find the most suitable size of the spheroids. Figure 37 shows representative images of spheroids and their average diameter, that were chosen as most suitable for extension flow measurements. HT-29 spheroids were cultured, according to the protocol described in Chapter 6.3.1.2 by seeding 1000, 2500, 5000 cells per well and in case of CCD-18Co it was 5000, 7500, 10000. Another parameter that was considered was the applied pressure. The value ranged from 50kPa to 80kPa to verify which pressure allows to significantly deform spheroids while at the same time keeps velocity low enough to accurately capture flow of spheroids in frames.

Bubbles of air that formed during measurements were also considered in these studies as a suitable internal calibration system, since they represent a simplified model of spherical deformable particles in the extensional flow.

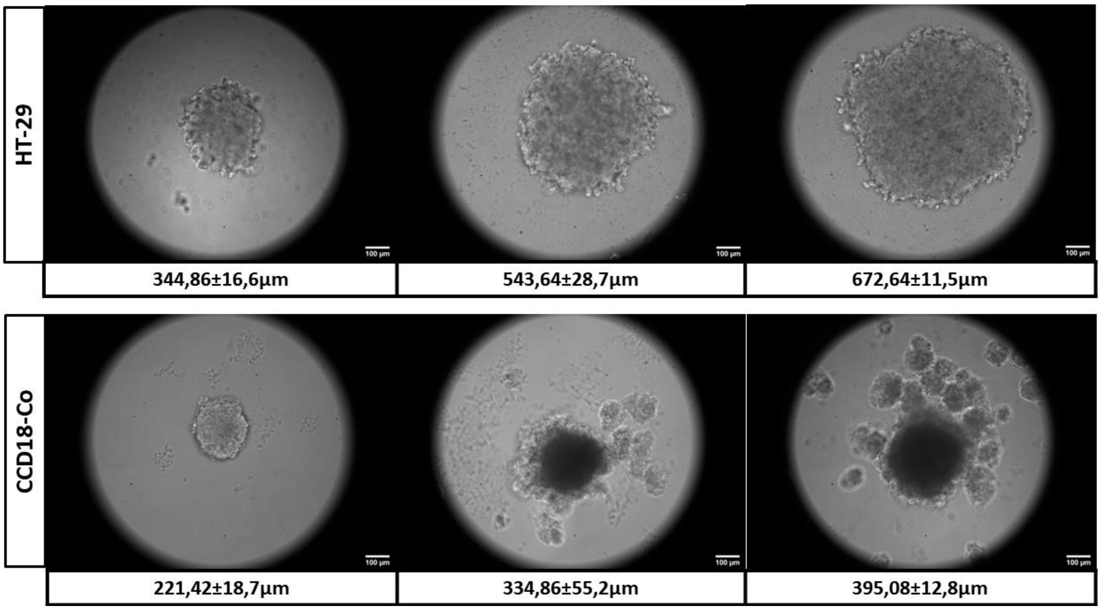

***Figure 37**. Images of spheroids of HT-29 and CCD-18Co cell lines prepared for studies.*

Obtained videos were analysed using Fiji extension of ImageJ software[253,262]. The most significant steps of video processing are shown in Figure 38. "Analyse particle" is a plug-in that allows to detect particles of a given size (in case of these studies air bubbles and spheroids) and track their movement, giving as an output:

- Major (a) and minor (b) axes and angle (β) between the primary axis and a line parallel to the X-axis of the image

- Perimeter - the length of the outside boundary of the ellipse
- Centroid - the center point of the
- Area (A) - area of selection in square pixels or in calibrated square units

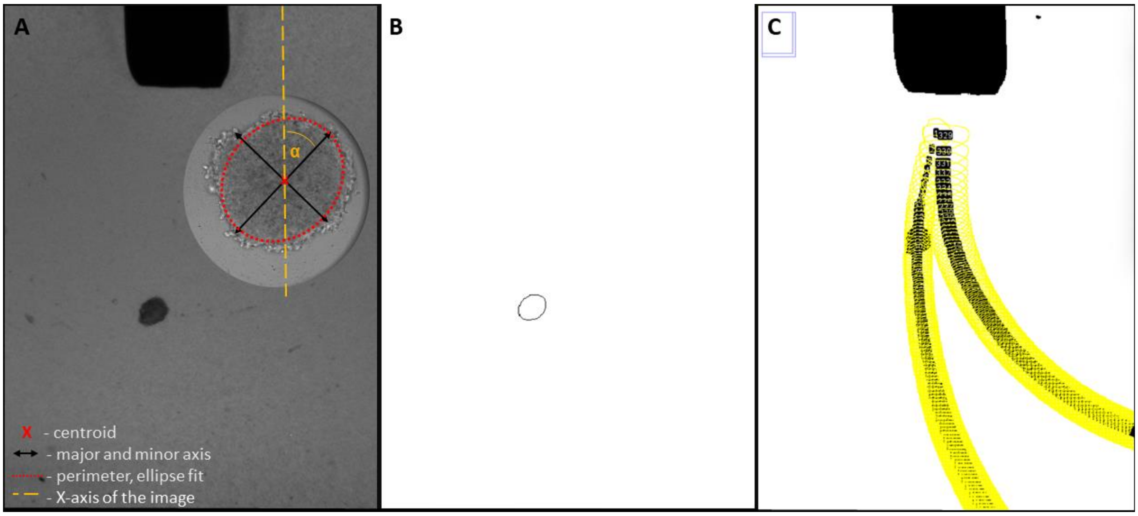

Figure 38. *Main steps of video processing presented on the same frame of video at different steps of analysis. The software detects particles of determined size and then tracks its trajectories based on position in every frame of video. Raw video capture (A). 8-bit binary image containing the best fit ellipse (B). Tracking of detected particles (compilation of all detected particles in each frame) (C).*

Using major and minor axis it was possible to calculate strain (ε) using equation:

$$\varepsilon = \tan\alpha = \frac{a-b}{\sqrt{ab}} \qquad \textit{Eq. 11}$$

, where α is angle between minor and major axis.

Assuming that the applied force is equal to the force at the needle exit, i.e. $F = pA_{needle}$, where A_{needle} is the needle sectional area and p is the pressure, the stress σ can be calculated from:

$$\sigma = \frac{F}{A} \qquad \textit{Eq. 12}$$

, where A is the measured sectional area of the spheroid. In the simplified model, the area A calculated from ImageJ software can be used. Regarding the force, further work is required to estimate it with better accuracy; in particular, the force is decreasing as the spheroids flows away from the needle. When both strain and stress are known, the Young's modulus can be calculated as:

$$E = \frac{\varepsilon}{\sigma} \qquad \textit{Eq. 13}$$

The flow around the drop is totally defined by a single dimensionless parameter, Ca, the capillary number, which is the ratio of shear forces (which tend to distort the particle) to surface tension forces (which tend to maintain the particle spherical)[263]:

$$\mathrm{Ca} = \frac{\tau r}{\sigma} = \frac{\mu \gamma r}{\sigma} \qquad \textit{Eq. 14}$$

, where τ is the shear stress, *r* is the equivalent radius (radius of a sphere of equal volume of the spheroid; here *r* considered as the radius of the sphere in the relaxed state) and γ is the surface tension, μ is a continuous-phase viscosity. Surface tension is a change in energy divided by a projected length. Projected length corresponds to macroscopic perimeter of the entire cell aggregate – spheroid[245].

The spheroid was considered as an ellipsoid that is oriented along the main axis of deformation in the simple shear flow. Introducing the parameter $\mathrm{D}=\frac{a-b}{a+b}$, the Taylor deformation parameter, the capillary number Ca turns out to be equal to D, i.e. it can be calculated using major and minor axes of the deformed spheroid[263]:

$$\mathrm{D} = \frac{a-b}{a+b} = \mathrm{Ca} \qquad \textit{Eq. 15}$$

This equation can be applicable considering few assumptions like isothermal conditions, incompressible Newtonian fluids, steady creeping flow with negligible inertial effects. Currently, data analysis is performed manually using Fuji software as described in chapter 3.1. Described steps are very time consuming what makes data analysis less efficient, in contrast to measurements which have high throughput. Automatized procedure to apply suitable physical model and extract values of spheroids elastic properties is under development, using Python environment.

6.4.2. Preliminary measurements and development of data analysis procedure.

To prove the effectiveness of the developed data analysis procedure, an example is presented in Fig. 39. This is a first seed of data analysis aimed to verify the quality of particle detection and parameter estimation.

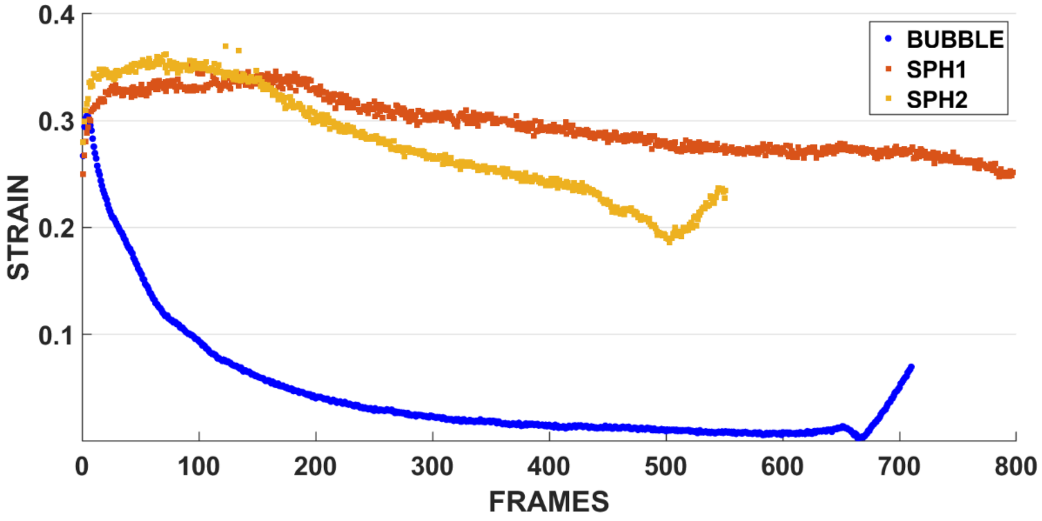

Figure 39 *Strain of two different spheroids and one air bubble in the alginate extensional flow, measured from the images recorded as described in the main text. The applied pressure was 50 kPa and the duration of videos was 3 seconds (equivalent to 800 frames, as reported in the graph).*

It can be observed that deformation decreases as the object leaves the needle, what can be especially visible in the case of air bubble. As the objects drifts away from needle they are returning to relaxed state.

Unfortunately, in extensional flow, some of the spheroids at some point deviates too much from the region in the field of view of the camera that would enable to precisely track their path and determine accurately the deformation, and in particular to characterize the relaxed geometry (far away from the needle) (Fig. 38) This issue is visible for one of the tracked spheroids in Figure 32, whose trajectory is shorter.

Another issue that can be observed in Figure 32 for the air bubble and spheroid 2 is the sudden increase of the strain in the last frames. When the object leaves the camera field of view the detection of object shape is altered, which causes incorrect calculation of major and minor axes.

Despite the issues observed, this preliminary work demonstrated that microfluidic cytometry in the alginate extensional flow can be applied successfully to characterize the mechanical response of the whole spheroid to a shear stress. It is generally difficult to comprehend these mechanical stress response processes because of the interaction between the complex rheology of the alginate. Further work is required to fully develop this promising approach, by expanding and adjusting physical models of viscoelastic bodies. The next challenge is to optimize data acquisition and to develop mathematical model that will allow to extract values of Young’s modulus. It will enable to make a full comparison with other techniques studying mechanics, including AFM.

6.5 Conclusions

The effective transition of 2D to 3D mechanobiology research will be achievable only if a set of conceptual hurdles, of both technological and operational origin, are addressed. Spheroid model is a new approach of studying cell and tumour mechanics, what is crucial for future medicine research. In this section, two new approaches to study elasticity of spheroids were presented and discussed.

AFM has proved its versality by enabling to study elasticity with different approach by using different AFM tips. It allowed to study the mechanical properties of different elements of multicellular spheroids (i.e. at different length scales). The remaining challenge is to set the procedure that enables to sufficiently immobilize spheroids for the time of measurements. Thanks to that, measurements will proceed faster and quality of collected FCs will be improved. The main disadvantage of studying elastic properties of spheroids with AFM was low throughput of measurements since it took 1-2 days to measure 10 spheroids. On the other hand, AFM allowed for more precise measurements with focus on studied layers of spheroids (see Fig. 25) and contact mechanics (Fig. 26).

Higher throughput can be obtained with microfluidic cytometry in the extensional flow, which is based on basic viscoelasticity mechanics. The extensional flow setup is far simpler than the standard microfluidic deformability cytometric tests based on narrow channelled devices. In principle, with the new method, much higher number of spheroids could be studied within one day of measurements (up to 200) with respect to AFM. Moreover, this method allows to characterize the mechanical properties of the spheroid as a whole, a limit that is hardly achievable by AFM, even with the largest probes. At present, besides the promising preliminary results, the real challenges to describe mechanical properties of spheroids successfully are to collect higher-quality and to further develop the theoretical framework to properly model the deformation of spheroids in the extensional flow.

7. Conclusions and perspectives

Mechanobiology is an interdisciplinary field of science that applies physics and mechanics to biology research that gains popularity and importance. The number of scientific papers related to mechanobiology increases rapidly in recent years, reaching number of more than 13500 articles in 2022. There are still a lot of unanswered questions in cancer research, however, application of biomechanical methods presented in this work shed a light on this issue. It was possible by adapting AFM into new approaches to the study various biological models.

Freezing is a standard procedure to store biological samples like tissue or ECM. Preliminary studies on bladder tissue suggest that some of freezing technique can affect mechanical properties of tissue. Considering importance of storage of biological specimens, this topic requires further investigation to optimize the procedure what will be beneficial for all laboratories performing studies on biological specimens.

As an improvement to studies on bladder tissue and to eliminate factors like freezing and fixation, vibratome sectioning method was developed. It allowed to prepare the sample of peritoneal tissue that will be suitable for AFM nanoindentation measurements.

Transition from 2D to 3D models in cancer research is common practice in cancer research in recent years, as it better mimics the tumour microenvironment and tissue homeostasis. To improve the research on PM from CRC, ex vivo engineered PM lesion model was successfully developed using ECM and organoids derived from clinical biopsies. Such model will allow to skip the stage of research on animals and to perform more patient oriented studies.

The same model was later applied in studies on influence of neoplastic organoids on normal and neoplastic ECM. The results provided better understanding of the mechanical changes during PM and the role of the tumour cells in changing ECM to create a more favourable and conducive environment for cancer progression. This is a promising topic that requires more research both on aspects of mechanics but also in context of molecular biology to investigate early hallmarks of cancer. Further research will focus on using organoids of different invasiveness for development of ex vivo engineered PM lesions. Another step is to supplement AFM measurements with additional molecular biology experiments.

Studies on dECM from PM patients have revealed a wide range of mechanobiological characteristics, which may be related to clinical data of patients. This also underlined the diversity among patients and the need to study patient-derived samples if we aim to obtain results that can be applied in cancer treatment. Research found a clear association between CAF activity, collagen deposition, and the nanomechanical characteristics of the ECM.

In search for another model that can resemble tissue complexity and allow to study cell-ECM interaction, research described in Chapter 6 focus on spheroids. To fully exploit advantages of spheroids in cancer research it is necessary to first develop and optimize suitable techniques. Hence, AFM in indentation mode turned out to be appealing tool to investigate spheroids on multicellular level. To supplement this approach, work on developing microfluidic in extensional flow method has been carried out. This is a very promising tool to investigate rigidity of spheroids as a single particle, however further optimization is required, especially in matter of data acquisition and data analysis.

To conclude, AFM is a versatile tool in mechanobiology that can be adapted to study many biological models. In this work, focus was on peritoneal metastasis and mutual interaction between cells and their microenvironment. Using AFM as main investigation tool it was possible to better understand cancer progression. Presented work has a great potential to be converted into a tool for early diagnosis in cancer.

Bibliography

1. Lee, G. Y. H. & Lim, C. T. Biomechanics approaches to studying human diseases. *Trends Biotechnol* **25**, 111–118 (2007).
2. Rianna, C. & Radmacher, M. Cell mechanics as a marker for diseases: Biomedical applications of AFM. in *AIP Conference Proceedings* vol. 1760 (American Institute of Physics Inc., 2016).
3. Stylianou, A., Lekka, M. & Stylianopoulos, T. AFM assessing of nanomechanical fingerprints for cancer early diagnosis and classification: From single cell to tissue level. *Nanoscale* **10**, 20930–20945 (2018).
4. Tian, M. *et al.* The nanomechanical signature of liver cancer tissues and its molecular origin. *Nanoscale* **7**, 12998–13010 (2015).
5. Goetz, J. G. *et al.* Biomechanical remodelling of the microenvironment by stromal caveolin-1 favors tumor invasion and metastasis. *Cell* **146**, 148–163 (2011).
6. Vineis, P. & Wild, C. P. Global cancer patterns: Causes and prevention. *The Lancet* **383**, 549–557 (2014).
7. Sung, H. *et al.* Global Cancer Statistics 2020: GLOBOCAN Estimates of Incidence and Mortality Worldwide for 36 Cancers in 185 Countries. *CA Cancer J Clin* **71**, 209–249 (2021).
8. Lekka, M. Discrimination Between Normal and Cancerous Cells Using AFM. *Bionanoscience* **6**, 65–80 (2016).
9. Lekka, M. *et al.* Cancer cell detection in tissue sections using AFM. *Arch Biochem Biophys* **518**, 151–156 (2012).
10. Zemła, J. *et al.* AFM-based nanomechanical characterization of bronchoscopic samples in asthma patients. *Journal of Molecular Recognition* **31**, (2018).
11. Najafi, M., Farhood, B. & Mortezaee, K. Extracellular matrix (ECM) stiffness and degradation as cancer drivers. *J Cell Biochem* **120**, 2782–2790 (2019).
12. Cox, T. R. The matrix in cancer. *Nat Rev Cancer* **21**, 217–238 (2021).
13. Holuigue, H. *et al.* Force Sensing on Cells and Tissues by Atomic Force Microscopy. *Sensors* **22**, (2022).
14. Deptuła, P. *et al.* Tissue Rheology as a Possible Complementary Procedure to Advance Histological Diagnosis of Colon Cancer. *ACS Biomater Sci Eng* **6**, 5620–5631 (2020).
15. Ansardamavandi, A., Tafazzoli-Shadpour, M., Omidvar, R. & Jahanzad, I. Quantification of effects of cancer on elastic properties of breast tissue by Atomic Force Microscopy. *J Mech Behav Biomed Mater* **60**, 234–242 (2016).
16. Rodríguez-Ortiz, L. *et al.* Colorectal peritoneal metastases: Optimal management review. *World J Gastroenterol* **25**, 3484–3502 (2019).
17. Ng, D. *et al.* Investigating the mechanisms of peritoneal metastasis in gastric adenocarcinoma using a novel ex vivo peritoneal explant model. *Sci Rep* **12**, 11499 (2022).

18. Ceelen, W., Ramsay, R. G., Narasimhan, V., Heriot, A. G. & de Wever, O. Targeting the Tumor Microenvironment in Colorectal Peritoneal Metastases. *Trends Cancer* **6**, 236–246 (2020).
19. Lemoine, L., Sugarbaker, P. & Speeten, K. van der. Pathophysiology of colorectal peritoneal carcinomatosis: Role of the peritoneum. *World journal of gastroentology* **22**, 7692–7707 (2016).
20. Jayne, D. Molecular biology of peritoneal carcinomatosis. *Cancer Treat Res* **134**, 21–33 (2007).
21. Deville, S. S. & Cordes, N. The Extracellular, Cellular, and Nuclear Stiffness, a Trinity in the Cancer Resistome—A Review. *Front Oncol* **9**, 1376 (2019).
22. Frantz, C., Stewart, K. M. & Weaver, V. M. The extracellular matrix at a glance. *J Cell Sci* **123**, 4195–4200 (2010).
23. Lu, P., Weaver, V. M. & Werb, Z. The extracellular matrix: A dynamic niche in cancer progression. *Journal of Cell Biology* **196**, 395–406 (2012).
24. Winkler, J., Abisoye-Ogunniyan, A., Metcalf, K. J. & Werb, Z. Concepts of extracellular matrix remodelling in tumour progression and metastasis. *Nat Commun* **11**, 5120 (2020).
25. Hoshiba, T. Decellularized extracellular matrix for cancer research. *Materials* **12**, (2019).
26. Chighizola, M. *et al.* Adhesion force spectroscopy with nanostructured colloidal probes reveals nanotopography-dependent early mechanotransductive interactions at the cell membrane level. *Nanoscale* **12**, 14708–14723 (2020).
27. Engler, A. J., Sen, S., Sweeney, H. L. & Discher, D. E. Matrix Elasticity Directs Stem Cell Lineage Specification. *Cell* **126**, 677–689 (2006).
28. Nebuloni, M. *et al.* Insight On Colorectal Carcinoma Infiltration by Studying Perilesional Extracellular Matrix. *Nature Publishing Group* **6**, 1–13 (2016).
29. Jaalouk, D. E. & Lammerding, J. Mechanotransduction gone awry. *Nat Rev Mol Cell Biol* **10**, 63–73 (2009).
30. Bissell, M. J. & Hines, W. C. Why don’t we get more cancer? A proposed role of the microenvironment in restraining cancer progression. *Nat Med* **17**, 320–329 (2011).
31. Chaudhuri, O. *et al.* Extracellular matrix stiffness and composition jointly regulate the induction of malignant phenotypes in mammary epithelium. *Nat Mater* **13**, 970–978 (2014).
32. Lansky, Z. *et al.* 3D mapping of native extracellular matrix reveals cellular responses to the microenvironment. *J Struct Biol X* **1**, (2019).
33. Alcaraz, J., Otero, J., Jorba, I. & Navajas, D. Bidirectional mechanobiology between cells and their local extracellular matrix probed by atomic force microscopy. *Semin Cell Dev Biol* **73**, 71–81 (2018).
34. Liu, H. *et al.* In situ mechanical characterization of the cell nucleus by atomic force microscopy. *ACS Nano* **8**, 3821–3828 (2014).
35. Muiznieks, L. D. & Keeley, F. W. Molecular assembly and mechanical properties of the extracellular matrix: A fibrous protein perspective. *Biochim Biophys Acta Mol Basis Dis* **1832**, 866–875 (2013).

36. Knudson, K. M. *et al.* M7824, a novel bifunctional anti-PD-L1/TGFβ Trap fusion protein, promotes anti-tumor efficacy as monotherapy and in combination with vaccine. *Oncoimmunology* **7**, (2018).
37. Bourboulia, D. & Stetler-Stevenson, W. G. Matrix metalloproteinases (MMPs) and tissue inhibitors of metalloproteinases (TIMPs): Positive and negative regulators in tumor cell adhesion. *Semin Cancer Biol* **20**, 161–168 (2010).
38. Levental, K. R. *et al.* Matrix Crosslinking Forces Tumor Progression by Enhancing Integrin Signaling. *Cell* **139**, 891–906 (2009).
39. Gkretsi, V. & Stylianopoulos, T. Cell adhesion and matrix stiffness: Coordinating cancer cell invasion and metastasis. *Front Oncol* **8**, (2018).
40. Gilkes, D. M., Semenza, G. L. & Wirtz, D. Hypoxia and the extracellular matrix: Drivers of tumour metastasis. *Nat Rev Cancer* **14**, 430–439 (2014).
41. Duval, K. *et al.* Modeling physiological events in 2D vs. 3D cell culture. *Physiology* **32**, 266–277 (2017).
42. Paradiso, F., Serpelloni, S., Francis, L. W. & Taraballi, F. Mechanical studies of the third dimension in cancer: From 2D to 3D model. *Int J Mol Sci* **22**, (2021).
43. Kim, W., Gwon, Y., Park, S., Kim, H. & Kim, J. Therapeutic strategies of three-dimensional stem cell spheroids and organoids for tissue repair and regeneration. *Bioact Mater* **19**, 50–74 (2022).
44. Fatehullah, A., Tan, S. H. & Barker, N. Organoids as an in vitro model of human development and disease. *Nat Cell Biol* **18**, 246–254 (2016).
45. Gilazieva, Z., Ponomarev, A., Rutland, C., Rizvanov, A. & Solovyeva, V. Promising applications of tumor spheroids and organoids for personalized medicine. *Cancers (Basel)* **12**, 1–19 (2020).
46. Sato, K. *et al.* Organoids and Spheroids as Models for Studying Cholestatic Liver Injury and Cholangiocarcinoma. *Hepatology* vol. 74 491–502 Preprint at https://doi.org/10.1002/hep.31653 (2021).
47. Pineda, E. T., Nerem, R. M. & Ahsan, T. Differentiation patterns of embryonic stem cells in two-versus three-dimensional culture. *Cells Tissues Organs* **197**, 399–410 (2013).
48. Mark, C. *et al.* Collective forces of tumor spheroids in three-dimensional biopolymer networks. *Elife* **9**, (2020).
49. McKenzie, A. J. *et al.* The mechanical microenvironment regulates ovarian cancer cell morphology, migration, and spheroid disaggregation. *Sci Rep* **8**, 1–20 (2018).
50. Varinelli, L. *et al.* Decellularized extracellular matrix as scaffold for cancer organoid cultures of colorectal peritoneal metastases. *J Mol Cell Biol* (2022) doi:10.1093/jmcb/mjac064.
51. Ferreira, L. P., Gaspar, V. M. & Mano, J. F. Decellularized Extracellular Matrix for Bioengineering Physiomimetic 3D in Vitro Tumor Models. *Trends Biotechnol* **38**, 1397–1414 (2020).

52. Dolznig, H. *et al.* Modeling colon adenocarcinomas in vitro: A 3D co-culture system induces cancer-relevant pathways upon tumor cell and stromal fibroblast interaction. *American Journal of Pathology* **179**, 487–501 (2011).
53. Lu, H. *et al.* Cultured cell-derived extracellular matrix scaffolds for tissue engineering. *Biomaterials* **32**, 9658–9666 (2011).
54. D'angelo, E. *et al.* Patient-Derived Scaffolds of Colorectal Cancer Metastases as an Organotypic 3D Model of the Liver Metastatic Microenvironment. *Cancers (Basel)* **12**, 364 (2020).
55. García-Gareta, E. *et al.* Decellularised scaffolds: just a framework? Current knowledge and future directions. *J Tissue Eng* **11**, 1–18 (2020).
56. Jin, Q. *et al.* Decellularized breast matrix as bioactive microenvironment for in vitro three-dimensional cancer culture. *J Cell Physiol* **234**, 3425–3435 (2019).
57. Lim, C. T., Zhou, E. H., Li, A., Vedula, S. R. K. & Fu, H. X. Experimental techniques for single cell and single molecule biomechanics. *Materials Science and Engineering C* **26**, 1278–1288 (2006).
58. Li, M., Dang, D., Liu, L., Xi, N. & Wang, Y. Atomic force microscopy in characterizing cell mechanics for biomedical applications: A review. *IEEE Trans Nanobioscience* **16**, 523–540 (2017).
59. Wu, P. H. *et al.* A comparison of methods to assess cell mechanical properties. *Nat Methods* **15**, (2018).
60. Hajjarian, Z. & Nadkarni, S. K. Technological perspectives on laser speckle micro-rheology for cancer mechanobiology research. *J Biomed Opt* **26**, (2021).
61. Alessandrini, A. & Facci, P. AFM: A versatile tool in biophysics. *Meas Sci Technol* **16**, (2005).
62. Trache, A. & Meininger, G. A. Atomic Force Microscopy (AFM). *Curr Protoc Microbiol* (2008) doi:10.1002/9780471729259.mc02c02s8.
63. Radmacher, M. Measuring the elastic properties of biological samples with the AFM. *IEEE Engineering in Medicine and Biology Magazine* **16**, 47–57 (1997).
64. Hochmuth, R. M. Micropipette aspiration of living cells. *J Biomech* **33**, (2000).
65. Wu, P. H. *et al.* Particle tracking microrheology of cancer cells in living subjects. *Materials Today* **39**, 89–109 (2020).
66. Wu, P. H. *et al.* High-throughput ballistic injection nanorheology to measure cell mechanics. *Nat Protoc* **7**, 155–170 (2012).
67. Zhang, H. & Liu, K. K. Optical tweezers for single cells. *J R Soc Interface* **5**, 671–690 (2008).
68. Laurent, V. M. *et al.* Assessment of mechanical properties of adherent living cells by bead micromanipulation: Comparison of magnetic twisting cytometry vs optical tweezers. *J Biomech Eng* **124**, 408–421 (2002).
69. Hosu, B. G., Jakab, K., Bánki, P., Tóth, F. I. & Forgacs, G. Magnetic tweezers for intracellular applications. *Review of Scientific Instruments* **74**, 4158–4163 (2003).

70. Berardi, M. *et al.* Dynamic Mechanical Analysis of Suspended Soft Bodies via Hydraulic Force Spectroscopy. *Soft Matter* (2022) doi:10.1039/d2sm01173e.
71. Gerum, R. *et al.* Viscoelastic properties of suspended cells measured with shear flow deformation cytometry. *Elife* (2022) doi:10.1101/2022.01.11.475843.
72. Mietke, A. *et al.* Extracting Cell Stiffness from Real-Time Deformability Cytometry: Theory and Experiment. *Biophys J* **109**, 2023–2036 (2015).
73. Lange, J. R. *et al.* Microconstriction Arrays for High-Throughput Quantitative Measurements of Cell Mechanical Properties. *Biophys J* **109**, 26–34 (2015).
74. Viji Babu, P. K., Rianna, C., Mirastschijski, U. & Radmacher, M. Nano-mechanical mapping of interdependent cell and ECM mechanics by AFM force spectroscopy. *Sci Rep* **9**, 12317 (2019).
75. Zemła, J. *et al.* Atomic force microscopy as a tool for assessing the cellular elasticity and adhesiveness to identify cancer cells and tissues. *Semin Cell Dev Biol* **73**, 115–124 (2018).
76. Lekka, M. *et al.* Cancer cell detection in tissue sections using AFM. *Arch Biochem Biophys* **518**, 151–156 (2012).
77. Lorenc, E. *et al.* The nanomechanical fingerprint of colorectal-derived peritoneal metastasis. *Biorvix* (2022) doi:/10.1101/2022.08.17.504271.
78. Gnanachandran, K., Kędracka-Krok, S., Pabijan, J. & Lekka, M. Discriminating bladder cancer cells through rheological mechanomarkers at cell and spheroid levels. *J Biomech* **144**, (2022).
79. Kontomaris, S.-V. The Hertz Model in AFM Nanoindentation Experiments: Applications in Biological Samples and Biomaterials. *Micro and Nanosystems* **10**, 11–22 (2018).
80. Allison, D. P., Mortensen, N. P., Sullivan, C. J. & Doktycz, M. J. Atomic force microscopy of biological samples. *Wiley Interdiscip Rev Nanomed Nanobiotechnol* **2**, 618–634 (2010).
81. Kubiak, A., Zieliński, T., Pabijan, J. & Lekka, M. Nanomechanics in monitoring the effectiveness of drugs targeting the cancer cell cytoskeleton. *Int J Mol Sci* **21**, 1–15 (2020).
82. Binnig, G., Quate, C. F. & Gerber, C. Atomic Force Microscope. *Phys Rev Lett* **56**, 930–934 (1986).
83. Indrieri, M., Podestà, A., Bongiorno, G., Marchesi, D. & Milani, P. Adhesive-free colloidal probes for nanoscale force measurements: Production and characterization. *Review of Scientific Instruments* **82**, (2011).
84. West, P. E. *Introduction to Atomic Force Microscopy:Theory Practice Applications*. (Pacific Nanotechnology, 2006).
85. Eaton, P. Jonathan. & West, Paul. *Atomic force microscopy*. (Oxford University Press, 2010).
86. Müller, D. J. & Dufrêne, Y. F. Atomic force microscopy as a multifunctional molecular toolbox in nanobiotechnology. *Nat Nanotechnol* **3**, (2008).
87. Gould, S. A. C. *et al.* The Atomic Force Microscope: A Tool For Science And Industry. *Ultramicroscopy* **33**, 93–98 (1990).

88. Krieg, M. *et al.* Atomic force microscopy-based mechanobiology. *Nature Reviews Physics* **1**, 41–57 (2019).
89. Puricelli, L., Galluzzi, M., Schulte, C., Podestà, A. & Milani, P. Nanomechanical and topographical imaging of living cells by atomic force microscopy with colloidal probes. *Review of Scientific Instruments* **86**, (2015).
90. Waters, C. M., Roan, E. & Navajas, D. Mechanobiology in lung epithelial cells: Measurements, perturbations, and responses. *Compr Physiol* **2**, 1–29 (2012).
91. Jorba, I., Uriarte, J. J., Campillo, N., Farré, R. & Navajas, D. Probing Micromechanical Properties of the Extracellular Matrix of Soft Tissues by Atomic Force Microscopy. *J Cell Physiol* **232**, 19–26 (2017).
92. Plodinec, M. & Lim, R. Y. H. Nanomechanical characterization of living mammary tissues by atomic force microscopy. *Methods in Molecular Biology* **1293**, 231–246 (2015).
93. Plodinec, M. *et al.* The nanomechanical signature of breast cancer. *Nat Nanotechnol* **7**, 757–765 (2012).
94. Lopez, J. I., Kang, I., You, W. K., McDonald, D. M. & Weaver, V. M. In situ force mapping of mammary gland transformation. *Integrative Biology* **3**, 910–921 (2011).
95. Lorenc, E., Holuigue, H., Rico, F. & Podestà, A. AFM Cantilever and Tips. in *Mechanics of Cells and Tissues in Diseases* vol. 1 (2023).
96. Casuso, I. *et al.* Atomic Force Microscope AFM. in *Mechanics of Cells and Tissues in Diseases* vol. 1 67–68 (2023).
97. Kontomaris, S. V., Malamou, A. & Stylianou, A. A new approach for the AFM-based mechanical characterization of biological samples. *Scanning* **2020**, (2020).
98. Lacaria, L., Rico, F., Radmacher, M. & Podestà, A. Contact Mechanics. in *Mechanics of Cells and Tissues in Diseases* vol. 1 21–63 (2023).
99. Butt, H. J., Cappella, B. & Kappl, M. Force measurements with the atomic force microscope: Technique, interpretation and applications. *Surf Sci Rep* **59**, 1–152 (2005).
100. Kontomaris, S. V., Malamou, A. & Stylianou, A. The Hertzian theory in AFM nanoindentation experiments regarding biological samples: Overcoming limitations in data processing. *Micron* **155**, 103228 (2022).
101. Stolz, M. *et al.* Early detection of aging cartilage and osteoarthritis in mice and patient samples using atomic force microscopy. *Nat Nanotechnol* **4**, 186–192 (2009).
102. Efremov, Y. M. *et al.* Mechanical properties of fibroblasts depend on level of cancer transformation. *Biochim Biophys Acta Mol Cell Res* **1843**, 1013–1019 (2014).
103. Li, Q. S., Lee, G. Y. H., Ong, C. N. & Lim, C. T. AFM indentation study of breast cancer cells. *Biochem Biophys Res Commun* **374**, 609–613 (2008).
104. Strasser, S., Zink, A., Janko, M., Heckl, W. M. & Thalhammer, S. Structural investigations on native collagen type I fibrils using AFM. *Biochem Biophys Res Commun* **354**, 27–32 (2007).

105. Wenger, M. P. E., Bozec, L., Horton, M. A. & Mesquidaz, P. Mechanical properties of collagen fibrils. *Biophys J* **93**, 1255–1263 (2007).
106. Chighizola, M. *et al.* Large colloidal probes for atomic force microscopy: fabrication and calibration issues. *Journal of Molecular Recognition* **34**, (2021).
107. Ebner, A., Wildling, L. & Gruber, H. J. Functionalization of AFM tips and supports for molecular recognition force spectroscopy and recognition imaging. in *Methods in Molecular Biology* vol. 1886 117–151 (Humana Press Inc., 2019).
108. Carl, P. & Schillers, H. Elasticity measurement of living cells with an atomic force microscope: Data acquisition and processing. *Pflugers Arch* **457**, 551–559 (2008).
109. Genovese, L. *et al.* Cellular Localization, Invasion, and Turnover Are Differently Influenced by Healthy and Tumor-Derived Extracellular Matrix. *Tissue Eng* **20**, 2005–2018 (2014).
110. Rigato, A., Miyagi, A., Scheuring, S. & Rico, F. High-frequency microrheology reveals cytoskeleton dynamics in living cells. *Nat Phys* **13**, 771–775 (2017).
111. Marsal, M. *et al.* AFM and microrheology in the zebrafish embryo yolk cell. *Journal of Visualized Experiments* **2017**, (2017).
112. Schillers, H. *et al.* Standardized Nanomechanical Atomic Force Microscopy Procedure (SNAP) for Measuring Soft and Biological Samples. *Sci Rep* **7**, (2017).
113. Rico, F. *et al.* Probing mechanical properties of living cells by atomic force microscopy with blunted pyramidal cantilever tips. *Phys Rev E Stat Nonlin Soft Matter Phys* **72**, 1–10 (2005).
114. Dimitriadis, E. K., Horkay, F., Maresca, J., Kachar, B. & Chadwick, R. S. Determination of elastic moduli of thin layers of soft material using the atomic force microscope. *Biophys J* **82**, 2798–2810 (2002).
115. Howland, R. & Benatar, L. *A practical guide to scanning probe microscopy*. (DIANE Publishing Company, 1993).
116. Rico, F., Roca-Cusachs, P., Sunyer, R., Farre, R. & Navajas, D. Cell dynamic adhesion and elastic properties probed with cylindrical atomic force microscopy cantilever tips. *Journal of Molecular Recognition* **20**, 459–466 (2007).
117. Mahaffy, R. E., Park, S., Gerde, E., Käs, J. & Shih, C. K. Quantitative Analysis of the Viscoelastic Properties of Thin Regions of Fibroblasts Using Atomic Force Microscopy. *Biophys J* **86**, 1777–1793 (2004).
118. Harris, A. R. & Charras, G. T. Experimental validation of atomic force microscopy-based cell elasticity measurements. *Nanotechnology* **22**, (2011).
119. Alcalá, J., Giannakopoulos, A. E. & Suresh, S. Continuous measurements of load-penetration curves with spherical microindenters and the estimation of mechanical properties. *J Mater Res* **13**, 1390–1400 (1997).

120. Swadener, J. G., George, E. P. & Pharr, G. M. The correlation of the indentation size eeect measured with indenters of various shapes. *J Mech Phys Solids* **50**, 681–694 (2002).
121. Garcia, P. D. & Garcia, R. Determination of the Elastic Moduli of a Single Cell Cultured on a Rigid Support by Force Microscopy. *Biophys J* **114**, 2923–2932 (2018).
122. Butt, H.-J. & Jaschke, M. Calculation of thermal noise in atomic force microscopy Calculation of thermal noise in atomic force microscopy. *Nanotechnology 6 1 Nanotechnology* **6**, 1–7 (1995).
123. Laurent, J., Steinberger, A. & Bellon, L. Functionalized AFM probes for force spectroscopy: Eigenmode shapes and stiffness calibration through thermal noise measurements. *Nanotechnology* **24**, (2013).
124. Hutter, J. L. & Bechhoefer, J. Calibration of atomic-force microscope tips. *Review of Scientific Instruments* **64**, 1868–1873 (1993).
125. Scouten, C. W. & Cunningham, M. Freezing Biological Samples. (2006).
126. Adam Moser, Kevin Range, and D. M. Y. Thermomechanical analysis of freezing-induced cell-fluid-matrixinteractions in engineered tissues. *Bone* **23**, 1–7 (2008).
127. Usukura, E. *et al.* A Cryosectioning Technique for the Observation of Intracellular Structures and Immunocytochemistry of Tissues in Atomic Force Microscopy (AFM). *Sci Rep* **7**, (2017).
128. Neidert. Michael R., Devireddy, R. v., Tranquillo, R. T. & Bischof, J. Cryopreservation of Collagen-Based Tissue Equivalents. II. Improved Freezing in the Presence of Cryoprotective Agents. *Tissue Eng* **10**, (2004).
129. Grant, C. A., Twigg, P. C. & Tobin, D. J. Static and dynamic nanomechanical properties of human skin tissue using atomic force microscopy: Effect of scarring in the upper dermis. *Acta Biomater* **8**, 4123–4129 (2012).
130. Schillers, H., Millet, A., Lekka, M., Alfano, M. & Podestà, A. *Standardised procedures for sample shipping*.
131. Experimental Pathology Research Laboratory. Freezing tissues for histology: Embedding protocol for Frozen Samples. Preprint at http://www.bdbiosciences.com/us/resources/s/frozentissue (2016).
132. Buhl, T., Legler, T. J. & Rosenberger, A. Controlled-rate freezer cryopreservation of highly concentrated peripheral blood mononuclear cells results in higher cell yields and superior autologous T-cell stimulation for dendritic cell-based immunotherapy. *Cancer Immunology, Immunotherapy* **61**, 2021–2031 (2012).
133. Biocision, L. Snap Freezing Using Dry Ice or Liquid Nitrogen. (2013).
134. Rondeau, R. E. Slush Baths. *Treasury Dept. Internal Revenue Service* **5**, 124–124 (1965).
135. Thomas Jefferson University. Step by Step instruction for frozen sample preparation for histology assay in non-histopathology lab environment.
136. van Zwieten, R. W. *et al.* Assessing dystrophies and other muscle diseases at the nanometer scale by atomic force microscopy. *Nanomedicine* **9**, 393–406 (2014).

137. Wowk, B. How Cryoprotectants Work. *Cryonics* 3–7 (2007).
138. Pegg, D. E. The History and Principles of Cryopreservation. *Semin Reprod Med* **20**, (2002).
139. Best, B. P. Cryoprotectant Toxicity: Facts, Issues, and Questions. *Rejuvenation Res* **18**, 422–436 (2015).
140. Tykocki, N. R. & Monson, F. C. Excitability and contractility in arterioles and venules from the urinary bladder. *Curr Top Membr* **85**, 301–326 (2020).
141. Nenadic, I. Z. *et al.* Ultrasound bladder vibrometry method for measuring viscoelasticity of the bladder wall. *Phys Med Biol* **58**, 2675–2695 (2013).
142. Neuhaus, J. & Schwalenberg, T. Intravesical treatments of bladder pain syndrome/interstitial cystitis. *Nat Rev Urol* **9**, 707–720 (2012).
143. Lekka, M., Pabijan, J. & Orzechowska, B. Morphological and mechanical stability of bladder cancer cells in response to substrate rigidity. *Biochim Biophys Acta Gen Subj* **1863**, 1006–1014 (2019).
144. Li, C. *et al.* Quantitative elasticity measurement of urinary bladder wall using laser-induced surface acoustic waves. *Biomed Opt Express* **5**, 4313 (2014).
145. Roberts, K. & Tuck, L. Embedding and freezing fresh human tissue in OCT using isopentane V.3 Human Cell Atlas Method Development Community. *protocols.io* https://dx.doi.org/10.17504/protocols.io.95mh846 (2019).
146. Hintze, J. L. & Nelson, R. D. Violin Plots: A Box Plot-Density Trace Synergism Statistical Computing and Graphics Violin Plots: A Box Plot-Density Trace Synergism. *Source: The American Statistician* **52**, 181–184 (1998).
147. Smith, R. E. Comparative evaluation of 2 instruments and procedures to cut nonfrozen section. *Journal of Histochemistry & Cytochemistry* **18**, (1970).
148. Babu, P. K. V. & Radmacher, M. Mechanics of brain tissues studied by atomic force microscopy: A perspective. *Front Neurosci* **13**, 1–9 (2019).
149. Oh, Y. J. & Hinterdorfer, P. Investigation of bacterial curli production and adhesion using AFM. in *Methods in Molecular Biology* vol. 1886 221–231 (Humana Press Inc., 2019).
150. Graham, H. K. *et al.* Tissue section AFM: In situ ultrastructural imaging of native biomolecules. *Matrix Biology* **29**, 254–260 (2010).
151. Xu, X., Li, Z., Cai, L., Calve, S. & Neu, C. P. Mapping the nonreciprocal micromechanics of individual cells and the surrounding matrix within living tissues. *Sci Rep* **6**, (2016).
152. Yarmolenko, P. S. *et al.* Thresholds for thermal damage to normal tissues: An update. *International Journal of Hyperthermia* **27**, 320–343 (2011).
153. Dewhirst, M., Viglianti, B. L., Lora-Michiels, M., Hoopes, P. J. & Hanson, M. A. Thermal dose requirement for tissue effect: experimental and clinical findings. *Thermal Treatment of Tissue: Energy Delivery and Assessment II* **4954**, 37 (2003).
154. Liu, F. & Tschumperlin, D. J. Micro-mechanical characterization of lung tissue using atomic force microscopy. *Journal of visualized experiments* **54**, (2011).

155. Cabourne, E. J. *et al.* Investigation of tumor-peritoneal interactions in the pathogenesis of peritoneal metastases using a novel ex vivo peritoneal model1. *Journal of Surgical Research* **164**, (2010).
156. Levy, A. D., Shaw, J. C. & Sobin, L. H. Secondary tumors and tumorlike lesions of the peritoneal cavity: Imaging features with pathologic correlation. *Radiographics* **29**, 347–373 (2009).
157. Ubink, I. *et al.* Histopathological and molecular classification of colorectal cancer and corresponding peritoneal metastases. *British Journal of Surgery* **105**, 204–211 (2018).
158. Akhtar, M., Haider, A., Rashid, S. & Al-Nabet, A. D. M. H. Paget's "Seed and Soil" Theory of Cancer Metastasis. *Adv Anat Pathol* **26**, 69–74 (2019).
159. Schlaeppi, M. *et al.* Role of Integrins and Evidence for two Distinct Mechanisms Mediating Human Colorectal Carcinoma Cell Interaction with Peritoneal Mesothelial Cells and Extracellular Matrix. *Cell Adhes Commun* **4**, 439–455 (1996).
160. Peinado, H. *et al.* Pre-metastatic niches: organ-specific homes for metastases. *Nat Rev Cancer* **17**, 302–317 (2017).
161. Liu, C., Pei, H. & Tan, F. Matrix stiffness and colorectal cancer. *Onco Targets Ther* **13**, 2747–2755 (2020).
162. Drost, J. & Clevers, H. Organoids in cancer research. *Nat Rev Cancer* doi:10.1038/s41568-018-0007-6.
163. Handorf, A. M., Zhou, Y., Halanski, M. A. & Li, W. J. Tissue stiffness dictates development, homeostasis, and disease progression. *Organogenesis* **11**, 1–15 (2015).
164. Karsdal, M. A. *et al.* Extracellular matrix remodeling: The common denominator in connective tissue diseases possibilities for evaluation and current understanding of the matrix as more than a passive architecture, but a key player in tissue failure. *Assay Drug Dev Technol* **11**, 70–92 (2013).
165. Butcher, D. T., Alliston, T. & Weaver, V. M. A tense situation: Forcing tumour progression. *Nat Rev Cancer* **9**, 108–122 (2009).
166. Hunter Joyce, M. *et al.* Phenotypic basis for matrix stiffness-dependent chemoresistance of breast cancer cells to doxorubicin. *Front Oncol* **8**, 337 (2018).
167. Czekay, R.-P., Cheon, D.-J., Samarakoon, R., Kutz, S. M. & Higgins, P. J. Cancer-Associated Fibroblasts: Mechanisms of Tumor Progression and Novel Therapeutic Targets. *Cancers (Basel)* **14**, 1231 (2022).
168. Nurmik, M., Ullmann, P., Rodriguez, F., Haan, S. & Letellier, E. In search of definitions: Cancer-associated fibroblasts and their markers. *Int J Cancer* **146**, 895–905 (2020).
169. Chiarugi, P. & Cirri, P. Cancer associated fibroblasts: the dark side of the coin. *Am J Cancer Res* **1**, 482–497 (2011).
170. Gavara, N. A beginner's guide to atomic force microscopy probing for cell mechanics. *Microsc Res Tech* **80**, 75–84 (2017).
171. Shimshoni, E. *et al.* Distinct extracellular–matrix remodeling events precede symptoms of inflammation. *Matrix Biology* **96**, 47–68 (2021).

172. Jorba, I. *et al.* Nonlinear elasticity of the lung extracellular microenvironment is regulated by macroscale tissue strain. *Acta Biomater* **92**, 265–276 (2019).
173. Alfano, M. *et al.* Linearized texture of three-dimensional extracellular matrix is mandatory for bladder cancer cell invasion. *Sci Rep* **6**, 1–12 (2016).
174. Kohn, J. C., Lampi, M. C. & Reinhart-King, C. A. Age-related vascular stiffening: Causes and consequences. *Front Genet* **6**, 112 (2015).
175. Arthroplasty, T. K. *et al.* Stiffening of human skin fibroblasts with age. *Biophys J* **99**, 2434–2442 (2010).
176. Berdyyeva, T. K., Woodworth, C. D. & Sokolov, I. Human epithelial cells increase their rigidity with ageing in vitro: Direct measurements. *Phys Med Biol* **50**, 81–92 (2005).
177. Huynh, J. *et al.* Age-related intimal stiffening enhances endothelial permeability and leukocyte transmigration. *Sci Transl Med* **3**, (2011).
178. Lieber, S. C. *et al.* Aging increases stiffness of cardiac myocytes measured by atomic force microscopy nanoindentation. *Am J Physiol Heart Circ Physiol* **287**, 645–651 (2004).
179. White, A. *et al.* A review of sex-related differences in colorectal cancer incidence, screening uptake, routes to diagnosis, cancer stage and survival in the UK. *BMC Cancer* **18**, 1–11 (2018).
180. Mosca, L., Barrett-Connor, E. & Kass Wenger, N. Sex/gender differences in cardiovascular disease prevention: What a difference a decade makes. *Circulation* **124**, 2145–2154 (2011).
181. Acerbi, I. *et al.* Human breast cancer invasion and aggression correlates with ECM stiffening and immune cell infiltration. *Integrative Biology (United Kingdom)* **7**, 1120–1134 (2015).
182. Seo, B. R. *et al.* Collagen microarchitecture mechanically controls myofibroblast differentiation. *Proc Natl Acad Sci U S A* **117**, 11387–11398 (2020).
183. Alcaraz, J. *et al.* Collective epithelial cell invasion overcomes mechanical barriers of collagenous extracellular matrix by a narrow tube-like geometry and MMP14-dependent local softening. *Integrative Biology* **3**, 1153–1166 (2011).
184. Mishra, D. K., Miller, R. A., Pence, K. A. & Kim, M. P. Small cell and non small cell lung cancer form metastasis on cellular 4D lung model. *BMC Cancer* **18**, (2018).
185. Grey, J. F. E., Campbell-Ritchie, A., Everitt, N. M., Fezovich, A. J. & Wheatley, S. P. The use of decellularised animal tissue to study disseminating cancer cells. *J Cell Sci* **132**, (2019).
186. Miyauchi, Y. *et al.* A novel three-dimensional culture system maintaining the physiological extracellular matrix of fibrotic model livers accelerates progression of hepatocellular carcinoma cells. *Sci Rep* **7**, 9827 (2017).
187. Sensi, F., D'Angelo, E., D'Aronco, S., Molinaro, R. & Agostini, M. Preclinical three-dimensional colorectal cancer model: The next generation of in vitro drug efficacy evaluation. *J Cell Physiol* **234**, 181–191 (2018).

188. Hertz, H. Ueber die Berührung fester elastischer Körper. *Journal Für Die Reine Und Angewandte Mathematik* (1882).
189. Gavara, N. & Chadwick, R. S. Determination of the elastic moduli of thin samples and adherent cells using conical atomic force microscope tips. *Nat Nanotechnol* **7**, 733–736 (2012).
190. Varinelli, L. *et al.* Decellularized Normal and Tumor Extracellular Matrix as Scaffold for Cancer Organoid Cultures of Colorectal Peritoneal Metastases. *bioRxiv* 2021.07.15.452437 (2021) doi:10.1101/2021.07.15.452437.
191. David, F. N. & Cramer, H. Mathematical Methods of Statistics. *Biometrika* **34**, 374 (1947).
192. Alper, J. S. & Gelb, R. I. Standard Errors and Confidence Intervals in Nonlinear Regression: Comparison of Monte Carlo and Parametric Statistics. *J. Phys. Chem* **94**, 4741–4151 (1990).
193. Kao, A. P., Connelly, J. T. & Barber, A. H. 3D nanomechanical evaluations of dermal structures in skin. *J Mech Behav Biomed Mater* **57**, 14–23 (2016).
194. Nyga, A., Loizidou, M., Emberton, M. & Cheema, U. A novel tissue engineered three-dimensional in vitro colorectal cancer model. *Acta Biomater* **9**, 7917–7926 (2013).
195. Asadishekari, M. *et al.* Three-Dimensional Tunable Fibronectin-Collagen Platforms for Control of Cell Adhesion and Matrix Deposition. *Front Phys* **10**, (2022).
196. Roy, P. *et al.* Organoids as preclinical models to improve intraperitoneal chemotherapy effectiveness for colorectal cancer patients with peritoneal metastases: Preclinical models to improve HIPEC. *Int J Pharm* **531**, 143–152 (2017).
197. Wirtz, D., Konstantopoulos, K. & Searson, P. C. The physics of cancer: The role of physical interactions and mechanical forces in metastasis. *Nat Rev Cancer* **11**, 512–522 (2011).
198. Ubink, I. *et al.* Organoids from colorectal peritoneal metastases as a platform for improving hyperthermic intraperitoneal chemotherapy. *British Journal of Surgery* **106**, 1404–1414 (2019).
199. Grebenyuk, S. *et al.* Large-scale perfused tissues via synthetic 3D soft microfluidics. *Nat Commun* **14**, 193 (2023).
200. Fujii, M., Matano, M., Nanki, K. & Sato, T. Efficient genetic engineering of human intestinal organoids using electroporation. *Nat Protoc* **10**, 1474–1485 (2015).
201. Mahajan, V. *et al.* Mapping Tumor Spheroid Mechanics in Dependence of 3D Microenvironment Stiffness and Degradability by Brillouin Microscopy. *Cancers (Basel)* **13**, 5549 (2021).
202. Condeelis, J. & Segall, J. E. Intravital imaging of cell movement in tumours. *Nat Rev Cancer* **3**, 921–930 (2003).
203. Sun, D. *et al.* Novel decellularized liver matrix-alginate hybrid gel beads for the 3D culture of hepatocellular carcinoma cells. *Int J Biol Macromol* **109**, 1154–1163 (2018).

204. Soofi, S. S., Last, J. A., Liliensiek, S. J., Nealey, P. F. & Murphy, C. J. The elastic modulus of Matrigel^{TM} as determined by atomic force microscopy. *J Struct Biol* **167**, 216–219 (2009).
205. Nunes, A. S., Barros, A. S., Costa, E. C., Moreira, A. F. & Correia, I. J. 3D tumor spheroids as in vitro models to mimic in vivo human solid tumors resistance to therapeutic drugs. *Biotechnol Bioeng* **116**, 206–226 (2019).
206. Han, W. *et al.* In vitro bone metastasis dwelling in a 3D bioengineered niche. *Biomaterials* **269**, (2021).
207. Jin, Q. *et al.* Decellularized breast matrix as bioactive microenvironment for in vitro three-dimensional cancer culture. *J Cell Physiol* **234**, 3425–3435 (2018).
208. McAllister, S. S. & Weinberg, R. A. Tumor-host interactions: A far-reaching relationship. *Journal of Clinical Oncology* **28**, 4022–4028 (2010).
209. Azadi, S., Tafazzoli Shadpour, M. & Warkiani, M. E. Characterizing the effect of substrate stiffness on the extravasation potential of breast cancer cells using a 3D microfluidic model. *Biotechnol Bioeng* **118**, 823–835 (2021).
210. Riehl, B. D., Kim, E., Bouzid, T. & Lim, J. Y. The Role of Microenvironmental Cues and Mechanical Loading Milieus in Breast Cancer Cell Progression and Metastasis. *Front Bioeng Biotechnol* **8**, (2021).
211. Alcoser, T. A. *et al.* Probing the Biophysical Properties of Primary Breast Tumor-Derived Fibroblasts. *Cell Mol Bioeng* **8**, 76–85 (2015).
212. Decarli, M. C. *et al.* Cell spheroids as a versatile research platform: Formation mechanisms, high throughput production, characterization and applications. *Biofabrication* **13**, (2021).
213. Edmondson, R., Broglie, J. J., Adcock, A. F. & Yang, L. Three-dimensional cell culture systems and their applications in drug discovery and cell-based biosensors. *Assay Drug Dev Technol* **12**, 207–218 (2014).
214. Conrad, C., Gray, K. M., Stroka, K. M., Rizvi, I. & Scarcelli, G. Mechanical Characterization of 3D Ovarian Cancer Nodules Using Brillouin Confocal Microscopy. *Cell Mol Bioeng* **12**, 215–226 (2019).
215. Blumlein, A., Williams, N. & McManus, J. J. The mechanical properties of individual cell spheroids. *Sci Rep* **7**, (2017).
216. Giannetti, A., Revilloud, J. & Verdier, C. Mechanical properties of 3D tumor spheroids measured by AFM. *Comput Methods Biomech Biomed Engin* **23**, S125–S127 (2020).
217. Pinto, B., Henriques, A. C., Silva, P. M. A. & Bousbaa, H. Three-dimensional spheroids as in vitro preclinical models for cancer research. *Pharmaceutics* **12**, 1–38 (2020).
218. Cui, X., Hartanto, Y. & Zhang, H. Advances in multicellular spheroids formation. *J R Soc Interface* **14**, (2017).
219. Glimelius, B., Norling, B., Nederman, T. & Carlsson, J. Extracellular matrices in multicellular spheroids of human glioma origin: Increased incorporation of proteoglycans and fibronectin as compared to monolayer cultures. *APMIS* **96**, 433–444 (1988).

220. Vyas, V., Solomon, M., D’Souza, G. G. M. & Huey, B. D. Nanomechanical Analysis of Extracellular Matrix and Cells in Multicellular Spheroids. *Cell Mol Bioeng* **12**, 203–214 (2019).
221. el Harane, S. *et al.* Adipose-derived stem cell spheroids are superior to single-cell suspensions to improve fat autograft long-term survival. *J Cell Mol Med* **26**, 1421–1433 (2022).
222. Ng, W. H. *et al.* Extracellular matrix from decellularized mesenchymal stem cells improves cardiac gene expressions and oxidative resistance in cardiac C-kit cells. *Regen Ther* **11**, 8–16 (2019).
223. Yamada, S., Wirtz, D. & Kuo, S. C. Mechanics of living cells measured by laser tracking microrheology. *Biophys J* **78**, 1736–1747 (2000).
224. Puig-de-morales, M. *et al.* Measurement of cell microrheology by magnetic twisting cytometry with frequency domain demodulation. *J Appl Physiol* **91**, 1152–1159 (2001).
225. Bu, Y., Li, L., Yang, C., Li, R. & Wang, J. Measuring Viscoelastic Properties of Living Cells. *Acta Mechanica Solida Sinica* **32**, 599–610 (2019).
226. Guillou, L. *et al.* Measuring Cell Viscoelastic Properties Using a Microfluidic Extensional Flow Device. *Biophys J* **111**, 2039–2050 (2016).
227. Nyberg, K. D. *et al.* Quantitative Deformability Cytometry: Rapid, Calibrated Measurements of Cell Mechanical Properties. *Biophys J* **113**, 1574–1584 (2017).
228. Qi, S., Yi, C. & Yang, M. Biosensors Using Atomic Force Microscopes. in *Encyclopedia of Microfluidics and Nanofluidics* 1–10 (Springer US, 2014). doi:10.1007/978-3-642-27758-0_98-2.
229. de Laat, M. L. C., Garza, H. H. P. & Ghatkesar, M. K. In situ stiffness adjustment of AFM probes by two orders of magnitude. *Sensors (Switzerland)* **16**, (2016).
230. Slattery, A. D. *et al.* Characterisation of the material and mechanical properties of atomic force microscope cantilevers with a plan-view trapezoidal geometry. *Applied Sciences (Switzerland)* **9**, (2019).
231. Berthold, T., Benstetter, G., Frammelsberger, W., Rodríguez, R. & Nafría, M. Numerical study of hydrodynamic forces for AFM operations in liquid. *Scanning* **2017**, (2017).
232. Damircheli, M. & Eslami, B. Design of V-shaped cantilevers for enhanced multifrequency AFM measurements. *Beilstein Journal of Nanotechnology* **11**, 1525–1541 (2020).
233. Alunda, B. O. & Lee, Y. J. Review: Cantilever-based sensors for high speed atomic force microscopy. *Sensors (Switzerland)* **20**, 1–39 (2020).
234. Slattery, A. D., Blanch, A. J., Ejov, V., Quinton, J. S. & Gibson, C. T. Spring constant calibration techniques for next-generation fast-scanning atomic force microscope cantilevers. *Nanotechnology* **25**, (2014).
235. Sader, J. E. & White, L. Theoretical analysis of the static deflection of plates for atomic force microscope applications. *J Appl Phys* **74**, 1–9 (1993).
236. Liu, B. H., Chuang, S. K. & Huang, A. L. Shape effect of torsional resonance mode AFM cantilevers operated in fluids. *Surf Topogr* **2**, V (2014).

237. Guan, D., Charlaix, E., Qi, R. Z. & Tong, P. Noncontact Viscoelastic Imaging of Living Cells Using a Long-Needle Atomic Force Microscope with Dual-Frequency Modulation. *Phys Rev Appl* **8**, (2017).
238. Minary-Jolandan, M., Tajik, A., Wang, N. & Yu, M. F. Intrinsically high-Q dynamic AFM imaging in liquid with a significantly extended needle tip. *Nanotechnology* **23**, (2012).
239. Daeinabi, K. & Korayem, M. H. Indentation analysis of nano-particle using nano-contact mechanics models during nano-manipulation based on atomic force microscopy. *Journal of Nanoparticle Research* **13**, 1075–1091 (2011).
240. Alcaraz, J. *et al.* Laminin and biomimetic extracellular elasticity enhance functional differentiation in mammary epithelia. *EMBO Journal* **27**, 2829–2838 (2008).
241. Gill, N. K. *et al.* A scalable filtration method for high throughput screening based on cell deformability. *Lab Chip* **19**, 343–357 (2019).
242. Rosendahl, P. *et al.* Real-time fluorescence and deformability cytometry. *Nat Methods* **15**, 355–358 (2018).
243. Qi, D. *et al.* Screening cell mechanotype by parallel microfiltration. *Sci Rep* **5**, (2015).
244. Navajas, D. & Radmacher, M. Viscoelasticity. in *Mechanics of cells and Tissues in Disease* vol. 1 (De Gruyte, 2023).
245. Manning, M. L., Foty, R. A., Steinberg, M. S. & Schoetz, E.-M. Coaction of intercellular adhesion and cortical tension specifies tissue surface tension. *PNAS* **107**, (2010).
246. Fabry, B. *et al.* Scaling the microrheology of living cells. *Phys Rev Lett* **87**, (2001).
247. Otto, O. *et al.* Real-time deformability cytometry: On-the-fly cell mechanical phenotyping. *Nat Methods* **12**, 199–202 (2015).
248. Mietke, A. *et al.* Extracting Cell Stiffness from Real-Time Deformability Cytometry: Theory and Experiment. *Biophys J* **109**, 2023–2036 (2015).
249. Byun, S. *et al.* Characterizing deformability and surface friction of cancer cells. *Proc Natl Acad Sci U S A* **110**, 7580–7585 (2013).
250. Nyberg, K. D. *et al.* The physical origins of transit time measurements for rapid, single cell mechanotyping. *Lab Chip* **16**, 3330–3339 (2016).
251. Müller, S. J., Fabry, B. & Gekle, S. Predicting cell stress and strain during extrusion bioprinting. (2022) doi:10.1101/2022.09.28.509836.
252. Efremov, Y. M. *et al.* Mechanical properties of cell sheets and spheroids: the link between single cells and complex tissues. doi:10.1007/s12551-021-00821-w/Published.
253. Schneider, C. A., Rasband, W. S. & Eliceiri, K. W. NIH Image to ImageJ: 25 years of image analysis. *Nat Methods* **9**, 671–675 (2012).
254. Jeong, S. Y., Lee, J. H., Shin, Y., Chung, S. & Kuh, H. J. Co-culture of tumor spheroids and fibroblasts in a collagen matrix-incorporated microfluidic chip mimics reciprocal activation in solid tumor microenvironment. *PLoS One* **11**, 1–17 (2016).

255. Park, J. il *et al.* Scaffold-free coculture spheroids of human colonic adenocarcinoma cells and normal colonic fibroblasts promote tumorigenicity in nude mice. *Transl Oncol* **9**, 79–88 (2016).

256. Ivascu, A. & Kubbies, M. Rapid generation of single-tumor spheroids for high-throughput cell function and toxicity analysis. *J Biomol Screen* **11**, 922–932 (2006).

257. Laurent, J. *et al.* Multicellular tumor spheroid models to explore cell cycle checkpoints in 3D. *BMC Cancer* **13**, (2013).

258. Targosz-Korecka, M., Daniel Brzezinka, G., Danilkiewicz, J., Rajfur, Z. & Szymonski, M. Glutaraldehyde fixation preserves the trend of elasticity alterations for endothelial cells exposed to TNF-α. *Cytoskeleton* **72**, 124–130 (2015).

259. Rodríguez-Nieto, M. *et al.* Viscoelastic properties of doxorubicin-treated HT-29 cancer cells by atomic force microscopy: the fractional Zener model as an optimal viscoelastic model for cells. *Biomech Model Mechanobiol* **19**, 801–813 (2020).

260. Maares, M. *et al.* Time-and zinc-related changes in biomechanical properties of human colorectal cancer cells examined by atomic force microscopy. *Biology (Basel)* **9**, 1–25 (2020).

261. Beton, K. & Brożek-Płuska, B. Biochemistry and Nanomechanical Properties of Human Colon Cells upon Simvastatin, Lovastatin, and Mevastatin Supplementations: Raman Imaging and AFM Studies. *Journal of Physical Chemistry B* **126**, 7088–7103 (2022).

262. Schindelin, J. *et al.* Fiji: An open-source platform for biological-image analysis. *Nat Methods* **9**, 676–682 (2012).

263. Canedo, E. L., Favelukis, M., Tadmor, Z. & Talmon, Y. An Experimental Study of Bubble Deformation in Viscous Liquids in Simple Shear Flow. *AIChE* **39**, (1993).